



THE HONG KONG  
POLYTECHNIC UNIVERSITY

香港理工大學

Pao Yue-kong Library

包玉剛圖書館

---

## Copyright Undertaking

This thesis is protected by copyright, with all rights reserved.

**By reading and using the thesis, the reader understands and agrees to the following terms:**

1. The reader will abide by the rules and legal ordinances governing copyright regarding the use of the thesis.
2. The reader will use the thesis for the purpose of research or private study only and not for distribution or further reproduction or any other purpose.
3. The reader agrees to indemnify and hold the University harmless from and against any loss, damage, cost, liability or expenses arising from copyright infringement or unauthorized usage.

### IMPORTANT

If you have reasons to believe that any materials in this thesis are deemed not suitable to be distributed in this form, or a copyright owner having difficulty with the material being included in our database, please contact [lbsys@polyu.edu.hk](mailto:lbsys@polyu.edu.hk) providing details. The Library will look into your claim and consider taking remedial action upon receipt of the written requests.

DEVELOPMENT OF A NOVEL LOW-  
PRESSURE LAPPING METHOD FOR  
SUPERFINISHING ALUMINIUM ALLOYS

YU NINGHUI

PhD

The Hong Kong Polytechnic University

2019

**The Hong Kong Polytechnic University**

**Department of Industrial and Systems Engineering**

**Development of a Novel Low-Pressure Lapping  
Method for Superfinishing Aluminium Alloys**

YU NingHui

A thesis submitted in partial fulfilment of the requirement for the degree of

Doctor of Philosophy

February 2019

# CERTIFICATE OF ORIGINALITY

I hereby declare that this thesis is my own work and that, to the best of my knowledge and belief, it reproduces no material previously published or written, nor material that has been accepted for the award of any other degree or diploma, except where due acknowledgement has been made in the text.

\_\_\_\_\_ (Signed)

YU NINGHUI (Name of student)

## ABSTRACT

Aluminium alloy (Al6061) is a common material used for reflective mirrors. It can be machined with a good surface finish by Single Point Diamond Turning (SPDT). As a high optical reflectance is needed for mirrors. Due to the material is relatively soft, it is difficult to apply post-processing such as ultra-precision lapping and ultra-precision polishing, as they may scratch the diamond turned surface. In addition, a recent study showed that the reflectance on a diamond turned aluminium alloy (Al6061) does not have a simple correlation with good surface finish. The highest reflectance is found on a surface with small tool marks, but how the tool marks affect the optical properties is not fully known. In this study, a novel low-pressure lapping method has been developed to reduce the surface roughness and preserve the reflectance at the same time.

In this thesis, the research work consisted of four parts. The first part focuses on the study of the influence of feed rate on the surface roughness and reflectance of Aluminium alloy (Al6061) by single-point diamond turning (SPDT). The results show that even through the surface roughness is decreased when the feed rate is reduced. When the feed rate is lower than a critical value, the reflectance is also decreased due to the  $Mg_2Si$  particles being embedded on the machined surface rather than being removed by the cutting. As a result, the low-pressure lapping technology in this research is focused on reducing the surface roughness and preserving the reflectance

of the aluminium alloy (Al6061) surface is machined under the critical feed rate.

The second part of the research focuses on the investigation of the relationship between the lapping parameters and surface roughness of the aluminium alloy (Al6061) surface by using a novel lapping technology. This novel lapping method uses a brush to drive the abrasive particles over the workpiece surface. During the lapping process, the fiber on the rotating brush provides a small normal force and sufficient lateral force for the abrasive particles to roll at high speed on the surface of the workpiece. When the moving abrasive particles reach adequate speed, they impinge and damage the asperities of the surface and eventually wear away the material. In this section, Taguchi method was used to determine the optimal lapping parameters. The lapped surface under the optimal lapping parameters was further analyzed by the spectrum analysis method so as to evaluate the performance of the lapping technology. The results showed that the new low-pressure lapping technology can successfully remove the tool marks, reduce the surface roughness and preserve the reflectance of aluminium alloy (Al6061) surfaces.

In the third part of the research, the mechanism of the lapping technology was investigated. To gain a deeper understanding of the surface generation mechanism, the hydrodynamic effect, different lapping tools and slurry in the lapping technology were investigated. The influence function was further studied in this chapter. Finally, the surface generation mechanism was discussed.

A Finite Element model has been built to simulate the mechanism of the lapping technology in the fourth part of the research. The simulation results were compared with the experimental results so as to gain a better understanding of the lapping mechanism.

The present study does not only contribute to determine the relationship between the optical reflectance and surface finish on machining aluminium alloy (Al6061), but also contributes significantly in the development of a novel low-pressure lapping technology which can be used to lap soft aluminium alloy (Al6061) workpiece with nanometric surface finish. The results provide an important means for superfinishing of soft materials.

## **PUBLICATIONS ARISING FROM THE STUDY**

### **Journal papers:**

Yu NH, Chan CY\*, Li LH, Lee WB. Spectral analysis of surface roughness features of a lapped ultraprecision single-point diamond machined surface. The International Journal of Advanced Manufacturing Technology. 88(5-8), pp.1407-1415, 2017.

Li, LH, Yu, NH\*, Chan, CY and Lee, WB. Al6061 surface roughness and optical reflectance when machined by single point diamond turning at a low feed rate. PloS one, 13(4), 2018 p.e0195083.

### **Conference paper:**

N.H.Yu, W.B.Lee, C.Y.Chan and L.H.Li "Investigation of novel low pressure lapping technology on aluminium moulds "Proceedings of the 16th euspen International Conference & Exhibition (EUSPEN2016), 01-05 June, Nottingham, UK, 2016: P6.19



# ACKNOWLEDGEMENTS

I would like to express my sincerely thanks to my supervisors, Prof. W.B. Lee Chair Professor of the Department of Industrial and Systems Engineering and Prof. Benny C.F. Cheung, Professor and Interim Head of the State Key Laboratory of Ultra-precision Machining Technology of The Hong Kong Polytechnic University, for their valuable guidance, encouragement, and support throughout my PhD study.

I would also like to express my thanks to Dr. Joe Chan and Dr. Lihua Li for their valuable guidance and kind encouragement. Many thanks are also due to the technical support provided by the technicians in the State Key Laboratory of Ultra-precision Machining Technology of The Hong Kong Polytechnic University.

Moreover, I would also like to thank for my friends Mr. Yuan Wei, Mr. Han JiDe, Mr. Kero, Dr. Peter Huang, Dr. Julia Li and Dr. Zhang XiaoDong for their encouragement and kind support. Finally, I would also like to express my sincerely thanks to my wife Mrs. Zhou Yuan and my parents for their support for my PhD study.

# CONTENTS

<b>ABSTRACT .....</b>	<b>i</b>
<b>PUBLICATIONS ARISING FROM THE STUDY.....</b>	<b>iv</b>
<b>ACKNOWLEDGEMENTS .....</b>	<b>v</b>
<b>CONTENTS .....</b>	<b>vi</b>
<b>LIST OF FIGURES.....</b>	<b>viii</b>
<b>CHAPTER 1 INTRODUCTION.....</b>	<b>1</b>
1.1 Motivation .....	1
1.2 Objectives .....	2
1.3 Organization of the thesis .....	3
<b>CHAPTER 2 LITERATURE REVIEW.....</b>	<b>5</b>
2.1. Ultra-precision machining and post-process techniques for diamond turned surface.....	5
2.1.1 Ultra-precision machining and SPDT .....	5
2.1.2 Overview of polishing and lapping technology .....	7
2.1.3 Principles of precision polishing and lapping technology.....	23
2.1.4 Modelling and simulation of current polishing and lapping method.....	39
2.2 Surface measurement and characterization methods .....	41
2.2.1 Surface characterization parameters .....	41
2.2.2 Power spectrum analysis method in characterizing surface texture .....	45
2.2.3 Methods for measuring reflectance.....	46
2.3 Summary .....	50
<b>CHAPTER 3 STUDY ON REFLECTANCE CHARACTERISTICS OF AL6061 ALLOY SURFACE USED FOR THE LOW-PRESSURE LAPPING TECHNOLOGY .....</b>	<b>53</b>
3.1 Introduction .....	53
3.2. Materials and methods.....	55
3.2.1 Materials and machine.....	55
3.2.2 Characterization methods.....	57
3.3. Results and Discussion.....	58

3.4. Summary .....	62
<b>CHAPTER 4 DEVELOPMENT OF A LOW-PRESSURE LAPPING TECHNOLOGY AND THE OPTIMIZATION OF THE LAPPING PARAMETERS .....</b>	<b>64</b>
4.1. Introduction .....	65
4.2. Experimental setup .....	68
4.3. Results and Discussion.....	73
4.4. Summary .....	82
<b>CHAPTER 5 INVESTIGATION ON SURFACE GENERATION MECHANISM OF THE LOW-PRESSURE LAPPING TECHNOLOGY .....</b>	<b>84</b>
5.1 Introduction .....	84
5.2 Part I: hydrodynamic effect.....	85
5.3 Part II: Influence function .....	91
5.4 Part III: surface generation mechanism.....	96
5.5 Summary .....	102
<b>CHAPTER 6 MODELLING AND SIMULATION OF THE SURFACE GENERATION MECHANISM OF THE LOW-PRESSURE LAPPING TECHNOLOGY .....</b>	<b>103</b>
6.1. Introduction .....	103
6.2 Modeling processes .....	106
6.2.1 Parameter setting .....	106
6.2.2 Software setting.....	111
6.3 Results and discussion .....	113
6.4 Summary .....	122
<b>CHAPTER 7 OVERALL CONCLUSION AND SUGGESTIONS FOR FURTHER WORK.....</b>	<b>124</b>
7.1 Overall conclusion.....	124
7.2 Suggestions for further work .....	126
<b>REFERENCES.....</b>	<b>128</b>

# LIST OF FIGURES

Figure. 2.1 Relationship of workpiece dimension and tolerance for Normal machining, precision machining and ultra-precision machining (Trent and Wright 2000).....	5
Figure 2.2 Ultra-precision diamond turning of aluminum alloy on a Nanotech 450 machine.....	6
Figure.2.3 Ideal surface machined by a round diamond tool.....	7
Figure 2.4 Polishing tool of Bonnet Polishing (Cheung et al.2010).....	9
Figure 2.5 Schematic of Magnetorheological Finishing (Ganapathy et al. 2016)	11
Figure 2.6 Schematic of Electrorheological fluid-assisted polishing (Kuriyagawa et al. 2002) .....	12
Figure 2.7 Configuration of Fluid Jet Polishing (Cao et al. 2014) .....	13
Figure 2.8 Fluid under different magnet condition in Magnetorheological Jet Polishing (Tricard et al. 2006) .....	14
Figure 2.9 Schematic of Elastic emission machine (Jain. 2009).....	15
Figure 2.10 Schematic of Ion Beam Figuring (Liao et al. 2014).....	16
Figure 2.11 Schematic of Plasma Jet Machining (Arnold and Bohm, 2012) .....	18
Figure. 2.12 Aluminum surface after bonnet polishing .....	19
Figure. 2.13 The basic CMP mechanism. (Kevin et al. 2008).....	20

Figure. 2.14 A flat aluminum mirror during the direct polishing process (Horst et al. 2008).....	21
Figure. 2.15 Examples of lapping process (Evans et al. 2003) .....	22
Figure 2.16 Kinematics model of fixed eccentric polishing method (Zhao et al. 2009).....	26
Figure 2.17 Fixed eccentric polishing path (Zhao et al. 2009).....	26
Figure 2.18 Fixed eccentric polishing path with translational motion (Zhao et al. 2009).....	26
Figure 2.19 Schematic of linear polishing device (Yi. 2005).....	27
Figure 2.20 linear polishing device path (Zhao et al. 2009).....	28
Figure 2.21 Peano curve and Peano-like curve for polishing aspherical surface (Tam et al. 2013) .....	29
Figure 2.22 Rake angles of abrasive particle determines whether the material in the groove is cut out or plowed without material removal.....	32
Figure 2.23 Micromachining by abrasive particles embedded in cloth fibers.....	35
Figure 2.24 Micromachining by abrasives contained in a carrier paste .....	36
Figure.2.25 FEM model of the motion of a diamond grain in polishing process.	40
Figure.2.26 The material removal mechanism at the monoatomic layer (Si et al. 2010).....	41
Figure 2.27 Geometric components of a surface profile: (a) roughness, (b)	

waviness, and (c) form (Jiang et al. 2007) .....	43
Figure 2.28 Schematic of specular reflection and diffuse reflection (retrieved from <a href="https://en.wikipedia.org/wiki/Diffuse_reflection">https://en.wikipedia.org/wiki/Diffuse_reflection</a> ).....	47
Figure 2.29 Strong V-W type reflectometer (James 2001) .....	49
Figure 2.30 V-N type absolute reflectometer (Germer et al. 2014) .....	50
Figure 3.1 15 samples machined by SPDT with different feed rates .....	56
Figure 3.2. Measurement image of the diamond tool tip radius an Olympus BX60 microscope.....	57
Figure 3.3 Reflectance measuring device .....	58
Figure 3.4 Results of normalized reflectance of 15 samples machined by Single Point.....	59
Figure 3.5 Chips measured by the Hitachi electron microscope TM3000, (a) feed rate is 7 mm/min, (b) feed rate is 3 mm/min.....	59
Figure 3.6 SEM images and EDX results of surfaces when feed rate are 1mm/min (a) and 7mm/min (b) separately.....	61
Figure 3.7 Verification experiment: SEM images of surfaces when feed rate are 1mm/min (a) and 7mm/min (b) respectively .....	61
Figure 3.8 (a) Si phase was removed when feed rate is under optimal condition (b) Si phase embedded into surface when feed rate is too small .....	62
Figure 3.9 The reflectance decreased when the feed rate is lower than 3mm/min	

(tool radius: 0.318 mm, spindle speed: 1000 rpm/min, DoC: 5 $\mu$ m) .....	63
Figure 4.1 Experimental setup .....	69
Figure 4.2 Schematic of the low-pressure lapping technology .....	69
Figure 4.3 Workpiece machined by SPDT .....	70
Figure 4.4 Wyko NT8000 optical profiling system .....	72
Figure 4.5 Main effects plot of each factor .....	77
Figure 4.6 Workpiece surface before lapping (Ra:20.27 nm) .....	78
Figure 4.7 Workpiece surface under optimum lapping conditions in first trial (Ra:15.59 nm) .....	78
Figure 4.8 Workpiece surface under optimum conditions in second trial (Ra:11.71 nm).....	78
Figure 4.9 Spatial Distribution of surface profile comparison between original surface (Figure 4.6) and lapped surface (Figure 4.7). Most of the lapping work was done on group V(23.40%) .....	80
Figure 4.10 Spatial Distribution of surface profile comparison between lapped surface in first trial (Figure 4.7) and lapped surface in second trial (Figure 4.8). Major change in spatial groups shift from long and short period (IV) to middle periods (I II III) .....	80
Figure 4.11 SEM: The material surface under 2000X magnification. No scratch occurred on the surface when the workpiece is under non-excessive lapping	

.....	81
Figure 4.12 Reflectance of Al6061 mirror before lapping (a), after lapping by low-pressure lapping method (b), after lapping by conventional bonnet polishing	
.....	82
Figure 5.1 Result of Al6061 mirror surface polished by (a) Bonnet polishing method (Inclination angle: 5°, pressure: 0.1 bar, rotational speed: 1000 rpm, time: 1 min) and (b) low-pressure lapping method	86
Figure 5.2 Al6061 mirror surface lapped for 30 min (a) and the cross section plot of this surface (b)	92
Figure 5.3 Al6061 mirror lapped for 1 hour (a) and the cross section plot of this surface (b)	93
Figure 5.4 Cross section plot of Al6061 surface after lapping for 30 min (a) and 1 hour (b)	94
Figure 5.5 Al6061 surface lapped when the workpiece is continue moving through the lapping path	96
Figure 5.7 Mottled surface after lapping process (Rotational speed 1000 rpm, Time 15 min, Slurry: SiO <sub>2</sub> )	99
Figure 5.8 Platelet-like debris on the surface after lapping process (Rotational speed 1000 rpm, Time 15 min, Slurry: SiO <sub>2</sub> )	99
Figure 5.9 Long scratch on the lapped surface (Rotational speed 1000 rpm, Time	



15 min, Slurry particle: Al <sub>2</sub> O <sub>3</sub> ) .....	100
Figure 6.1. Schematic of the finite element model .....	106
Figure 6.2. Schematic of the lapping process. One fiber on the brush is swept from the workpiece surface.....	109
Figure 6.3 Abaqus interface .....	112
Figure 6.4 Stress-time curve of 1000nm tool mark surface under different speed .....	119
Figure 6.5 Stress-time curve of 20nm tool mark under different speed .....	120
Figure 6.6 Plastic strain map of the 1000 nm high tool mark surface .....	120
Figure 6.7 Plastic strain map of the 20 nm high tool mark surface .....	121
Figure 6.8 The asperities on the tool mark surface are removed first, then the tool mark itself are worn away .....	122

# CHAPTER 1 INTRODUCTION

## 1.1 Motivation

For aluminum and its alloys, Single Point Diamond Turning (SPDT) is commonly used because of its good machinability, and is widely used as a mould insert material.

Aluminum and its alloys are also the main materials used for cryogenic optical instruments, and the optical aluminum mirrors in these instruments are generally machined by SPDT (Horst et al. 2008, Kinast et al.2018).

However, SPDT inevitably generates tool marks on the workpiece since when the cutting tool cuts the workpiece successively along the feed direction of the rotating workpiece. The tool feed is defined as the interval to the small topical area. The tool marks reduce the optical performance by creating scattering and grating patterns (Yin and Yi, 2015). There are two methods that can be used to remove tool marks. One is to reduce the feed rate (Singh, 2016), while another is to polish the surface (Kevin et al.2006). However , the machined surface roughness increases if the feed rate is smaller than a particular critical value (Zhang, 1991, To, 1997) in SPDT Conventional ultra-precision polishing cannot be used on aluminum alloys because they are relatively soft and the surface is very easy to be scratched (Horst et al. 2012).

In addition, our recent work has revealed that the reflectance does not always increase monotonically with the surface roughness of the workpiece. The best reflectance occurs when the areal surface has small tool marks. As a result, a novel lapping

technology is developed to remove the tool marks from Al6061 alloy while reserving the reflectance of the machined surfaces at the same time.

## **1.2 Objectives**

The main focus of this research aims to develop a novel low-pressure lapping technology to remove the tool marks on the Al6061 alloy surface while maintaining high reflectance. As a result, the reflectance characteristics of the Al6061 alloy are investigated first, the surface with the best reflectance can be observed. A low-pressure lapping technology is then developed to remove the tool marks on this surface. Finally, a simulation model is developed to optimize and predict the surface generation in the new lapping technology. The objectives of the study are given below:

1. The reflectance characteristics is the key part of the whole research, in which a surface with high reflectance is to be lapped by the novel low-pressure lapping technology. As a result, the first objective is to investigate the reflectance characteristics when the roughness of the Al6061 alloy surface is attained in the nanometric range. The lapping technology is investigated based on the optimization of the surface in which the best reflectance can be achieved (feed rate of 7 mm/min in this research).
2. Based on the results of the study on the reflectance of Al6061 alloy surface, the second objective is to develop a novel low-pressure lapping technology and technology as well as to investigate the key factors affecting surface generation of the lapped surface. Spatial analysis method was used to evaluate the lapping technology.

The goal of the new lapping technology is to reduce the surface roughness of the Al6061 alloy surface and preserve the reflectance at the same time.

3. To investigate the surface generation mechanism of the new low-pressure lapping technology. The hydrodynamic effect, the lapping tool geometry and the slurry used in the lapping technology were studied. The Influence function describing the materials removal characteristics are further studied so as to gain a better understanding of the surface generation mechanisms.

4. To model the surface generation mechanism of the low-pressure lapping technology on Al6061 alloy surface by Finite Element Method (FEM). The results are compared with the experiment results in order to optimize and predict the surface generation in the low-pressure lapping technology.

### **1.3 Organization of the thesis**

The thesis is composed of seven chapters. In Chapter 1, an introduction to the research motivation and objectives of the study are presented. In Chapter 2, a literature review is presented to gain a better understanding of the background theories and related work done. The limitations of the traditional ultra-precision lapping and polishing methods are also identified in the literature review. Chapter 3 discusses the inter-relationship between the optical reflectance and surface roughness of the workpiece based on the results of the reflectance experiments. Based on the results in Chapter 3, a novel low-pressure lapping technology is investigated and presented in Chapter 4 for realizing the lapping of the Al6061 alloy with a soft lapping head, while

the relationship among various factors (speed, pressure, grit size, time) affecting surface generation and the surface roughness of the workpiece are described. In Chapter 5, the surface generation mechanisms are investigated by a series of experiments. Chapter 6 established a FEM model to simulate the surface generation mechanism of the low-pressure lapping technology on Al6061 alloy surface. Finally, an overall conclusion and suggestions for future work are presented in Chapter 7.

## CHAPTER 2 LITERATURE REVIEW

### 2.1. Ultra-precision machining and post-process techniques for diamond turned surface.

#### 2.1.1 Ultra-precision machining and SPDT

Ultra-precision machining has been widely used to obtain super mirror finished surfaces for optics industry. The ultra-precision machining technologies include Single Point Diamond Turning (SPDT) (Ikawa et al. 1991), ultra-precision raster milling (Cheung et al. 2006), ultra-precision grinding (Namba et al. 1993), ultra-precision lapping (Cha et al. 2009), ultra-precision polishing (Kuriyagawa et al. 2002) etc. Compared to traditional machining processes, ultra-precision machining can achieve an accuracy of an order of magnitude better than conventional machining (Figure. 2.1). Traditional machining methods can achieve 0.1  $\mu\text{m}$  arithmetic roughness ( $Ra$ ) values. However, ultra-precision machining can achieve nanometer range  $Ra$  values.

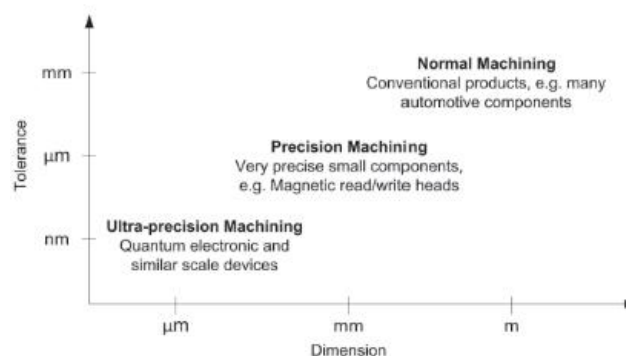


Figure. 2.1 Relationship of workpiece dimension and tolerance for Normal machining, precision machining and ultra-precision machining (Trent and Wright 2000)

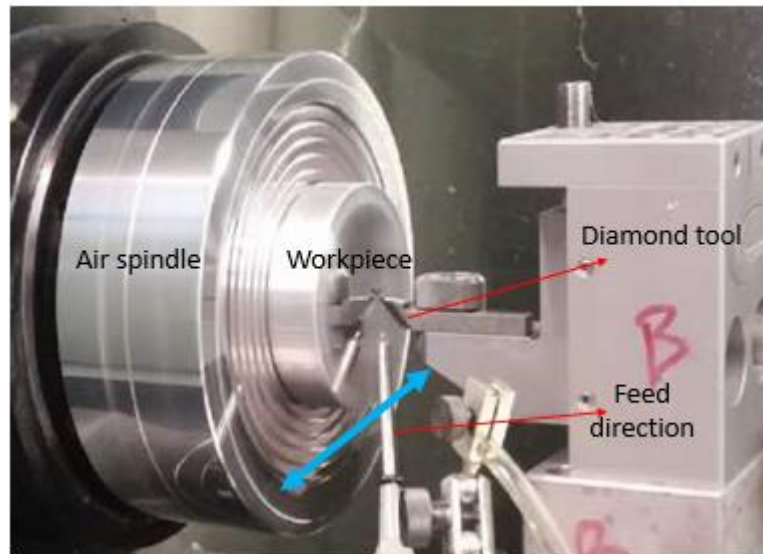


Figure 2.2 Ultra-precision diamond turning of aluminum alloy on a Nanotech 450 machine

As one of the key technologies, SPDT first appeared in the 1960s (Ikawa et al. 1991). It uses a diamond-made turning tool with a nanoscale edge radius to machine the workpiece. (Lee et al. 2003). Figure 2.2. shows the process of diamond turning of aluminum alloy In SPDT, the workpiece is rotated by the spindle, and the surface profile of the workpiece is generated under the continuous feed of the cutting tool. (Lee et al. 2003).as shown in Figure.2.3. The maximum peak-to-valley height ( $R_t$ ) on the ideal surface can be expressed as

$$R_t = \frac{f^2}{8RV^2} \quad (2.1)$$

where  $f$  is the feed rate in mm/min,  $R$  is the tool nose radius in mm,  $V$  is the rotational speed in r/min. From Eq. 2.1, the surface roughness decreases with

decreasing the feed rate or increasing the spindle rotational speed. However, Zhang (1991) claimed that the surface roughness increases if the feed rate is lower than a certain level in ultra-precision machining. Cheung and Lee (2007) also reported that when the rotational speed is higher than 1000 rpm, the maximum peak-to-valley height ( $R_t$ ) do not change much in SPDT. As a result, post-processing techniques need to be conducted on the diamond turned surfaces in order to further reduce the surface roughness.

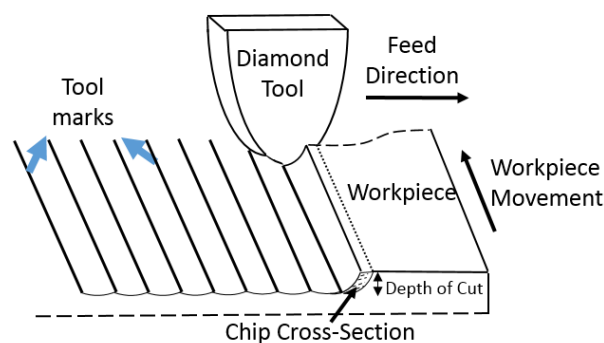


Figure.2.3 Ideal surface machined by a round diamond tool

### 2.1.2 Overview of polishing and lapping technology

Polishing and lapping are the oldest techniques among the various manufacturing processes (Evans 2003). Humans learned to polish and lap stones into weapons and polish jade into ornaments a long time ago. Although various polishing tools have been invented, polishing mainly relies on human effort to operate and judge the effect of polishing. With development of modern industrialization, automation gradually appeared and polishing equipment changed from machining plane, spherical surfaces



to aspheric surfaces and hence freeform surfaces, Moreover, the polishing accuracy was also largely improved. This section mainly introduces the current advanced polishing equipment, and discusses why a new polishing method is developed in this project.

In order to improve the performance of optical systems and reduce system cost and weight, aspherical mirrors and even freeform surfaces are gradually being applied to optical systems. As a result, the equipment for polishing complex surfaces, such as aspheric surfaces, has been developed. These devices can be broadly classified into flexible contact polishing equipment and non-contact polishing equipment. Among them, bonnet polishing equipment, magnetorheological polishing technology and electrorheological polishing technology are representatives of flexible contact devices. Kinetic energy abrasive flow polishing method, continuous particle flow impact polishing technique and chemical etching method are representatives of non-contact polishing methods.

### *2.1.2.1 Bonnet polishing technology*

Bonnet polishing technology was jointly proposed by University College London (UCL) and Zeeko Co. in 2000. The principle is shown in the Figure 2.4, the polishing head is a flexible spherical airbag. This polishing head is mounted on the rotating member of the system to form a cavity chamber. The chamber can be filled with a controlled low pressure gas. This polishing head can have a polishing film and conduct precision polishing with a suitable polishing solution. It is also possible to apply a grinding film to

correct the shape of the workpiece. The bonnet polishing has a Gaussian shape removal function, and the polishing texture is fine and uniform. The flexible polishing head can automatically adapt to the curved shape of the workpiece, and the same polishing head can be used to polish a variety of shapes, such as plane, spherical, and aspherical surfaces. However, this method still needs to be checked for quality control when polishing the edge of the workpiece. At the same time, this method has a poor polishing effect on soft metals such as aluminium alloy. Soft metal in this thesis means metals like Al6061 alloy, copper, brass or other metals with hardness is lower than 200 HB.

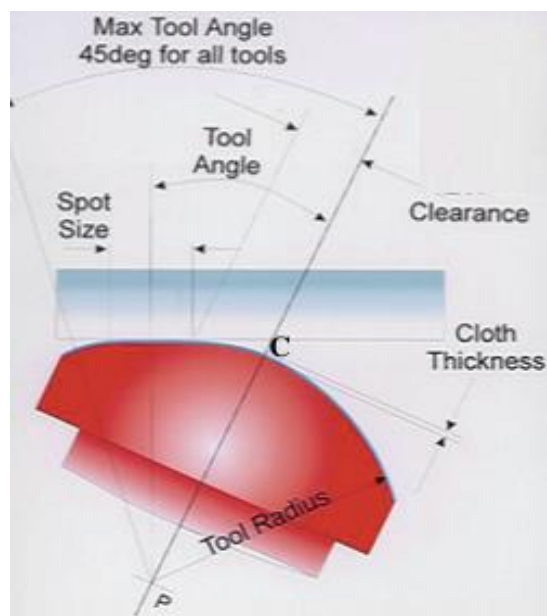


Figure 2.4 Polishing tool of Bonnet Polishing (Cheung et al.2010)

### 2.1.2.2 Magnetorheological finishing

Magnetorheological finishing, (MRF) was first proposed by Kordonski in 1988. The first

MRF prototype was produced in 1994. MRF makes use of a rheological fluid to polish the workpiece surface. During the polishing process, the rheological fluid is controlled by a variable magnetic field due to the rheological properties of the fluid. The MR fluid consists of magnetic particles, a base fluid and a stabilizer. The polishing principle is shown in Figure 2.5. The magnetic pole forms a high gradient magnetic field between the workpiece and the MR liquid conveyor belt. When the MR liquid is transmitted to the small gap between workpiece and conveyor belt with high velocity, the high gradient magnetic field makes it a viscoplastic Bingham medium and contact with the surface of the workpiece. The material is then removed by the large shear stress between the fluid and the workpiece. During the polishing process, selective removal can be achieved by controlling the residence time of the workpiece in the MR fluid.

MRF has many advantages, such as constant material removal rate, high efficiency, high surface finish quality, and removing the debris in real-time. MRF technology began to be applied in 1998. For example, Q22 Technology Co. and the Rochester University USA COM Lab jointly launched the Q22 MRF processing system, which is commonly used as a post processing method after aspheric finishing and SPDT. Companies such as Zeiss and Leica also use Schneider's SLP series polishing machine and the Q22 MRF processing system to machining SLR lenses. The disadvantage of this technique is that the shape of the workpiece is limited, in particular the curvature of concave workpiece. When using MRF processing to polish the workpiece, it is very easy to generate pitting effects especially when polishing a relatively soft metal like Al6061

alloy. Compared to MRF based processing, the major advantages of the low-pressure lapping method attempt to provide a scratch-free method to remove the material from Al6061 alloy and not generating scratches or damaging the surface form during the process.

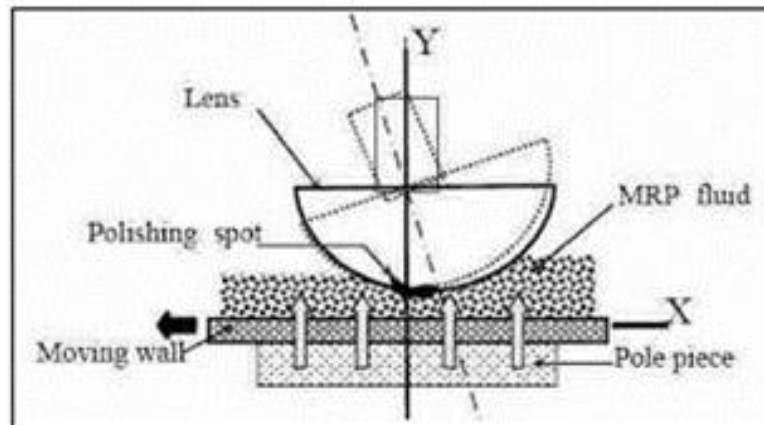


Figure 2.5 Schematic of Magnetorheological Finishing (Ganapathy et al. 2016)

### 2.1.2.3 Electrorheological fluid-assisted polishing EFP

This Electrorheological fluid-assisted polishing technique is based on the viscosity of the electrorheological fluid changing with the applied electric field strength (Figure 2.6).

The viscosity of the electrorheological fluid showing solid-like properties when the electric field is large enough. Material removal is achieved by controlling the external field to change the viscosity and local shape of the electrorheological fluid. This polishing method was first proposed by Kuriyagawa et al. in 1999. It is used to polish non-conductors such as BK7. The advantage is that the material removal rate is high, but the disadvantage is that when polishing a conductor workpiece, it is easily broken

due to the high voltage.

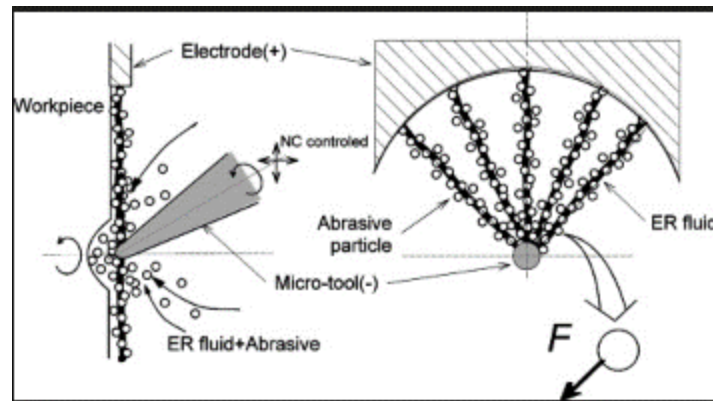


Figure 2.6 Schematic of Electrorheological fluid-assisted polishing (Kuriyagawa et al. 2002)

For non-contact polishing equipment, it mainly includes the kinetic energy abrasive flow polishing method, continuous particle flow polishing technique and chemical method.

#### 2.1.2.4 Kinetic energy abrasive flow polishing method

The kinetic energy abrasive flow polishing method includes Fluid Jet Polishing (FJP) and Magnetic Jet Polishing (MJP). The main material removal principle of these methods is using kinetic energy for impacting on the workpiece surface. The advantage of these methods is to eliminate some of the inevitable problems in contact polishing, such as matching the polishing tool with the special surface workpiece. Among them, Fluid jet polishing (FJP) is a method that shoots a liquid containing abrasive particles at the workpiece through a nozzle, and removes material by generating radial shear between the fluid and workpiece surface (Figure 2.7). The polishing effect of FJP is

controlled by the pressure, direction and residence time of the liquid jet. There are several advantages of this method such as the removal function makes it relatively easy to remain constant, the cross-sectional area of the jet beam is small, and the nozzle running track is not limited to the linear direction, and is particularly suitable for processing complex surfaces such as high-steep aspheric surfaces of hard and brittle materials etc.

However, for the FJP technology, the liquid beam is disturbed by the air which means its stability is affected by the distance between the nozzle and the workpiece surface, resulting in unstable removal rates in the polishing zone. As a result, a Magnetorheological Jet Polishing MJP was developed. The magnetorheological fluid rapidly transforms into a viscoplastic Bingham fluid under the action of a local axial magnetic field near the nozzle outlet. The surface stability of the jet beam is enhanced and the beam diameter remains substantially constant over a long distance as shown in Figure 2.8. The MJP technology has a good polishing removal function and is not sensitive to polishing distance. It is very suitable for polishing complex surfaces such as high-steep aspheric concave surfaces.

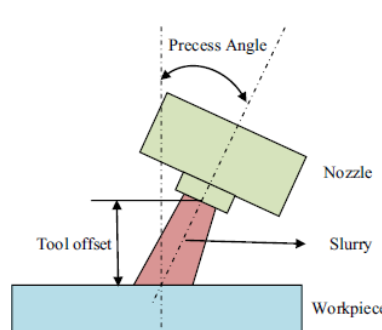


Figure 2.7 Configuration of Fluid Jet Polishing (Cao et al. 2014)

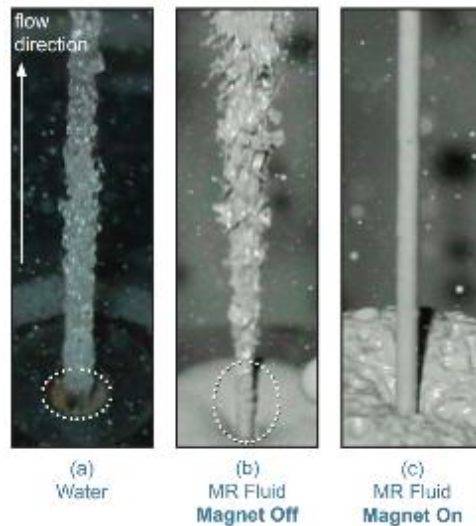


Figure 2.8 Fluid under different magnet condition in Magnetorheological Jet Polishing

(Tricard et al. 2006)

#### 2.1.2.5 Continuous particle flow impact polishing technique

Continuous particle flow impact polishing techniques make use of a continuous stream of kinetic energy particles to impact the surface of the workpiece. Typical methods include Elastic Emission Machine (EEM) and Ion Beam Figuring (IBF). The Elastic emission machine (EMM) was proposed by Tsuwa. It is an ultraprecision method which remove materials at the atomic level. The working principle is that the ultrafine abrasive particles impact on the workpiece surface, and the abrasive particles are firmly combined with the atoms of the workpiece surface. Since the binding energy of the first layer atoms and the second layer atoms on the workpiece surface is low, when the powder particles are removed, the first layer of atoms is separated from the second layer of atoms, thus achieving atomic level material removal with small elastic damage. The specific processing method is shown in Figure 2.9. The motor drives the

polyurethane ball to rotate and sweep in the liquid. The ball rotates at high speed forming a gap between the ball and the workpiece, and driving the abrasive grains with particle sizes of several tens of nanometers in the polishing liquid to strike the workpiece surface with a small incident angle. The abrasive particles and the surface of the workpiece form atomic-level bonds in a narrow area and are removed by the suspension flows. This method controls the material removal rate by controlling the dwell time of each point. The feed rate is linear with the processing speed (sweep times). The surface polished by this method has no plastic deformation or lattice defects, but the material removal rate is low.

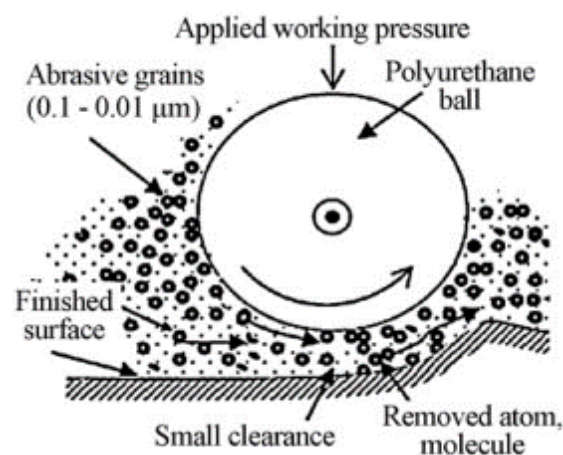


Figure 2.9 Schematic of Elastic emission machine (Jain. 2009)

Another continuous particle flow impact finishing method is Ion Beam Figuring (IBF). This method accelerates the neutral ions in an electric field under a vacuum environment, to impact on the atoms or molecules of the workpiece surface, causing them to escape the surface (Figure 2.10). The material removal rate of IBF can be



accurate to the atomic level, and another benefit of this method is that the material removal function is not sensitive to changes in the curvature of the workpiece surface, the phase distance, and the small deviation of the vertical incident angle of the beam, and is very suitable for reshaping aspherical surfaces (Dai et al. 2008).

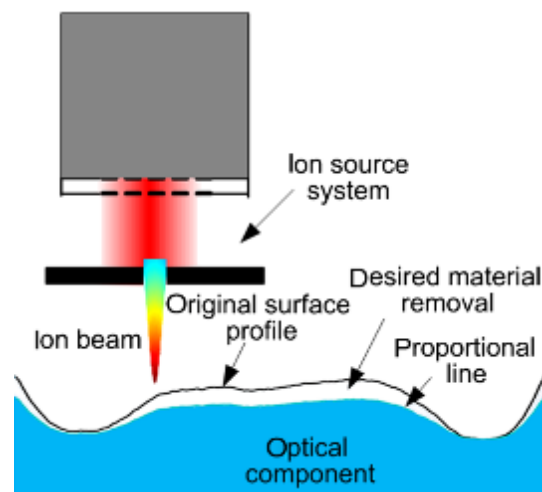


Figure 2.10 Schematic of Ion Beam Figuring (Liao et al. 2014)

#### 2.1.2.6 Chemical etching method

The chemical etching method is also a non-contact polishing method, and it is used to remove trace material from the surface with no subsurface damage. The typical method is plasma etching processing technology.

Plasma etching processing technology converts activated radicals in the plasma with atoms on the surface of the workpiece, turning them into volatile molecules, and removes the material by gas evaporation. Plasma etching processing techniques can be used to process siliceous or silicon-based materials (such as molten silicon, zero-expansion glass, quartz crystals, single crystal silicon, and silicon carbide) as well as tantalum lenses. Since there are highly toxic compounds in the process, the treatment

of the reaction products has high requirements for the equipment. Conventional plasma etching processing methods, such as Plasma Assisted Chemical Etching (PACE), excite a halogen-based gas into a plasma and react with the surface of the workpiece, which has high processing efficiency and no surface contamination and sub-surface damage layer. However, the original PACE equipment discharges gas in vacuum environment during processing, the equipment cost was high, and the scope of use was limited. As a result, researchers subsequently and gradually developed atmospheric plasma processing technology. By optimizing the ratio of the reaction gas and the plasma gas, the reaction gas in the plasma is excited by the Radio Frequency (RF) electric field excitation after being sufficiently mixed, so that a large-area uniform low-temperature plasma can be generated at one atmosphere.

Current atmospheric plasma processing techniques include plasma jet processing and plasma chemical evaporation processing. The principle of Plasma Jet Machining (PJM) is shown in Figure 2.11 (Arnold and Bohm, 2012). The plasma torch consists of a cylindrical electrode (anode) and a grounded shield (cathode), with an inert shield between the cathode and the anode. The reaction gas, oxygen and argon are mixed and sent to the barrel electrode, and the arc discharge is generated by the microwave or the RF power source between the barrel electrode and the ground shield. The gas ionization generates an active chemical group and is rapidly heated under the high temperature of the arc. It is ejected and chemically reacts with the surface material of the workpiece to form a volatile substance to remove the material.

A similar technique is Plasma Chemical Vaporization Machining (PCVM), which was proposed by Mori et al (2000). The high temperature reaction gas is directed to the surface of the workpiece through the tubular electrode. During the polishing process, the reaction gas is excited by the RF power source to form a plasma, and its chemical reaction is similar to that of PJM.

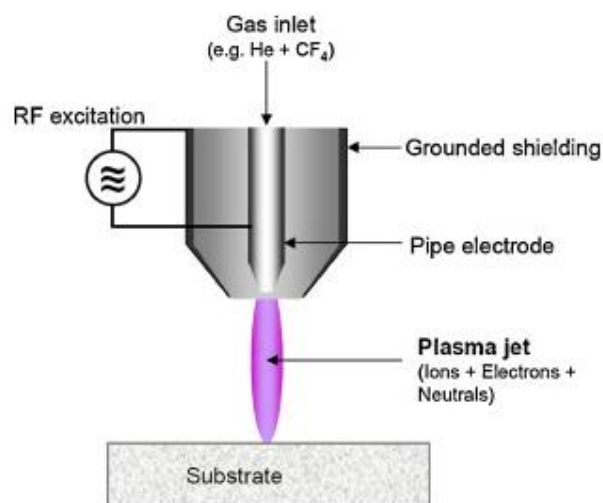


Figure 2.11 Schematic of Plasma Jet Machining (Arnold and Bohm, 2012)

The polishing methods described above all achieve nano-scale ultra-precision polishing and all of them have a constant material removal function. Since these techniques are combined with polishing path planning and dwell time to achieve quantitative material removal, the machining tool and the workpiece surface are essentially in point contact, and only a single workpiece can be machined at a time. As a result, the machining accuracy requires a complicated CNC system and high Precision, high rigidity machine tool system which means high processing costs.

In the meantime, these ultra-precision polishing processes such as Fluid Jet Polishing

(FJP) (Fahnle et al. 1998), bonnet polishing (Bingham et al. 2000) and Magneto Rheological Finishing (MRF) (Jacobs et al. 1995) experienced difficulty in polishing aluminum alloy surfaces because it is very easy to scratch the surface (Horst et al. 2012). Figure. 2.12 shows an aluminum alloy surface after bonnet polishing, where it can be seen that the surface is full of scratches.

At present, most of the common precision aluminum alloy polishing methods are still only at the micron-scale roughness level. There are other less precise polishing methods that can applied to aluminum alloy surfaces. One such technique for polishing aluminum is Chemical Mechanical Polishing (CMP) which can successfully polish an aluminum alloy surface to the nanometer scale roughness (Kevin et al. 2006).

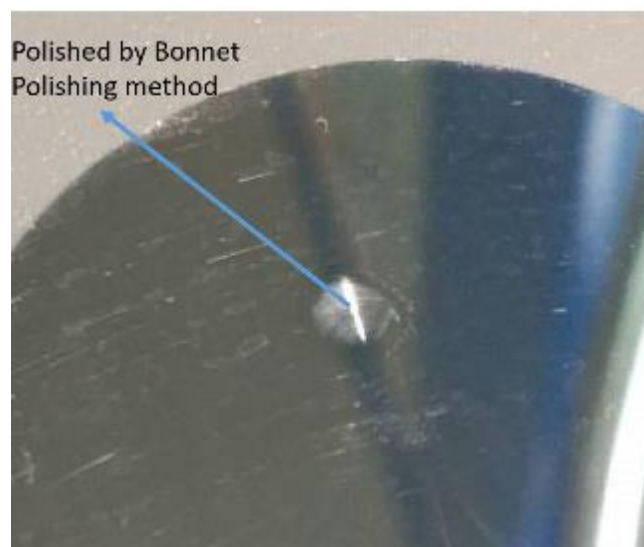


Figure. 2.12 Aluminum surface after bonnet polishing

Chemical Mechanical Polishing (CMP) is a polishing method that produces a material

removal by a combination of a chemical reaction and a mechanical force. (Lee and Jeong 2009). As shown in Figure.2.13, the first step is the reaction between the chemical additive and metal surface to form a layer of oxide. Hence, the oxidized layer is removed by the abrasive particles through the rotation of the polishing pad. However, the limitation of CMP is that the process is very sensitive to oxidizing and scratching (Horst et al. 2008).

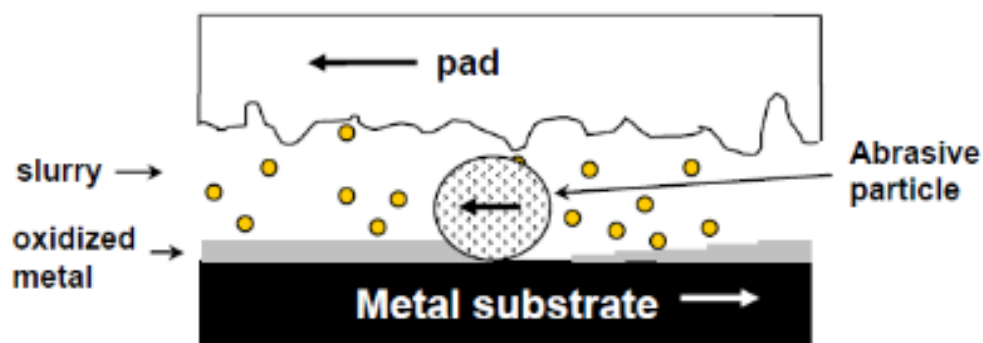


Figure. 2.13 The basic CMP mechanism. (Kevin et al. 2008)

Another method for polishing aluminum alloy was investigated by Horst et al. (2008) by directly applying a polishing tool with a 5 mm thick layer of specially prepared polishing pitch, as shown in Figure. 2.14. A surface accuracy of  $0.5 \lambda$  and 1 nm surface roughness (Ra) can be achieved. Yin and Yi (2015) also investigated the optimal polishing conditions of the direct polishing technique by using the Taguchi method. However, the limitation of CMP and the mechanical polishing method is that they only can be applied on flat surfaces because the polishing tool is flat. In addition, the relationship between the surface roughness and reflectance of the surface after SPDT

is not known. As a result, a new lapping method was investigated to figure out the relationship between the surface finish and reflectance in this project.

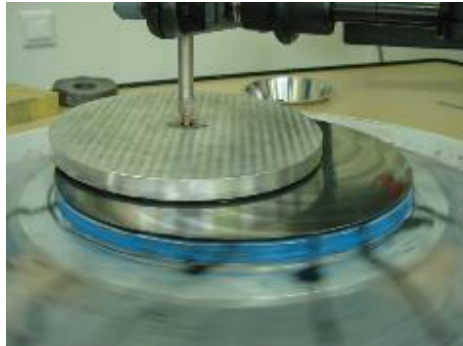


Figure. 2.14 A flat aluminum mirror during the direct polishing process (Horst et al. 2008)

As shown in Figure. 2.15, lapping is a process in which the lapping tool rubs against the workpiece with a lapping medium (lapping fluid and lapping grit). Material is removed by the countless loose particles between the carrier surface (lapping plate) and the workpiece pressed against it (St'aihli 1998). The polishing process is similar to lapping but the action is much smaller than lapping. In the polishing process, material is only removed by plastic deformation in order to generate a super fine surface. Marinescu et al. (2006) also claimed that the polishing process, not like lapping, was influenced by both mechanical actions and chemical actions. The comparison between the lapping and polishing processes is summarized in Table 2.1. Abrasives such as aluminum oxide,  $\text{SiO}_2$  or diamond are used in the lapping process. The rolling abrasives can provide a kind of kneading action on the workpiece surface,

as discovered by Martin using an electron microscope (St'aihli 1998). In this method, because the aluminum alloy surface is relatively soft compared to other metals, it is preferable to use rolling abrasives than sliding abrasives. The rolling abrasives can smooth the tool marks by bending the sharp edges over rather than breaking them, therefore, debris can be avoided during the lapping process.

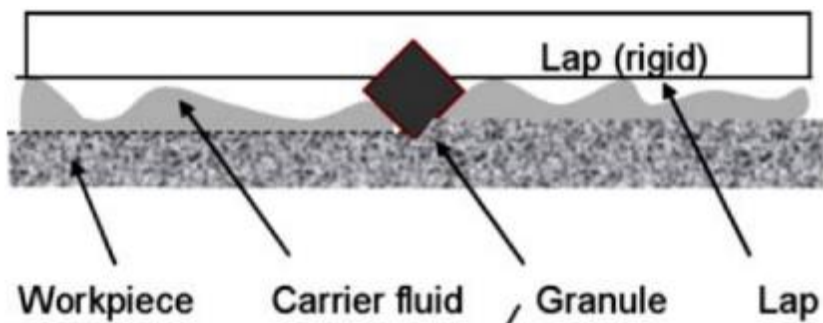


Figure. 2.15 Examples of lapping process (Evans et al. 2003)

Table 2.1 Comparison between lapping and polishing process

	Lapping	Polishing
Material removal mechanism	Mechanical mechanism, Abrasive roll on the surface	Interaction of mechanical and chemical mechanisms(Klocke and Kuchie 2009), Abrasive slide on the surface
Abrasive	Coarse grain with geometrically undefined cutting edges(Marinescu et al. 2006)	Fine grain
Surface characteristic	1.Undirected processing traces 2.Semi-gloss appearance 3.Little wear when under strain (Klocke and Kuchie 2009)	1.Mirror finish

### 2.1.3 Principles of precision polishing and lapping process

Polishing and lapping processes are varied. Different kinds of samples need particular equipment and skills to polish or lap (Baker et al. 1975). The material and shape of samples determine the process used to polish, such as which abrasive particles, whether the medium is oil or water, or even how to clean after polishing process.

Although most of the polishing industries now use automated polishing equipment, there is still a need for experienced technicians to do the final checks on the polishing of some high-end products. Researchers have been developing equipment to replace skilled workers who need years of learning to become skilled. In general, the strength and displacement accuracy of existing polishing equipment are already high enough, in order to replace experienced workers, a more in-depth study of the polishing process is required. At present, the polishing parameters can be generally divided into two types: process parameters and material parameters. The process parameters refer to parameters that need to be set in the equipment during the polishing process, such as polishing feed rate, head pressure, polishing head rotational speed, polishing path, etc. The material parameters mainly refer to the workpiece material, the type of polishing liquid, and the material of the polishing head.

Since the polishing process involves a lot of parameters, when faced with a new polishing project, a two-step experimental design is generally considered to determine the polishing process. The first step is to select possible process parameters and material parameters based on previous research. The second step is to explore the



effects of several major parameters and to find the best combination of polishing through the Analysis of variance (ANOVA) method (Kaplan et al. 1996). By using the ANOVA method, the number of experiments can be greatly reduced, and a suitable polishing combination of different parameters can be found more quickly. The ANOVA method itself is constantly being optimized, and a well-known one is the Taguchi method, which is used in many polishing studies (Chen et al. 2018, Ren et al. 2018).

Since the shape of the workpiece is now more and more complicated, the polishing head and the workpiece are usually in point contact during the polishing process, so the polishing path is an important research direction in the polishing process (Zhao et al. 2009). The polishing path is the relative trace of the abrasive particles and the workpiece during the polishing process. It generally includes two aspects: one is the path of the abrasive particles to the workpiece, and the other is the path of the workpiece relative to the polishing tool.

Uniform polishing path has a major impact on the polishing results, which not only ensures that every point of the material on the surface of the workpiece can be removed evenly, but also ensures uniform wear of the polishing tool. Both of these aspects are closely related to the polishing results (Tam and Cheng, 2010). The following assumptions are made during the study of the polishing path uniformity (Su et al, 2004):

- The workpiece, the abrasive grains and the polishing head are rigid bodies;
- The abrasive particles are fixed on the working surface of the polishing head;

- The abrasive grains are not broken or fall off;
- The rotation error of the workpiece and the polishing head are ignored.

On the basis of the above assumptions, the polishing uniformity can be evaluated by calculating the path between the workpiece and the abrasive particles. The wear uniformity of the polishing head can be evaluated if the path between the workpiece and the polishing head is determined.

For planar polishing, there are generally several common polishing paths. One is the polishing path produced by the fixed eccentric method as shown in Figure 2.16. This method is a very common method. The Eq. (2.2) of the motion of any particle P on the polishing pad relative to the workpiece is given as follows:

$$\begin{cases} X_p = r_p \cos(\theta + \omega_p t - \omega_w t) + e \cos \omega_w t \\ Y_p = r_p \sin(\theta + \omega_p t - \omega_w t) - e \sin \omega_w t \end{cases} \quad (2.2)$$

Where  $\omega_w$  is workpiece rotational speed,  $\omega_p$  is rotational speed of polishing pad,  $e$  is center distance between the workpiece and the polishing pad. The path of a particle P on the workpiece is shown in Figure 2.17. It can be determined from the formula that when the relative speed of the workpiece and the polishing pad are equal ( $\omega_w = \omega_p$ ), the material removal rate can be considered to be uniform. However, in actual production, the eccentric polishing method has poor uniformity in material removal, and is generally only used for processing small-sized workpiece which having a diameter of not more than 200 mm.

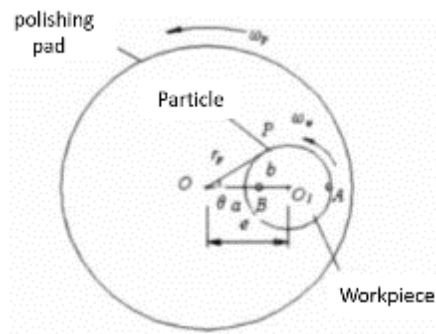


Figure 2.16 Kinematics model of fixed eccentric polishing method (Zhao et al. 2009)

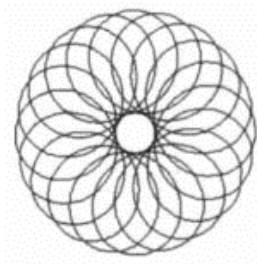


Figure 2.17 Fixed eccentric polishing path (Zhao et al. 2009)

In order to improve the uniformity of the polishing path of the fixed eccentric device, some researchers added the translational motion for the workpiece, so that the relative distance between the center of the workpiece and the center of the polishing pad changes with time.

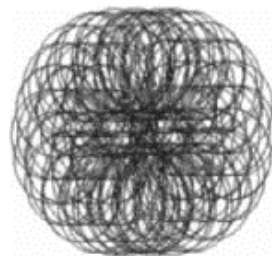


Figure 2.18 Fixed eccentric polishing path with translational motion (Zhao et al. 2009)

It can be seen from Figure 2.18 that the uniformity of the polishing path in this method

is obviously better than that of the fixed eccentric device, and is more conducive to the improvement of the surface precision of the workpiece, and is suitable for processing large-sized workpiece (i.e. diameter larger than 200 mm).

In addition to the above two polishing tracks, there is also a linear polishing device. The schematic of this method is shown in Figure 2.19. The workpiece is simply rotated, and a polishing belt is used as a polishing pad at the bottom for lateral movement or to swing around a fixed point. It is assumed that for any abrasive particle P on the abrasive belt, the relative motion path of point P relative to the workpiece is given as follows:

$$\begin{cases} X_p = r_p - v_p t \cdot \sin(\omega_w t) \\ Y_p = r_p + v_p t \cdot \cos(\omega_w t) \end{cases} \quad (2.3)$$

where  $r_p$  is the distance between  $p$  and the workpiece center.  $v_p$  is speed of the polishing belt,  $\omega_w$  is the rotational speed of the workpiece, the path of P on the workpiece is shown in Figure 2.20. This method has a simple movement form, and at the same time, it can be used in mass production if lengthening the polishing belt, which means the production efficiency is high. As a result, this polishing mechanism is widely used in industry.

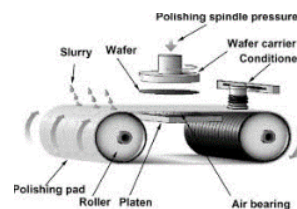


Figure 2.19 Schematic of linear polishing device (Yi. 2005)

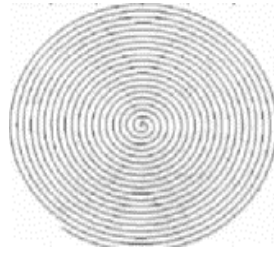


Figure 2.20 linear polishing device path (Zhao et al. 2009)

The common feature of the above methods is that the polishing pad is larger than the workpiece, and the advantage of these methods is that the material removal rate is even on every part of the workpiece. The disadvantage is that as the workpiece increases, the size of the device also increases greatly. The huge workbench is not only expensive, but also affects the accuracy of the spindle and polishing pad. Another type of polishing method is the point contact polishing described above for polishing complex surfaces. The workpiece can be fixed or rotated during this polishing process and the polishing head walks through the surface of the workpiece according to a certain route. Besides, the conventional zig-zag and ring polishing paths, Hilbert and Peano paths were also commonly used in the polishing process. The Peano curve (Figure 2.21) theoretically provides a uniform and non-intersecting polishing path that allows the polishing path to be distributed throughout the polished surface without irregular voids. Some studies have shown that this polishing path is more advantageous than other methods in achieving good polishing uniformity (Tam et al. 2013).

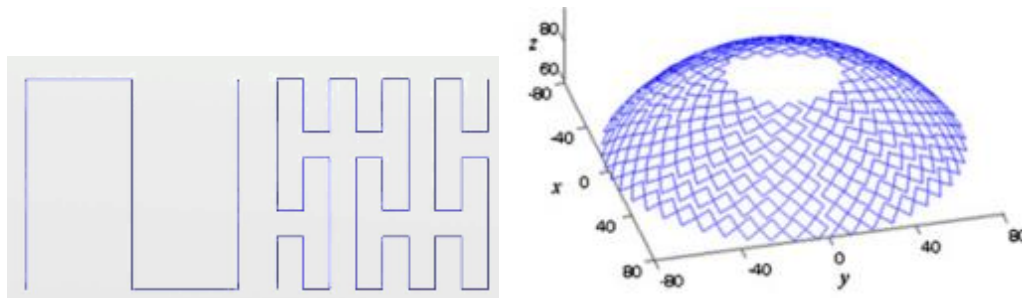


Figure 2.21 Peano curve and Peano-like curve for polishing aspherical surface (Tam et al. 2013)

It can be seen from various polishing parameters mentioned above that the polishing mechanism is a difficult research direction because of its many complicated parameters, but the polishing mechanism can help us control and predict the polishing process. Since the brush and the polishing solution are used in this study, some related polishing mechanisms are discussed below, mainly the abrasive polishing.

In the early view, polishing was the abrasive grains removed asperities from the rough surface. In the 20th century, due to limitations of experimental equipment, researchers believed that during the polishing process, the abrasive particles smear the asperities into the gap of the rough surface, thereby smoothing the surface (Belby, 1921, Bowden and Hughes, 1921). They assumed that asperities become liquid during the polishing process and then solidified again in the gaps of the rough surface. They concluded that the mechanism of this process is that the abrasive particles rubbed the asperities during the polishing process to produce a sufficiently high temperature. This temperature is close to the melting point of the material, so that the material of the

contact area becomes highly elastic and is brought into the gap of the rough surface by the shear forces. These materials cool rapidly after polishing and form an amorphous like structure, also known as the Beilby layer (Bowden and Tabor, 1950). However, with subsequent research, this Beilby layer assumption is basically incorrect. The Beilby layer hypothesis makes people feel that the polished surface is no longer the same as the original surface. However, with the development of modern optical microscopy technology, the microscopic surface becomes able to be observed. Researchers found that the polished surface is not as clean as seen with the naked eye, and still has many tiny grooves. At the same time, the new technology brings temperature detection equipment, and it was found that the contact area did not reach the melting point in the polishing process. Subsequent studies also found that the surface of the amorphous like structure is not rendered after polishing (Turley and Samuels, 1981). Although the polished surface did exhibit elastic deformation, the existence of the Beilby layer was not found, therefore researchers were more inclined to believe that the mechanism was mainly material removal during the polishing process.

As a result, the material removal mechanism during polishing can be consider as micromachining. When the polishing particles are large, many small machining chips are produced during polishing. These chips look very different, some are very slender, and some are tiny and irregular particles. Studies have shown that at the time of coarser polishing, these chips may be generated by particles that remove the material

from the edge of the chip grooves, but in fine polishing, the chips may be produced during the delamination process. Although these are two different generation mechanisms, but the difference is closer to scale than to kind. Based on this statement, the polishing process produces scratch grooves on the polished surface when the normal force applied to the polishing particles is small. Samuels (1992) suggested that better polishing results when the grooves produced during polishing process are narrower than 50 nm to 100 nm. To achieve this effect, the force needs to be less than 0.01N when polishing a workpiece with a hardness of 1000 HV, and less than 0.002 N when polishing a workpiece with a hardness of 100 HV.

For the grooves generated in the polishing process, rake angles (tool edge geometry) of the contacting point between the workpiece surface and abrasive particle determines whether the material in the groove is cut out by the particle or plowed without material removal (Figure 2.22). The shape of the contact point between the abrasive particles and the surface of the workpiece determines how much material is removed if a chip is cut, or the shape of the groove cross section if the surface is plowed.

In a follow-up study, there are two problems that have attracted much interest. One is during the polishing process, when the abrasive particles are in contact with the material, the surface of the material, especially the surface of a brittle material, is changed to ductile or is still brittle. Another interesting question is why the abrasive particles can stably produce a long scratch on the surface of the workpiece or can cut



the polishing chips during the polishing process.

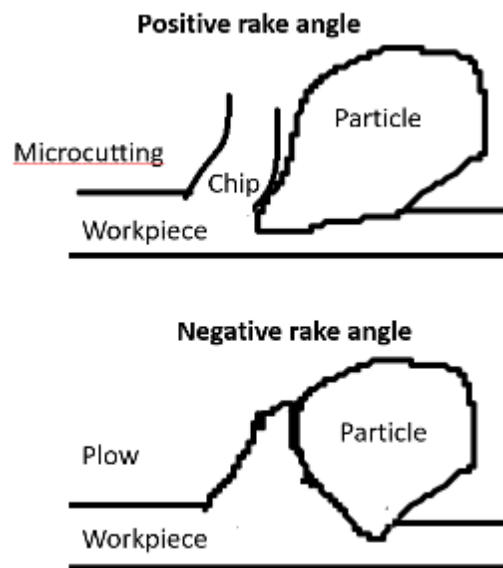


Figure 2.22 Rake angles of abrasive particle determines whether the material in the groove is cut out or plowed without material removal

Regarding the first question, researchers found that during the polishing process, randomly distributed pits and grooves appeared on the surface of a brittle material, and these tiny pits covered some parts of the grooves. These pits contain cracks below, and these cracks are not likely generated by micromachining, but are more like layers produced by elastic deformation. By using TEM detection on the polished surface of silicon, dislocation arrays also implied the existence of this elastic deformation region (Pugh and Samuels, 1963). However, due to this research mainly studies the process of polishing soft metals, the polishing mechanism of brittle materials is not discussed in depth. Regarding the second question, why can the abrasive particles form long

scratches, there are a lot of possibilities that are now discussed.

### *2.1.3.1 Slurry erosion mechanism*

In most polishing systems, the polishing particles are suspended in a polishing fluid. During the polishing process, the abrasive particles repeatedly circulate between the polishing pad and the surface of the workpiece due to the relative movement of the polishing disk and the workpiece. Some abrasive particles have enough momentum to make a groove on the surface of the workpiece. Moreover, even have enough momentum to remove the material by cutting a chip. This mechanism called slurry erosion.

Slurry erosion is a complex process, and many parameters in the polishing I affect the results. It is generally believed that the mechanism of material removal depends on the particle's rake angles and whether there is enough momentum when the particles are in contact with the surface. When the rake angle is negative, it may only plow without any material removal rate. When the rake angle is positive, chips are generated, like cutting, in the polishing process.

A single abrasive particle can remove very little material, but when the amount of abrasive grains is accumulated to a certain extent, the material removal rate is still could be considerable. However, this mechanism has a small removal rate relative to the mechanism described later. In this process, only relatively short, and random directions of the grooves are generated. In the traditional polishing experiment, the surface to be polished has a lot of consistent grooves. Some studies have shown that

this may be due to the polishing pad lengthening the grooves and covering the original grooves which are generated by the particles. There is also a possibility that the abrasive particles accumulate on the polishing pad, thereby causing parallel long grooves along with the movement of the polishing pad.

### *2.1.3.2 Micromachining by accumulated abrasive particles*

Some studies have shown that the polishing particles may be trapped by the polishing cloth fiber to form a large particle and produce a cutting action on the polished surface. It generally happens when the size of the abrasive particle is larger than the diameter of the cloth fiber (about 20 microns). Some studies have shown that the accumulated abrasive particles are also small, so it is conceivable that the removal rate of this mechanism is not high.

### *2.1.3.3 Micromachining by abrasive particles embedded in cloth fibers*

Some studies have shown that abrasive particles can also be embedded in the polishing heads or polished cloth fibers. For a fiber, only particles smaller than the diameter of the fiber can be embedded in the middle of the fiber. The particles embedded in the fiber are constantly in contact with the surface of the workpiece. Each hair is like a miniature machining system, and this micro system is softer than the abrasion process. Each individual tiny system either machines a chip or plows a groove during the polishing process. The result of the polishing depends on the contact point between the abrasive particles and the surface of the workpiece. Since arm movement by the fiber-driven abrasive particles is very light at the point of contact, the groove is

very shallow. This situation is relatively easy to polish a mirror surface. However, some qualitative analyses have shown that this mechanism does not usually occur, so the material removal rate through this mechanism is relatively small (Figure 2.23).

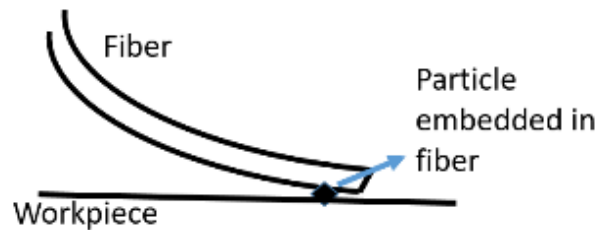


Figure 2.23 Micromachining by abrasive particles embedded in cloth fibers

#### *2.1.3.4 Micromachining by abrasives contained in a carrier paste*

A more common situation is that the fibers on the polishing pad are gradually coated with a layer of carrier paste film or a pile of particles during the polishing process (Figure 2.24). An elastic soft machining system is therefore generated. Even though not every micro system plays a cutting role during the polishing process, this mechanism is more common than the processing mechanism described above. Previous studies have shown that the distribution of such abrasive particles and the density are largely dependent on the processing parameters at the time of polishing.

This mechanism is generally considered to have a greater removal rate than the mechanisms previously discussed. Especially when the hardness of the fiber is smaller than the workpiece, and the size of the abrasive is at the sub micrometer level, the abrasive particles are easily wedged into the polishing pad, and then the fiber on the polishing pad directly contacts the workpiece with the abrasive particles. The number

of abrasive particles which participate in the material removal process depends on the contact range of the pad asperities and the workpiece (Evans et al 2003). This theory has been validated theoretically (Ahmedi and Xia 2001) and experimentally (Yu et al. 1994). The contact range is positively correlated with the pressure on the polishing pad and is inversely proportional to Young's modulus of the polishing head.

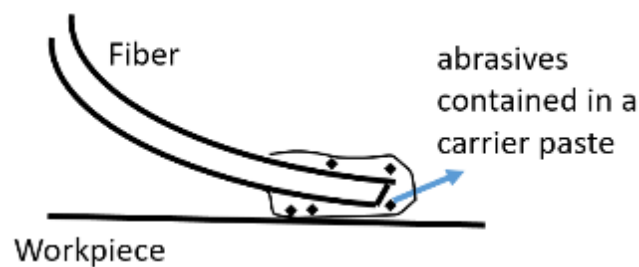


Figure 2.24 Micromachining by abrasives contained in a carrier paste

### 2.1.3.5 Delamination mechanisms

Some debris generated during the polishing process mixes with the abrasive particles and removes the material together. These types of debris are not very long, and there are some small, plate shape particles. Studies have shown that this mechanism is becoming more common when the size of the abrasive particles decrease. Some researchers believe that when the abrasive particles are small, to a certain extent, such as less than 0.5 microns, this mechanism is the main mechanism during the polishing process, called platelet delamination. The texture of the polished surface produced by this mechanism is different from micromachining. When the polished surface is mostly long grooved, the mechanism of the process is micromachining, and when the abrasive

particles become very small, the polished surface shows a lot of mottled surfaces, so it can be said that platelet delamination is the main mechanism in the process.

This new material removal process is one of the delaminations, but it is difficult to say which specific delamination occurs during polishing. In general, there are two cases of delamination, one is the sliding contact between metal and metal at low speed. Delamination occurs mainly due to nucleation and growth of subsurface cracks (Suh et al, 1977). Another reason for the formation of delamination is the high-speed friction between the abrasive particles and the metal surface. The principle of this mechanism is that when the abrasive particles pass through the surface of the workpiece, a local shear fracture is created (Doyle and Turley, 1978). However, there are still little mature evidence to explain which delamination is the mechanism at the time of fine polishing. At the same time, there is no satisfactory explanation why delamination occurs when the abrasive particles are less than a certain size.

### *2.1.3.6 Chemical-mechanical mechanisms*

Some indirect evidence suggests that in the polishing process, there is a case where the removal of the material is due to the simultaneous action of the chemical solution and the mechanical removal process. During this polishing process, a chemical that reacts slightly with the sample material is added to the solution to increase the material removal rate during polishing. In this process, it is difficult to observe whether the abrasive particles are removing the material or the polishing liquid itself is removing the material. The use of colloidal silica in the polishing process is a common example.

Silica particles are almost purely round. When this polishing fluid is used to polish harder materials, it is difficult to explain how pure mechanical action can result in material removal rates. The similar example is in using magnesium oxide as the polishing fluid. These polishing solutions can be used to polish surfaces with almost no scratches and no deformation, which is difficult to conduct with pure mechanical polishing. As a result, it means that etching may occur in these processes.

Silica sol was originally used to polish single crystals of silicon in the semiconductor industry. Many studies have suggested that the silica of the sol reacts with the silicon to form a softer surface. Then in mechanical polishing, the top of the asperities is first removed with little mechanical damage on the underlying silicon. A new layer of soft layer is then formed and removed by a mechanical polishing process again. During this iterative process, the asperities gradually decrease and the surface of the workpiece gradually become smooth.

For silica sol, this reaction with the surface of the material appears to be less likely to happen on other metals. In order to create a corrodible layer with a metal surface, the polishing solution can be replaced with a solution containing oxidizers as a primary chemically active ingredient such as hydrogen peroxide. In this process, it is also possible to assume that the abrasive particles wear away the asperities layer by layer to smooth the surface. This method is not suitable for use on noble metals such as gold and platinum, because corrodible layers do not form on the surface of these noble metals.

In chemical mechanical polishing, the shape of the polished particles is also important, and angular particles may be more likely to produce higher removal rates than spherical particles. At the same time, the fibers may also play the role of removing the asperities on the corrosion layer. In general, due to the complexity of chemical mechanical polishing, the corrosion and removal processes are still not well understood. Such as in the etching process, the state of the abrasive particles as they pass through the reaction zone is unknown.

#### **2.1.4 Modelling and simulation of current polishing and lapping method**

Modelling and simulation including Finite Element Method (FEM) and Molecular Dynamics (MD) are important methods to describe and improve the ultra-precision polishing and lapping processes. The most well-known semi-empirical model was built by Preston (1927). Polishing and lapping processes usually use Preston's equation as shown in Eq. (2.4) to predict the material removal rate,

$$W = \int Kpvdt \quad (2.4)$$

in which  $K$  equals Preston's coefficient [ $m^3s^2/kg$ ],  $p$  is the pressure [ $Pa$ ],  $v$  is the velocity of the lap relative to the workpiece [ $m/s$ ] and  $t$  is time. Preston's equation suitable for all the material and parameters (John et al. 1997). Brown (1982) built a model to verify the linear relationship with the applied pressure and velocity using Preston's equation. Xie et al. (2006) built a model to describe the linear relationship between material removal depth and dwell time based on the Preston's equation. Li et al. (2014) built a model by normalizing the Preston coefficients to



describe the material removal in vibration-assisted dry polishing. In addition, a number of researchers' models have also been built based on the Preston's equation (Kordonski and Golini, 1999; Shorey, 2000; Miao et al., 2009; Liu et al., 2011; Zeng, 2014).

The finite element method (FEM) and molecular dynamics (MD) are also common methods used in modelling and simulation. Srinivasa-Murthy et al. (1997) used a finite element model to simulate the Von Mises stress in chemical-mechanical polishing. as shown in Figure 2.25, Klocke et al. (2008) used FEM to model the contact behavior between the surface and tool,. Enomoto et al. (2011) studied the polishing pad by FEM. Si et al. (2010) used MD to simulate the material removal mechanism at the monoatomic layer in chemical-mechanical polishing as in Figure 2.26. Han et al. (2009) also used MD to simulate the material removal mechanism of a silicon wafer in chemical-mechanical polishing.

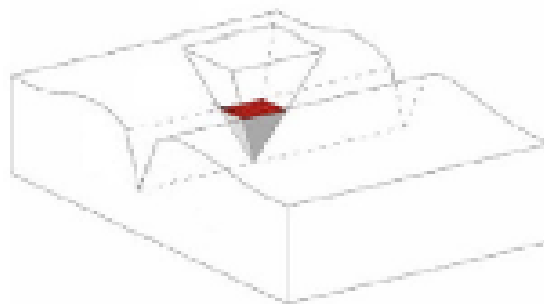


Figure.2.25 FEM model of the motion of a diamond grain in polishing process

(Klocke et al. 2008)

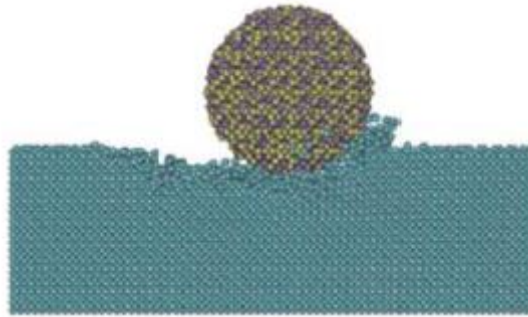


Figure.2.26 The material removal mechanism at the monoatomic layer (Si et al. 2010)

There are also some other methods developed by researchers to analyse the lapping/polishing process. Eitobgy et al. (2005) used Finnie's erosion model to describe the penetration depth and volume of material removed in water jet machining. Pitschke et al. (2009) used neural networks to describe the optical polishing process. The models aforementioned are good for describe the material removal in a small area. However, since the low-pressure lapping process in this study involves less material removal, the mechanism needs to be further investigated.

## **2.2 Surface measurement and characterization methods**

### **2.2.1 Surface characterization parameters**

Measuring capability decides the accuracy a machined surface that can be achieved. This is particularly true for ultra-precision machining. The form accuracy and surface roughness of the surface and are usually at micrometer to sub-micrometer scale and nanometer ranges respectively. These form error and surface roughness are

impossible to inspect by a human eye, and can only be measured by instruments. As a result, the development of ultra-precision machining depends on the progress of the measurement equipment. In this section, some surface characterization parameters are described first. Secondly, some existing techniques, which are used to measure the form and roughness of the ultra-precision machining components surface, are introduced. Thirdly, the method for measuring reflectance is presented.

During 1940s, engineers generally accepted the use of roughness, waviness and form errors to describe a surface. As shown in in Figure 2.27, the roughness is considered as the irregularities on the surface after the manufacturing process. Waviness represents the machine tool behavior and form arise from the designed surface. Usually, the three components, roughness, waviness and form, are divided into wavelength bands: the smallest wavelength represents roughness, intermediate wavelength represents waviness and large wavelength represents form errors. Usually filtering techniques were used to separate these three components. Raja, et al. (2002) claimed that only filtering techniques can separate meaningful wavelength bands from different surface texture measuring instruments. In these three bands, waviness is the most difficult band to be separated from the profile. In the waviness filtering process for waviness, it is necessary to determine whether the waviness is a periodic band that can be detected on the entire surface. (Whitehouse, 2004).

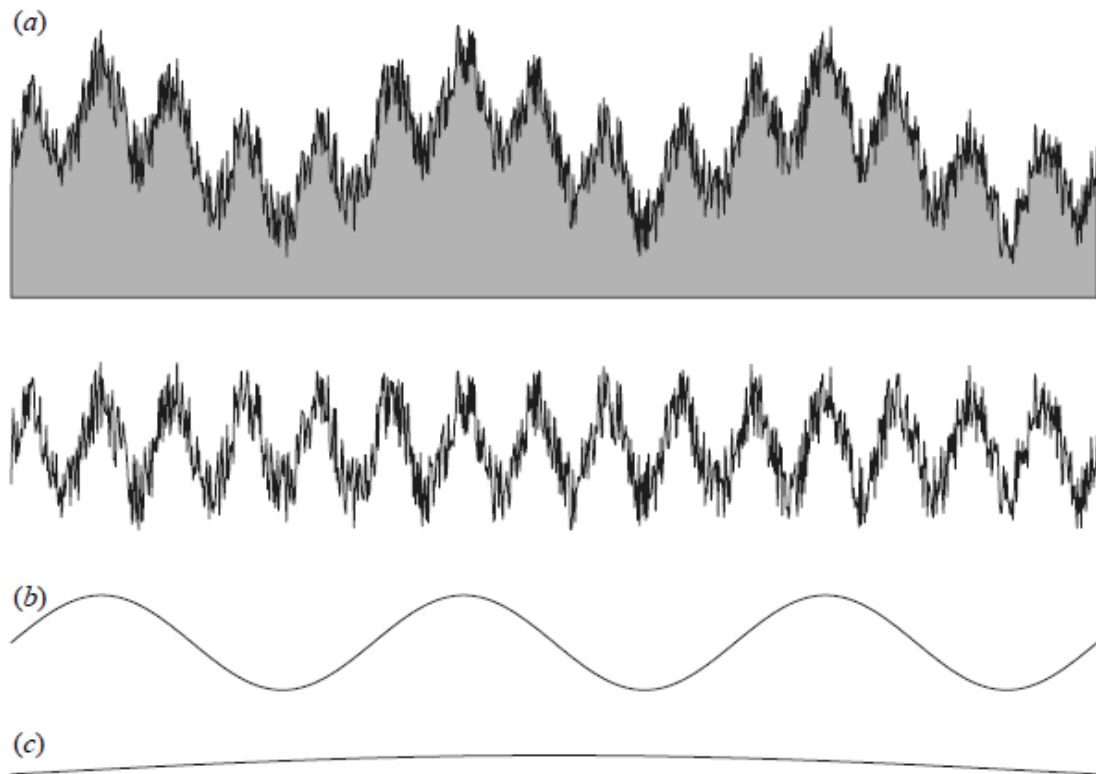


Figure 2.27 Geometric components of a surface profile: (a) roughness, (b) waviness, and (c) form (Jiang et al. 2007)

In 2002, TC-213 was created by the ISO Technical Committee to develop the Geometrical Product Specification (GPS) and Verification standards. After that, a paradigm shift occurred in surface metrology which meant that the surface measurement method changed from profile to areal (Jiang et al. 2007). All areal surface texture standards were covered in ISO 25178. The ISO 25178 standard contains two parts (Blateyron, 2013):

- a) The areal surface texture standards defined for specification and verification.
- b) Revises the existing profile standards to new areal standards.

Table 2.2 Height parameters for areal surface from ISO 25178-2:2012

Parameters	Notations	Definitions	Remark
$S_q$	Root mean square height of the scale-limited surface	$s_q = \sqrt{\frac{1}{NM} \sum_{x=0}^{N-1} \sum_{y=0}^{M-1} z_{x,y}^2}$	EUR 15178 EN report/ISO 25178-2:2012
$S_z$	Maximum height of the scale-limited surface	Sum of the maximum peak height value and the maximum pit height value	EUR 15178 EN report/ISO 25178-2:2012
$S_a$	Arithmetic mean height of the scale limited surface	$s_a = \frac{1}{NM} \sum_{x=0}^{N-1} \sum_{y=0}^{M-1}  z_{x,y} $	EUR 15178 EN report/ISO 25178-2:2012

The main document defining areal parameters is in ISO 25178-2, published in 2012.

The areal parameters are classified into five groups: height parameters, spatial parameters, hybrid parameters, functions parameters and miscellaneous parameters.

Height parameters (Table 2.2) only describe the distribution of height along the z axis, and in regard to a mean plane obtained through the leveling of the mean square plane of the measured surface. The height parameters, root mean square height of the surface, can be expressed as:

$$s_q = \sqrt{\frac{1}{A} \iint_A z^2(x, y) dx dy} \quad (2.5)$$

It is interesting to note that the integral in Eq. (2.5) is usually replaced by the trapezoidal rule (i.e. Eq. 2.6) when evaluating digital data in metrology instruments.

$$s_q = \sqrt{\frac{1}{NM} \sum_{x=0}^{N-1} \sum_{y=0}^{M-1} z_{x,y}^2} \quad (2.6)$$

Other groups of parameters such as the spatial parameters are not related to this research and are not listed here.

### 2.2.2 Power spectrum analysis method in characterizing surface texture

Power spectrum analysis method is widely used for obtaining more information on the characterizations of the fluctuations in the strength and periodicity of any signal no matter this is a force or undulations of a surface. The power spectrum method is an analyzing method which is used to assess the data through an autocorrelation function or Fourier transform of the data (Whitehouse, 2010). The autocorrelation function can be evaluated by using Fast Fourier Transform (FFT) to get the Power Spectrum Density (PSD) first, and then obtaining the autocorrelation. The relationship between autocorrelation function and PSD can be expressed as follows:

$$A(\tau) = \frac{1}{L-\tau} \int_0^{L-\tau} f(x)f(x+\tau)dx \quad (2.7)$$

where the measured surface  $L$  is finite. The limitation of measuring the autocorrelation function is that truncation may cause some problems in the frequency domain. Another way is to directly evaluate the data by measuring the power spectrum. The periodogram is obtained by transforming the real data, and the  $N$  transform points correspond to  $N$  real data points (Cheung, 2001). A convolution operation is usually used by applying a lag window in order to get a smooth main lobe. The PSD at a particular frequency can be expressed by

$$P(\omega_0) = 0.25(F(\omega_{-1}))^2 + 0.5(F(\omega_0))^2 + 0.25(F(\omega_{+1}))^2 \quad (2.8)$$

Where  $\omega_{-1}$ ,  $\omega_0$ , and  $\omega_1$  are adjacent frequencies. The power spectrum method is a useful method which can be used to extract several periodical components, like tool geometry and material properties, from the surface roughness profile in SPDT (Sata

et al. 1991). Jiang et al. (2007) also claimed that compared to the traditional machined surface, spectrum analysis is more suitable for obtaining a fine surface texture.

In SPDT, the spectrum analysis method can extract periodical components from the surface roughness profile. Cheung and Lee (2001) studied the spectrum of tool geometry components, feed components and relative tool-work vibration components from a surface roughness profile. Yuan et al. (2016) use the spectrum analyzing method to evaluate the vibration between a diamond tool and the workpiece in surface generation. However, few researchers have used the spectrum method to analyze the surface in the ultra-precision finishing process. There is a common belief that surface roughness is a surface with arbitrary asperities, which implies the surface do not have much patterns in a spectrum. Zheng et al. (2010) compared the profiles of two polished surfaces by PSD. Li et al. (2011) used PSD to evaluate the roughness of perpendicular veins before and after finishing. However, they did not analyze the spectrums in detail. In the present study, the power spectrum analysis method is used to evaluate the surface roughness of the lapped surface, and the spectrum will be sub-divided into several parts in order to further study the surface generation mechanism of the lapping process.

### **2.2.3 Methods for measuring reflectance**

Reflectance is a physical property which is used to describe the relationship between the incident light and the reflected light. Different materials have different reflectance

properties. These properties can be generally categorized as: specular and diffuse. Specular reflection (Figure.2.28 (a)) can be considered as mirror-like reflection which reflects the light to one angle. It usually occurs on glossy surfaces and is dominant for metals. Diffuse reflection (Figure. 2.28) on the contrary, reflects the incident light to many angles instead of a single angle as in the case of specular reflection. The mechanism of diffuse reflection can be explained by multiple scattering from a rough surface or subsurface scattering. As shown in Figure.2.28 (b), when the incident light propagates to the surface, part of the light is scattered on the surface and another part of the light directly goes through the surface and is scattered from the subsurface. As a result, the scattered light reflects back in random directions

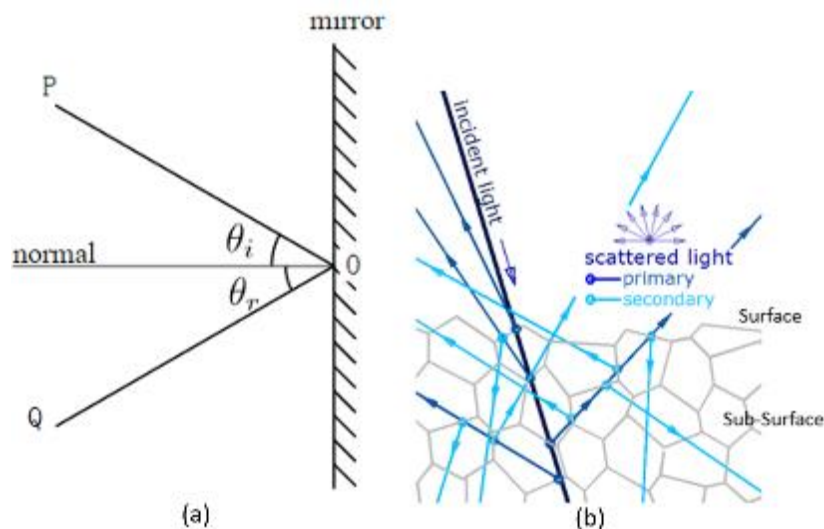


Figure 2.28 Schematic of specular reflection and diffuse reflection (retrieved from

[https://en.wikipedia.org/wiki/Diffuse\\_reflection](https://en.wikipedia.org/wiki/Diffuse_reflection))

The principle of specular reflection is that after incident light is applied to the specular



surface, reflected light is formed on the same surface, and the angle between the incident light and the surface normal is the same as the angle between the reflected light and the surface normal. This behavior was first discovered through the scientific measurements by Hero of Alexandria (AD c. 10-70). However, the mechanism of diffuse reflection is more complex and is still being investigated by the researchers even up to now. In diffuse reflection, when the incident light arrives at the surface of the material, most of the light rays are reflected based on the law of reflection. Due to the matte surface, the actual surface at the micrometer scale is a series of small surfaces with different directions causing the light to be scattered. On the other hand, some of the light goes through the surface and arrives at the sub-surface (Hanrahan, 1993). In the sub-surface, reflection occurs in the interface of the atoms in the material and finally is reflected back again. During the whole diffuse reflection process, some light rays are absorbed by particular materials that causes different reflectivity.

In the diffuse reflection process, metals can provide a high reflectance effect as compared to other materials. However, metals still cannot 100% reflect incident light. Gennaro (2004) reported that when a silver film becomes extremely thin, the silver starts to become transmissive and only reflects 10% of the incident light. This observation shows the reaction between the incident light and the sub-surface of metals. In this thesis, the aluminium alloy samples used in the reflectance test were thick enough and the diffuse reflection is not considered in the experiments.

The most common methods for the absolute measurement of specular reflectance are

the V-W methods developed by Strong in 1938. As shown in Figure 2.29, the reflectance of the auxiliary mirror is measured in the lower position (V) first, and then rotated 180 degree to the upper position (W). After that the sample is mounted in the center and the light is reflected in the same way as in the first measurement, except that the light is reflected twice on the sample. As a result, the reflectance of the sample can be determined as:

$$R_s = \sqrt{R_w / R_v} \quad (2.9)$$

where  $R_s$  is the reflectance of the sample,  $R_w$  is the reflectance measured the W position,  $R_v$  is the reflectance measured in the V position. The V-N method is also a common method for measuring absolute specular reflectance. As shown in Figure 2.30, it measures the reflectance of the reference surface and the reflectance of the sample by moving one mirror and rotating another mirror. Researchers also developed other methods to measure the absolute reflectance, like the goniometer method and the integrating sphere method.

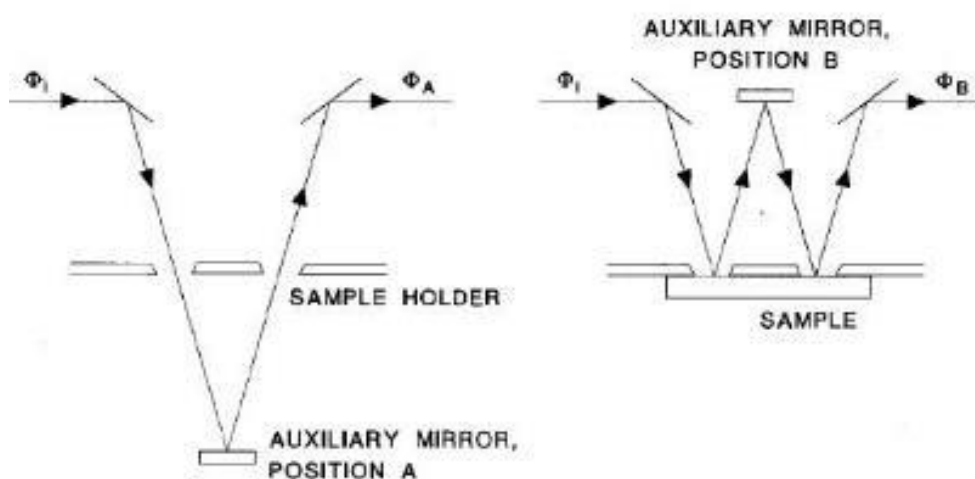


Figure 2.29 Strong V-W type reflectometer (James 2001)

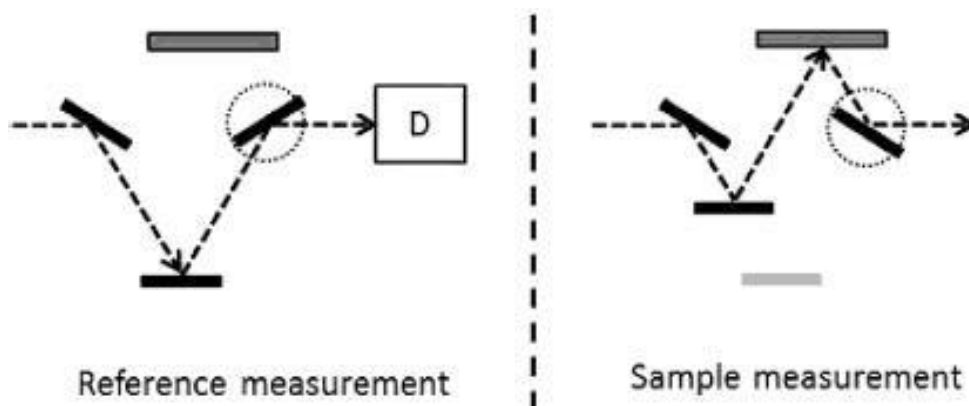


Figure 2.30 V-N type absolute reflectometer (Germer et al. 2014)

Besides the absolute measurement, there is another easier method that just compares the intensity of the incident light and the reflected light (Lei et al. 2010). In this method, the relative reflectance can be measured. This method is usually used in qualitative analysis rather than quantitative analysis. Since the purpose of this research is to study the changes of the reflectance on the same material with different machining parameters, the method for measuring relative reflectance is used.

### 2.3 Summary

The level of development of ultra-precision machining technology is an important symbol of the industrial strength of a nation. Aerospace, military, deep-sea exploration et al. are all inseparable from ultra-precision precision machining technology. In this literature review, ultra-precision turning and ultra-precision post-processing technology are introduced. The principle of the existing ultra-precision lapping and polishing technology and their surface generation mechanisms are also discussed.

These techniques are either costly and have very low material removal rates, or easy to cause scratches on the surface of the soft material such as aluminum alloy during the lapping/polishing process. However, the periodic tool marks on the surface machined by diamond turning may cause scattering and affect the optical performance, and it is necessary to develop a relatively inexpensive and versatile lapping/polishing method to remove tool marks from these surface which made of soft metals such as aluminium alloy (Al6061).

In addition, our recent work has revealed that the reflectance does not always increase monotonically with the surface roughness of the workpiece. The best reflectance occurs when the areal surface has small tool marks. As a result, a novel lapping/polishing method need to be developed to remove the tool marks from Al6061 alloy while reserving the reflectance of the machined surfaces at the same time.

# **CHAPTER 3 STUDY ON REFLECTANCE CHARACTERISTICS OF AL6061 ALLOY SURFACE USED FOR THE LOW-PRESSURE LAPPING TECHNOLOGY**

## **3.1 Introduction**

The aluminium alloy (Al6061) is commonly used in ultra-precision machining because of its good machinability (Hashmi 2014, Ji et al. 2016, Ahmed et al. 2017), and this aluminium alloy is the preferred material for mirrors in spaceborne applications (Zhang et al. 2017). Such aluminium mirrors machined by ultra-precision machining technology have more stringent requirements on both the form accuracy and the surface roughness as compared to that of optical lighting system (Jeon et al. 2016).

Previous studies have investigated the reflectance of metal alloy surfaces for different purposes, such as spaceborne applications or non-contact measurements. In these studies, factors such as the wavelength of the incident beam, the surface roughness and the material properties may affect the surface reflectance. Bennett and Porteus (1961) studied the reflectance of an optically polished surface, at normal incidence, with surface roughness. They determined that the reflectance was wavelength-dependent. Whitley et al. (1987) reported that the specular reflectance increases for both nickel and stainless steel as the surface roughness decreases. Peiponen and

Tsuboi (1990) further investigated the optical reflectance of nickel, aluminium, copper and brass and reported that the reflectance is strongly affected by the surface roughness. Although different factors have been studied by researchers, there has less focused on reflectance when the surface roughness machined by single point diamond turning (SPDT) is in the nanometre scale. Lei et al. (2010) determined that the reflectance decreased when the tool mark spacing was less than 6  $\mu\text{m}$  in single point diamond machining (SPDM), but they have not further studied this phenomenon. As a result, the reflectance characteristic of aluminium alloy (Al6061) mirrors when the surface roughness is in the nanometre range is investigated in this study, in order to optimize the machining parameters when turning the Al6061 mirror.

Single point diamond turning is a very well-known method for producing ultra-precise Al6061 mirrors with surface roughness less than 10 nm and form errors less than 200 nm (Abdullah et al. 2010). The surface roughness value of an ultra-precision face turned surface can be estimated by (Whitehouse 1994):

$$Ra = \frac{0.032f^2}{RV^2} \quad (3.1)$$

where  $Ra$  is the ideal arithmetic surface roughness,  $f$  is the feed rate,  $R$  is the tool radius and  $V$  is the spindle speed. Ultra-precision face turning, even when the feed rate is very low, is in general agreement with Eq. (3.1). As a result, a better surface finish can be expected with decreasing feed rate. However, the same trend does not apply to the reflectance. When the feed rate is very low, decreasing the feed rate produces a decrease in the surface roughness. However, in this study, it was observed

that the decrease in the surface roughness did not lead to a decrease in the reflectance of Al6061 mirrors when they are machined by SPDT.

Considering the function of mirrors, reflectance is always more important than surface roughness. Under such circumstances, surface roughness is simply used by convention to assist in indirectly gauging the reflectivity of an aluminium mirror. In general, good surface roughness of an aluminium mirror was assumed to be a guarantee of good reflectance. However, this assumption might fail when the feed rate is decreased to a certain level, such that continuous chip formation cannot be maintained. It is the prime objective of this research to study this phenomenon experimentally and systematically.

## **3.2. Materials and methods**

### **3.2.1 Materials and machine**

The Al6061-T6511 alloy (Figure 3.1) used in this study was supplied by Kaiser Aluminum Ltd., USA. The turning was performed on an ultra-precision machine 450UPL (Moore Nanotech). The diamond tool used was C0.30mLGC from Contour Fine Tooling Ltd (Figure 3.2). The details of the materials used in the experiment and the turning parameters are shown in Table 3.1.

Chapter 3 Study on Reflectance Characteristics of Al6061 Alloy Surface used for the Low-pressurelapping technology

Table 3.1 Workpiece properties and cutting conditions

Workpiece (Figure 3.1)	Al6061-T6511
Workpiece dimension (mm)	Diameter=23mm, Height=15mm
Number of samples	15
<i>Cutting conditions</i>	
Spindle speed (r/min)	1000
Feed rate (mm/min)	1,2,3,4,5,6,7,8,9,10,11,12,13,14,15
Depth of cut ( $\mu\text{m}$ )	5
Diamond tool radius (mm)	0.318

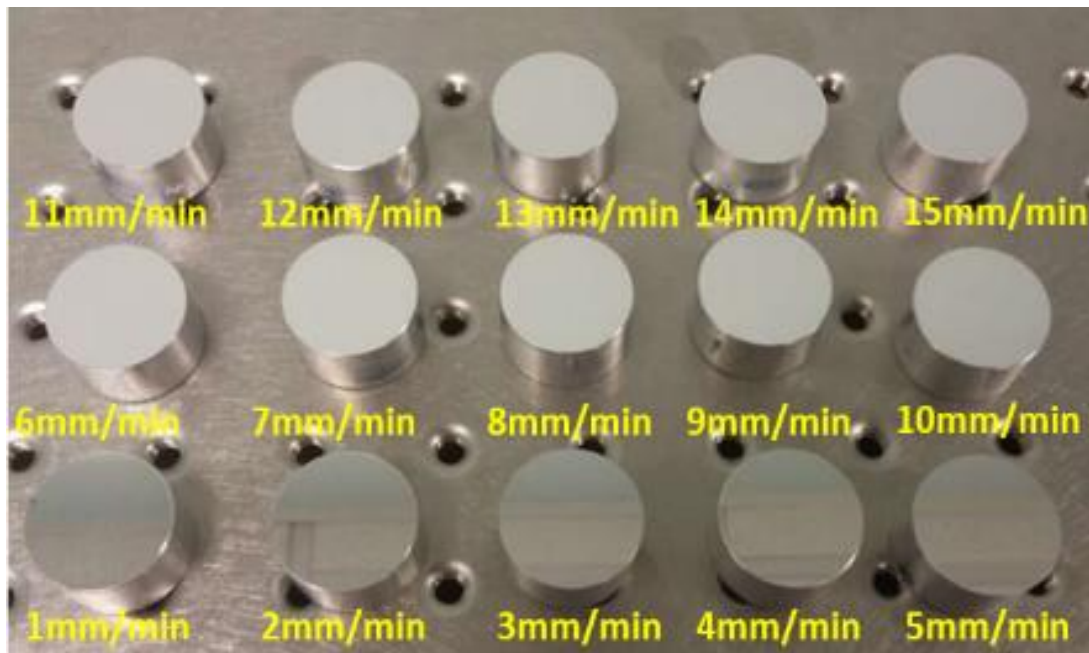


Figure 3.1 15 samples machined by SPDT with different feed rates



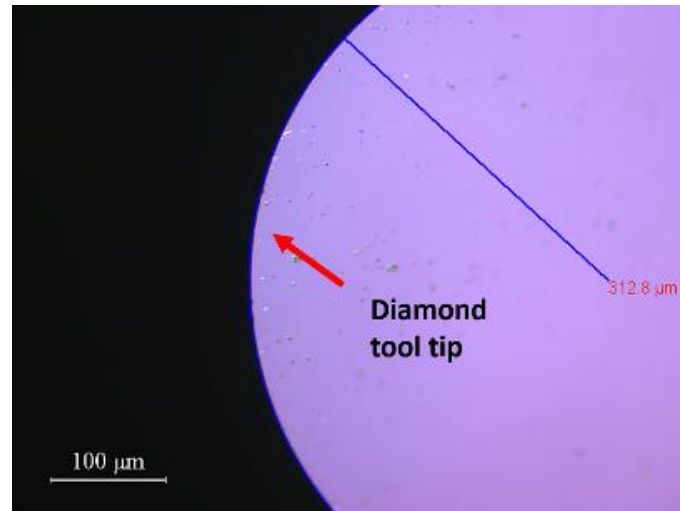


Figure 3.2. Measurement image of the diamond tool tip radius an Olympus BX60 microscope

### 3.2.2 Characterization methods

First, the surface roughness was measured by a white light interferometer (Zygo Nexview) in the range of  $700 \times 700 \mu\text{m}^2$ . Next, the reflectance of the same area on the samples was measured by the reflectance measuring system as shown in Figure 3.3, in which a 100 mW laser was used to measure on the workpiece surface (648 nm diode laser) and collected by a beam profiler (WinCamD UCD15). An integrating sphere was used to realize the photometric integration (Gindele et al. 1985, Huang et al. 2016). The reflectance was determined by a comparison between the relative power  $I_o$  of the sample and a flat mirror  $I_r$  (protected silver mirror PF-10-03-P01 from Thorlabs, Inc). The relative reflectance can be expressed as  $R_r = I_o / I_r$ .

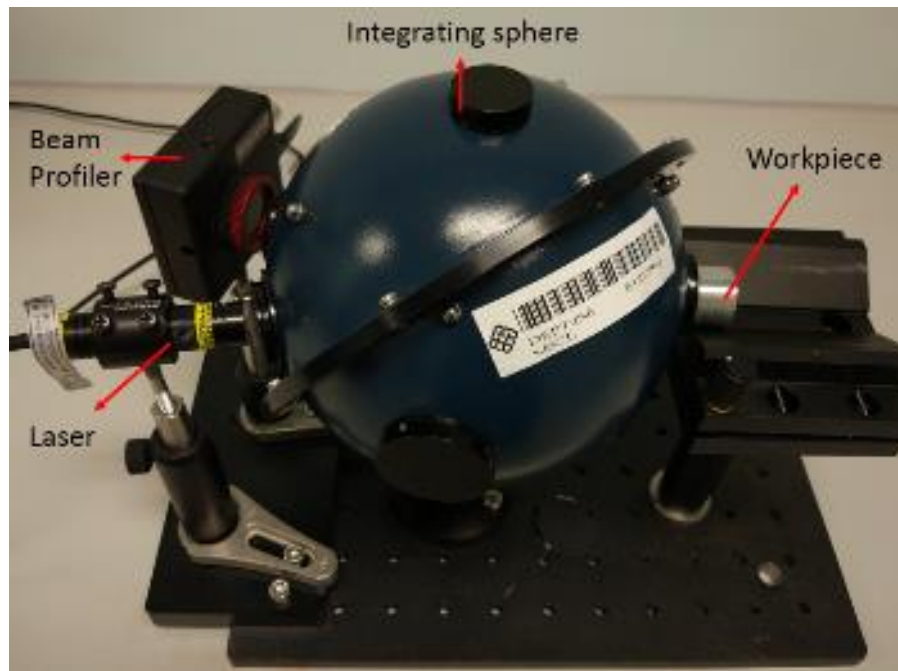


Figure 3.3 Reflectance measuring device

### 3.3. Results and Discussion

From the results, it is interesting to note that when the feed rate was below 7 mm/min, the values of the normalized reflectance became unstable (Figure 3.4) and tended to fluctuate between 84% and 90%. It is possible that the chip formation could not be consistently maintained as continuous because the decrease in the feed rate may have caused a burnishing or rubbing dominated mechanism, instead of the cutting process (Rahman et al. 2017).

The chip formation ceased to be continuous ( see Figure. 3.5) when the feed rate was below 3 mm/min. Due to the chip formation becoming unstable, the decrease of the surface roughness did not result in a decrease in the normalized reflectance.

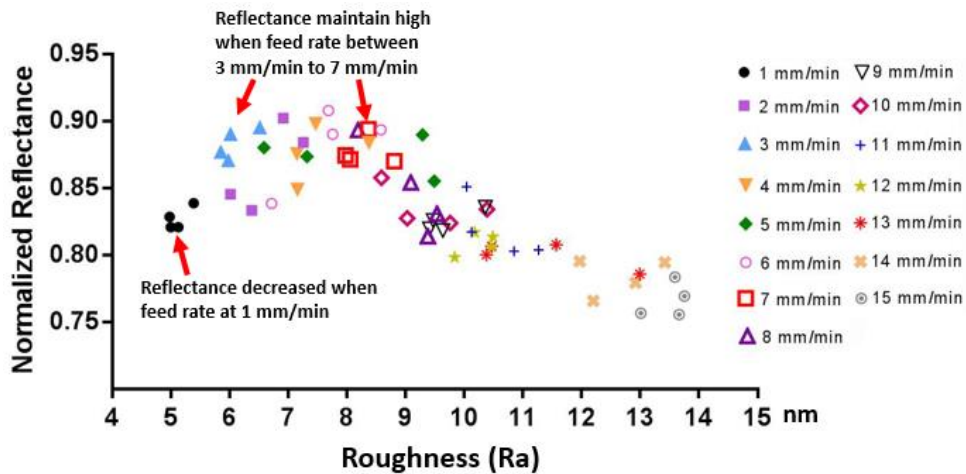


Figure 3.4 Results of normalized reflectance of 15 samples machined by Single Point Diamond Turning

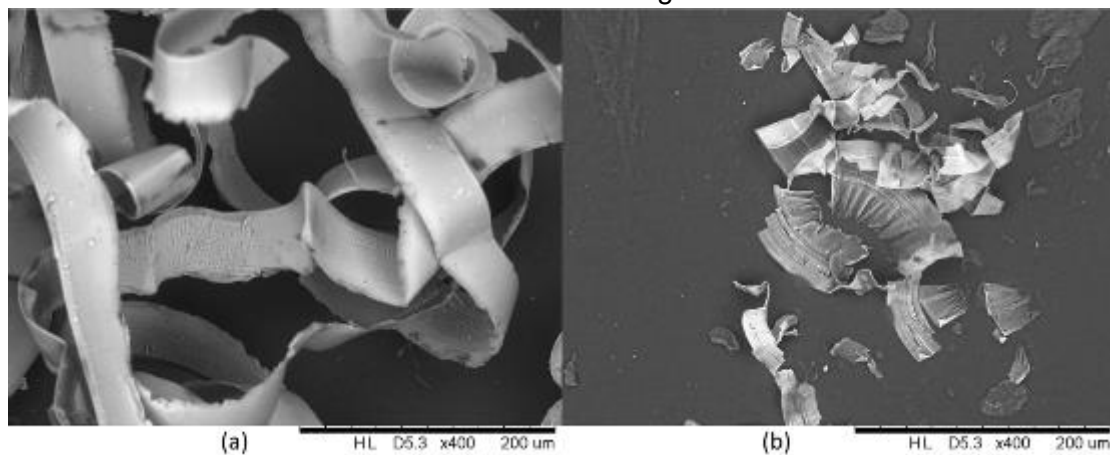


Figure 3.5 Chips measured by the Hitachi electron microscope TM3000, (a) feed rate is 7 mm/min, (b) feed rate is 3 mm/min

When the feed rate was further reduced from 3 mm/min to 1 mm/min, the surface roughness was reduced from 7 nm to 5 nm. However, such an improvement of the surface roughness is not favourable for aluminium mirrors because it is achieved at the cost of a reduction in the normalized reflectance, which decreased from 90% to 82%.

Based on the above results, the optimal feed rate for face turning Al6061 alloy is

between 3 mm/min and 7 mm/min for a depth of cut of 5  $\mu\text{m}$ . Using EDX analysis (Figure 3.6), it was determined that the  $\text{Mg}_2\text{Si}$  particles on the machined surface increased for samples being cut at a lower feed rate, and the  $\text{Mg}_2\text{Si}$  particles tended to align with the cutting direction when the surface was machined at a feed rate of 1 mm/min (see the arrow in Figure 3.6).

For the sample cut at a feed rate of 1 mm/min, the Mg and Si content was 1.07 wt% and 1.04 wt%, respectively, and for the 7 mm/min sample, they were 0.76 wt% and 0.81 wt%, respectively. To exclude the effect of the used material itself, a verification cutting experiment was conducted by separately machining two new samples with a feed rate of 1 mm/min and 7 mm/min, in order to confirm that the amount of  $\text{Mg}_2\text{Si}$  did increase when the feed rate was low. As shown in Figure. 3.7, the results indicate that the surface machined at a feed rate of 1 mm/min has more  $\text{Mg}_2\text{Si}$  (white colour particles on the surface) than the surface machined at a feed rate of 7 mm/min; the reflectances were 0.84 (1 mm/min) and 0.93 (7 mm/min). This result infers that the reflectance of Al6061 alloy does not always monotonically decrease with decreasing surface roughness.

Since the SPDT temperature is approximately 30°C to 70°C when cutting metals with hardness (HRB) less than 90 (Yen 2004, Mandal et al. 2013, Childs et al. 2015), it is unlikely to cause any phase transformation on the surface because the cutting temperature is not high enough. As a result, the reason for the changes in the amount of  $\text{Mg}_2\text{Si}$  particles is likely due to the low feed rate (1 mm/min) causing a burnishing

Chapter 3 Study on Reflectance Characteristics of Al6061 Alloy Surface used for the Low-pressurelapping technology

effect (Rahman et al 2017): the  $Mg_2Si$  particles were firmly pressed to the surface rather than being removed or knocked-out as shown in Figure 3.8, and these remaining  $Mg_2Si$  particles caused the reduction of the reflectance of the Al6061 alloy. However, further work is needed to gain better understanding about the possible mechanisms regarding this observation.

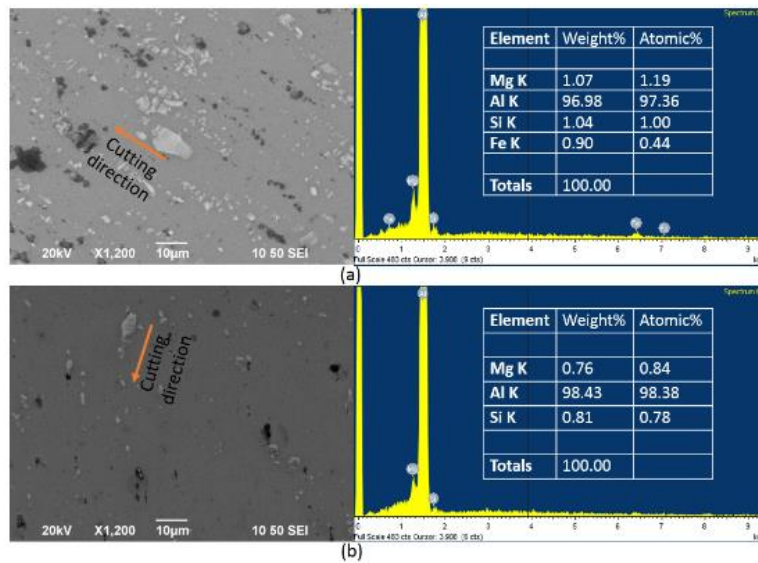


Figure 3.6 SEM images and EDX results of surfaces when feed rate are 1mm/min (a) and 7mm/min (b) separately

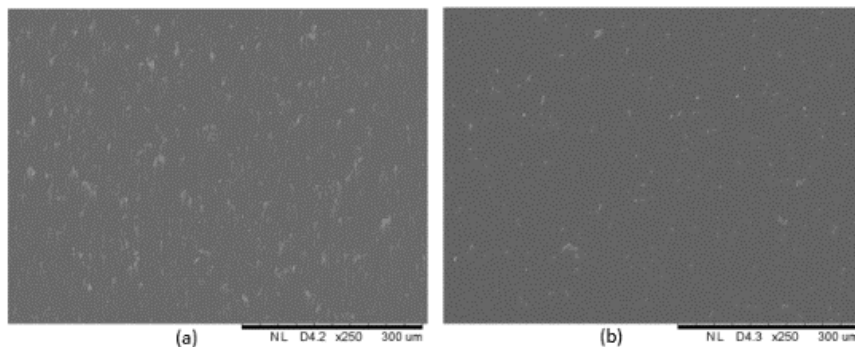


Figure 3.7 Verification experiment: SEM images of surfaces when feed rate are 1mm/min (a) and 7mm/min (b) respectively

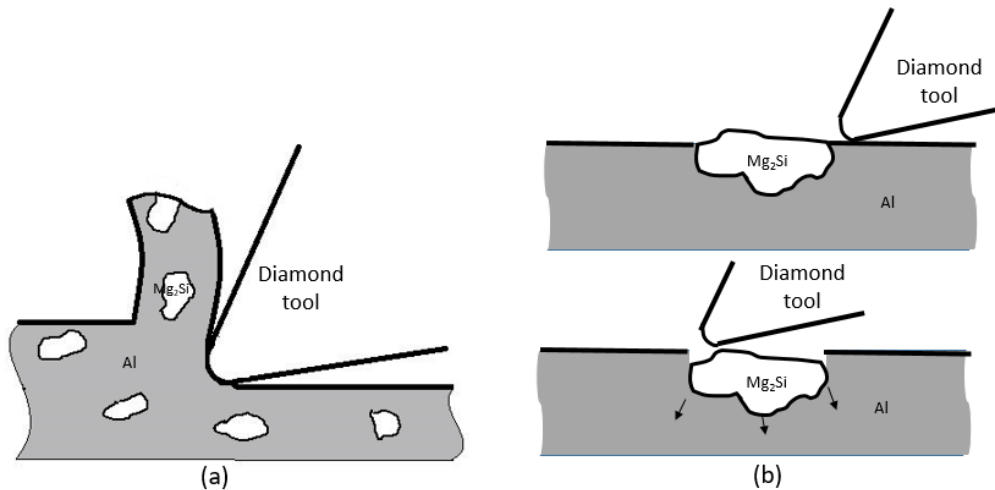


Figure 3.8 (a) Si phase was removed when feed rate is under optimal condition (b) Si phase embedded into surface when feed rate is too small

### 3.4. Summary

An assessment method was developed using an integrating sphere lumens measurement system to assess the reflectivity of a single point diamond turned surface of Al6061 alloy. This assessment method exhibited sufficient precision for assessing the reflectance of a machined surface.

Based on this method, it was determined that the reflectance of Al6061 alloy does not always monotonically increase with a decrease in the surface roughness. An optimal feed rate range exists (3 mm/min - 7 mm/min in this study), and when the feed rate is larger than 7 mm/min, the Al6061 surface roughness is decreased as the feed rate decreases; therefore, this smoother surface causes the reflectance to increase. When the feed rate is decreased from 7 mm/min to 3 mm/min, the surface roughness

### Chapter 3 Study on Reflectance Characteristics of Al6061 Alloy Surface used for the Low-pressurelapping technology

---

continues to decrease, but the reflectance stabilizes, remaining at the same level.

Below 3 mm/min, the chip formation is unstable, and the reflectance of the machined surface is unfavorably reduced as the feed rate decreases as shown in Figure 3.9.

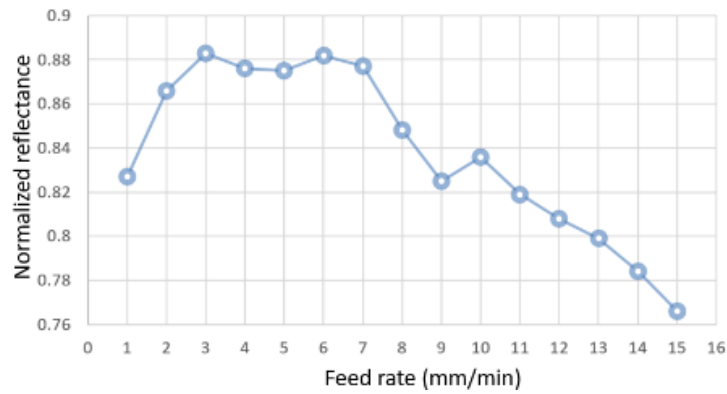


Figure 3.9 The reflectance decreased when the feed rate is lower than 3mm/min (tool

radius: 0.318 mm, spindle speed: 1000 rpm/min, DoC: 5 $\mu$ m)

## **CHAPTER 4 DEVELOPMENT OF A LOW-PRESSURE LAPPING TECHNOLOGY AND THE OPTIMIZATION OF THE LAPPING PARAMETERS**

Single point diamond turning of soft metals can provide shiny surfaces with optimal feed rate, however tool marks would be left on the surface. If the feed rate is too slow, the roughness of the surface can be improved but the reflectiveness would be decreased on Al6061 alloy surface. As a result, it is necessary to develop a lapping technology to reduce the roughness by removing the tool marks, while the reflectiveness can be kept at the original level simultaneously.

In this chapter, a novel lapping technology is developed which makes use of strands of wool fibers to deliver the abrasive slurry to rub against the moulds. It is proposed for removing the tool marks on the Al6061 alloy mould by lapping. Since the surface finish is mainly controlled in this study, form accuracy might be the focus.

Even though the normal pressure applied by the wool strands onto the mould surface is very low, the coefficient of friction would be increased significantly with the application of the abrasive slurry. The combined effect provides a relatively large shear force to lap the surface with a minimal normal force. As a result, the proposed method can theoretically avoid damaging the workpiece surfaces while effectively removing the irregularities that appeared on the surfaces.



In order to evaluate the proposed lapping method, the tool marks were lapped under different lapping conditions (e.g. speed, grit size, time and pressure) so as to find out the relationship between these parameters and the surface roughness, with the same profile of the mould. Secondly, the optimal lapping parameters were designed based on the above lapping results to deduce the best lapping solution for processing the tool marks. Thirdly, the lapped surface profile of the mould was tested by an optical profiling system and the features of the surface can be categorized into various spectral distribution groups. Finally, it is verified that based on our proposed methodology by comparing the variation of the spectral distribution groups. Selective removal of surface spectral groups of the features becomes possible.

### **4.1. Introduction**

There are ever increasing forces driving the miniaturization and higher optical performance of electronic products, which in turn demand smaller and smaller form errors together with better surface finish. However, it is never an easy task to cater for both of these demands simultaneously. In these circumstances, form errors are always prioritized because these lead to significant image quality deterioration. This does in no way imply that surface roughness is not important, but means that it needs to be taken care of right after the turning process, usually by a combination of lapping and polishing processes.

Lapping contains the mutual movement of the abrasive particles between the two contact surfaces (DIN 8589-15 1985). It can be roughly divided into two types: one is

grinding, that is, the abrasive grains are in contact with the hard surface to produce material removal, and the other is to generate a smooth surface by material removal. The common purpose of both types is to produce a smooth surface as much as possible to reduce the time for subsequent polishing (Marinescu et al. 2006). Lapping usually removes a small amount of material (Sanchez et al. 2011). Sanchez et al. (2011) described the lapping process as the lapping pad that drives the abrasive particles to move on the surface of the workpiece. Compare to polishing process, the abrasive particles are rolled on the surface of the workpiece rather than sliding under the driving of the lapping pad in lapping process.

Tool marks are usually removed by a polishing process. Cao et al (2014) used Fluid Jet Polishing to remove tool marks. They studied the material removal characteristics by proposing a computational fluid dynamic model. They pointed out that it is difficult to accurately describe the surface generation mechanism due to too many parameters involved in the polishing process. To polish relatively soft but brittle KDP crystals, Chen et al. (2015) adopted the magnetorheological (MRF) polishing method. The polishing is essential to enhance the performance of KDP crystal to be used in high power laser systems. The purpose of MRF was to improve the surface roughness and to remove the tool marks due to SDPT. To achieve this purpose, recrystallization of KDP during the polishing process must be prevented. Guo and Jiang (2015) proposed a corrective finishing method for micro-aspheric moulds made of tungsten carbide that aimed at obtaining form accuracy down to tens-of-nanometers and surface roughness to sub-

nanometers. The corrective polishing was based on a dwell time algorithm derived from a uniform polishing experiment. In order to maintain the stability of the polishing force, he also developed a tilting angle control method. Yin et al (2015) developed an optimal polishing conditions using the Taguchi Method for reducing surface roughness and for removing tool marks.

Even though the polishing process can improve the surface quality by removing tool marks (Shiou et al. 2016), Ho and Tso (Chuang et al. 2006) stated that if the lapping process was used before polishing to remove tool marks, the surface roughness would be improved and the form accuracy would be preserved. Also, they reported that there were three key factors affecting the lapping performance: abrasive particle size, type of lapping head and the uniform distribution of polishing pressure (Lewandowski et al. 2015).

To reduce the surface roughness and to maintain form accuracy, a low-pressure lapping process is much needed. The purpose of this process is to remove the tool marks on the mould without damage to the profile of the mould. Lapping is a finishing process. However, in this work, the process is named as lapping because the nature of the process is to remove tool marks and not to produce debris that is large enough to produce scratch marks. The success of the low-pressure lapping technology will improve the brightness and contrast of the captured images which in an aesthetic sense constitutes a definitive criterion for determining whether the lens is for amateur or for professional use.

## 4.2. Experimental setup

In this study, a low-pressure lapping system, which consists of four parts including: rotation spindle, brush, beaker and tilt platform, which has been developed in the State Key Laboratory of Ultra-precision Machining Technology. It is used to achieve the above purposes as shown in Figure 4.1, the workpiece is placed in the slurry. The abrasive particles in the slurry are driven by the rotating brush and roll on the workpiece surface. When the abrasive particles reach sufficient speed, the particles start to impinge on the asperities on the workpiece surface (Figure 4.2). When the impact force of abrasive particles is large enough to reach the yield strength of the workpiece material, the deformation of the contact area between abrasive particles and asperities on the workpiece surface changes from elastic deformation to plastic deformation and eventually cause the material to be worn off. As stated earlier, the objective of lapping is to remove the tool marks appearing on the mould by lapping without damaging the profile of the mound. In this regard, free abrasive lapping is always preferred and the abrasive grains are applied directly to a lapping plate.

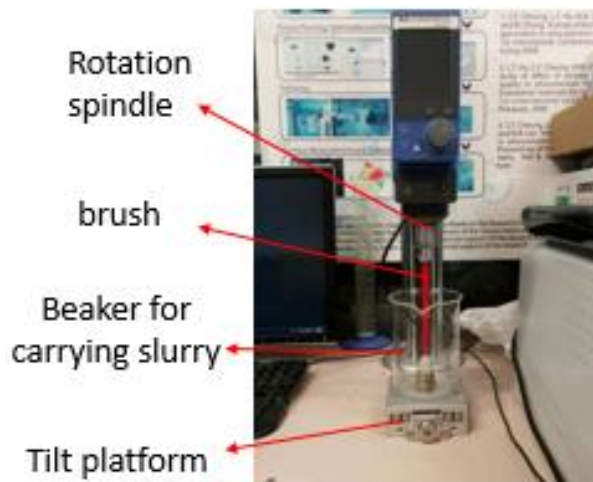


Figure 4.1 Experimental setup

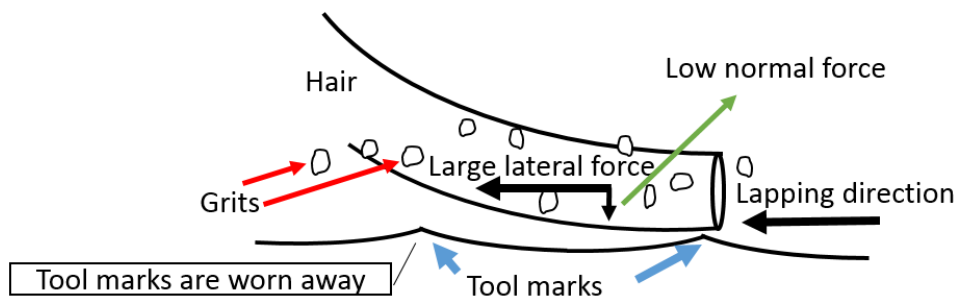


Figure 4.2 Schematic of the low-pressure lapping method

For shape preservation and the maintenance of form accuracy, the lapping pressure must be low. Strands of wool fibers can be used because they can effectively deliver the abrasive slurry onto the workpiece without inserting any significant normal pressure (5 times smaller than traditional pressure). Each strand consists of around 20,000 fibers, which are then rolled and mounted into a hollow cylindrical brush holder (8mm in diameter). Without inserting any normal force onto the workpiece, the  $\text{SiO}_2$  particles

## Chapter 4 Development of A Low-pressure Lapping technology and the Optimization of the Lapping Parameters

---

are expected to roll rather than to slide on the surface of the workpiece. The fibers drive the SiO<sub>2</sub> particles towards the workpiece by skin friction, facilitating the SiO<sub>2</sub> to rotate. As the fibers are very soft, a small vibration may occurred on the rotating brush when the brush is misaligned with the axis of the spindle clamp during installation, it does not notably affect the lapping performance in the experiment.

The brush was mounted on a rotational spindle (IKA EURO STAR60), with a rotational speed ranges from 0 rpm to 2000 rpm. 500ml of slurry was poured into a beaker, and was then placed on a tiltable platform (Figure 4.1). A Tilt platform is used to avoid the zero speed area in the center of the brush. The tillable platform together with slurry containing beaker was placed underneath the rotation spindle. The workpiece material used in this study was Al6061. The samples, used in the lapping experiment, were machined by single point diamond turning (SPDT) (Figure 4.3) and the cutting parameters are listed in Table 4.1. The surface roughness (Ra) was 20.27 nm. The height of the tool marks was 80nm.

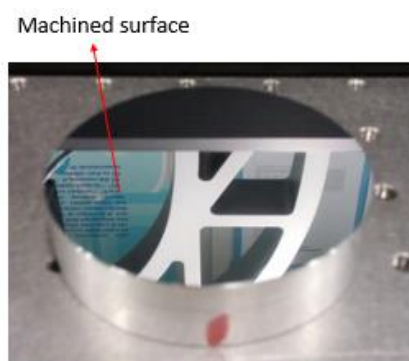


Figure 4.3 Workpiece machined by SPDT

## Chapter 4 Development of A Low-pressure Lapping technology and the Optimization of the Lapping Parameters

Table 4.1 Diamond turning parameters

Sample size	R=70mm H=15mm
Sample material	Al6061
Diamond tool radius	2.5 mm
Depth of cut	5 um
Feed rate	40 mm/min
Spindle speed	1000 rpm

In order to remove the tool marks from the surface, the workpiece was immersed in a bath of abrasive slurry. The Taguchi method was used to investigate the parameters affecting the surface generation in the lapping process (Choi et al. 2015), and is widely used in the ultra-precision manufacturing area (Cheung et al. 2010, Wang et al. 2010). In this Chapter, Taguchi analysis was used to investigate the factors which most affect the lapping process. Furthermore, the optimal lapping conditions that can generate a better surface roughness, with a higher form accuracy, would be identified. A Taguchi array (L9) was chosen for investigating and optimizing the lapping process. The four three-levelled factors are shown in Table 4.2. Table 4.3 shows the L9 orthogonal array used in the experimental design. The arithmetic roughness parameter Ra was used to analyze the results. The workpiece surface was measured by a Wyko NT8000 optical profiling system as Figure 4.4 shown.

Table 4.2 Factors and levels selected for the study

## Chapter 4 Development of A Low-pressure Lapping technology and the Optimization of the Lapping Parameters

<b>Factors</b>	<b>Level 1</b>	<b>Level 2</b>	<b>Level 3</b>
Rotational speed (rpm)	500	1000	1500
Grit size (nm)	15	72	1500
Lapping time (min)	5	10	20
Lapping pressure (bar)	0.0062	0.0124	0.0186

The 3D profile was first measured by Wyko. 2D files were then extracted numerically from the measured 3D profiles and transformed into a power spectra using FFT. The spatial spectra cover the spatial distribution groups as shown in Table 4.4



Figure 4.4 Wyko NT8000 optical profiling system



Chapter 4 Development of A Low-pressure Lapping technology and the Optimization of the Lapping Parameters

Table 4.3 Experimental design with L9 orthogonal array used

Trial	Rotational speed (rpm)	Grit size (nm)	Lapping time (min)	Pressure (bar)
1	500	15	5	0.0062
2	500	72	10	0.0124
3	500	1500	20	0.0186
4	1000	15	10	0.0186
5	1000	72	20	0.0062
6	1000	1500	5	0.0124
7	1500	15	20	0.0124
8	1500	72	5	0.0186
9	1500	1500	10	0.0062

Table 4.4 Spatial distribution groups

Spatial Distribution Group	I	II	III	IV
Spatial Period ( $\mu m$ )	0.5-0.7	0.7-0.9	0.9-1.1	1.1-1.3

### 4.3. Results and Discussion

The results of surface roughness measurement using the Taguchi method are

summarized in Table 4.5. Table 4.6 shows the improvement and effectiveness of surface roughness under different lapping conditions.

$$\Delta R_a = (R_{a-bef} - R_{a-af}) \quad (4.1)$$

$$\eta = (\Delta R_a / R_{a-af}) \times 100 \quad (4.2)$$

where  $\Delta R_a$  is the improvement of the surface roughness,  $R_{a-bef}$  is surface roughness before the lapping process,  $R_{a-af}$  is surface roughness after lapping process, and  $\eta$  is effectiveness.

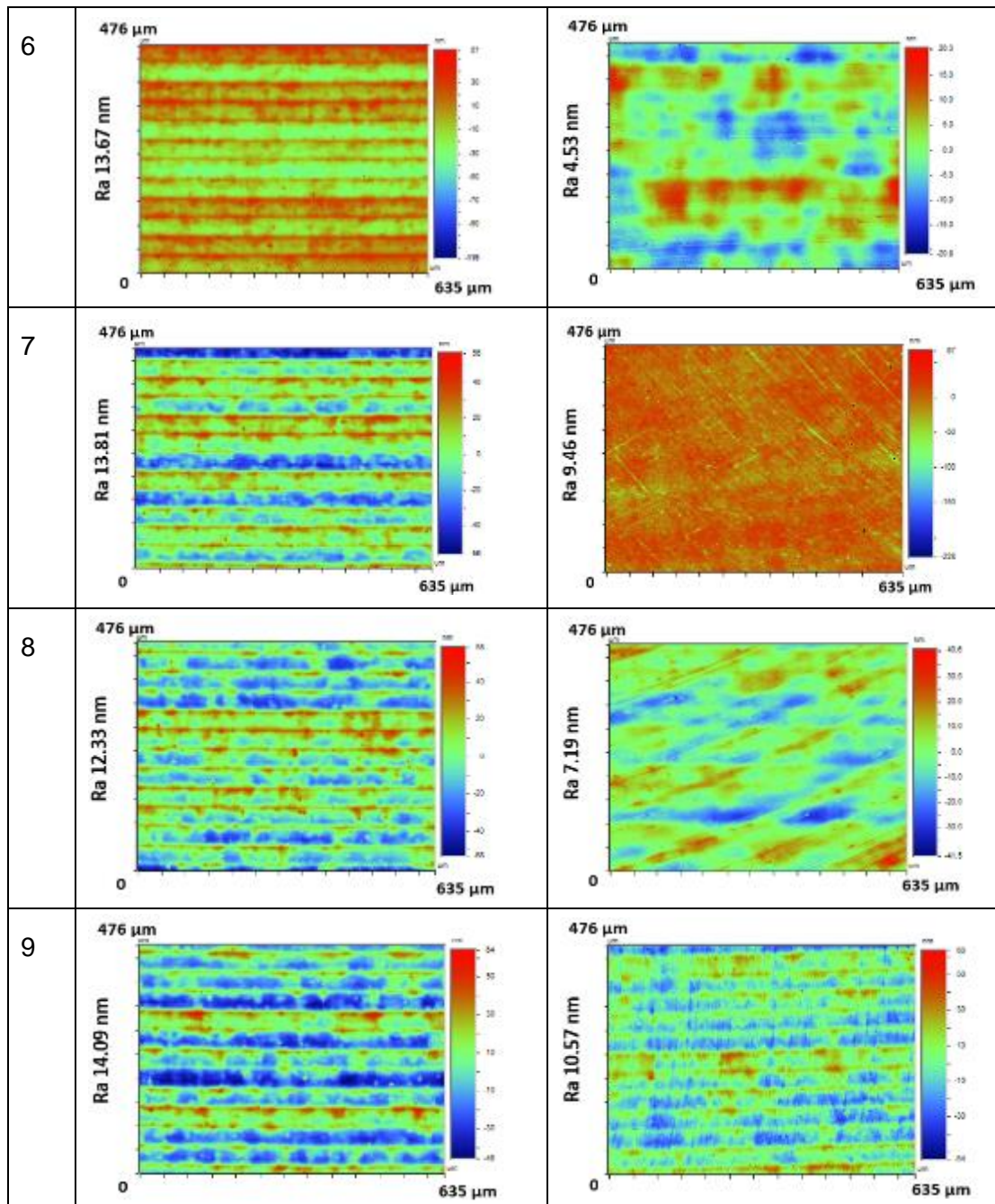
The analytical process estimates the improvement of the surface roughness. In addition, the main effect plot of each parameter is shown in Figure 4.5. It is interesting to note that some combinations of lapping parameters could remove materials from the surface more effectively, and the smallest surface roughness is generated in trial 6. This indicates that different combinations of lapping parameters can significantly affect the surface generation. As mentioned previously, the low-pressure lapping method prioritizes form accuracy over roughness. A lapping trial was conducted under the predicted condition, from the results, it can be seen that the surface roughness decreases from 20.27 nm (Figure 4.6) to 15.59 nm (Figure 4.7). The subsequent lapping under optimal conditions further improves the surface roughness to 11.73 nm as shown in Figure 4.8. The tool marks on the surface were almost completely removed from the surface, and it is difficult to see any scratches on the surface by the Wyko NT8000 optical profiling system.

Table 4.5 Effect of process parameters on tool marks removal

Chapter 4 Development of A Low-pressure Lapping technology and the Optimization of the Lapping Parameters

No	Before lapping	After lapping
1		
2		
3		
4		
5		

Chapter 4 Development of A Low-pressure Lapping technology and the Optimization of the Lapping Parameters



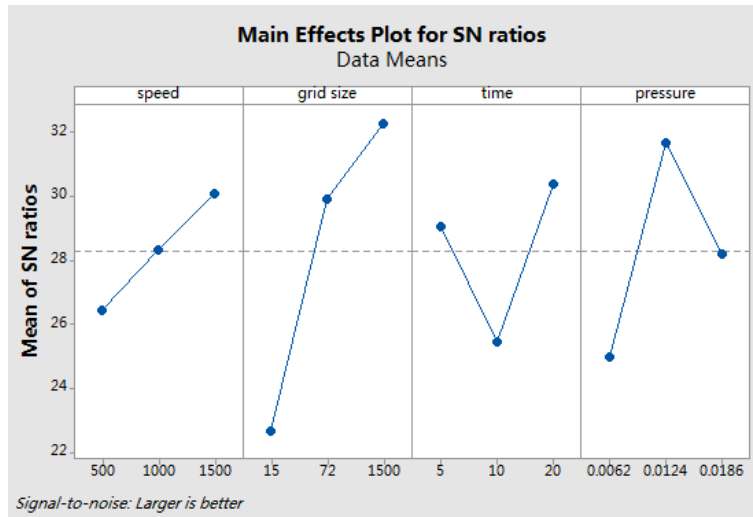


Figure 4.5 Main effects plot of each factor

Table 4.6 Results of surface roughness measurement

No	$R_a$ before lapping ( $R_{a\text{ bef}}$ )(nm)	$R_a$ after lapping ( $R_{a\text{ aft}}$ )(nm)	Improvement (nm)	Effectiveness %
1	12.67	11.63	1.04	8.20
2	12.39	9.06	3.33	26.87
3	12.78	7.41	5.37	42.02
4	12.27	11.07	1.20	9.77
5	12.17	8.83	3.34	27.44
6	13.67	4.53	9.14	66.86
7	13.81	9.46	4.35	31.49
8	12.33	7.19	5.14	41.68
9	14.09	10.57	3.52	24.98

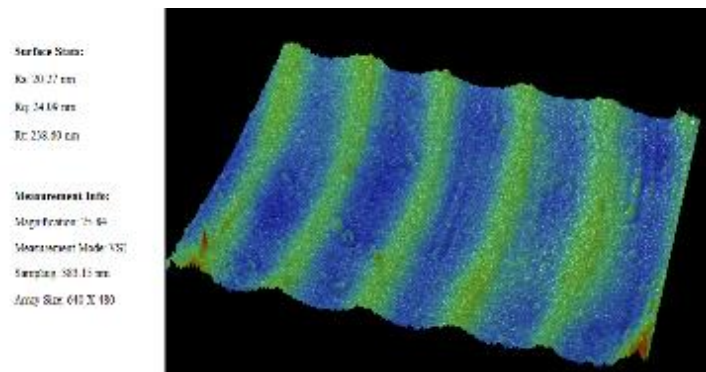


Figure 4.6 Workpiece surface before lapping (Ra:20.27 nm)

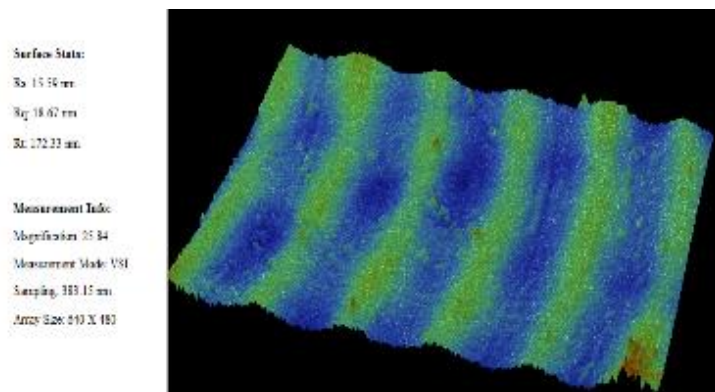


Figure 4.7 Workpiece surface under optimum lapping conditions in first trial (Ra:15.59 nm)

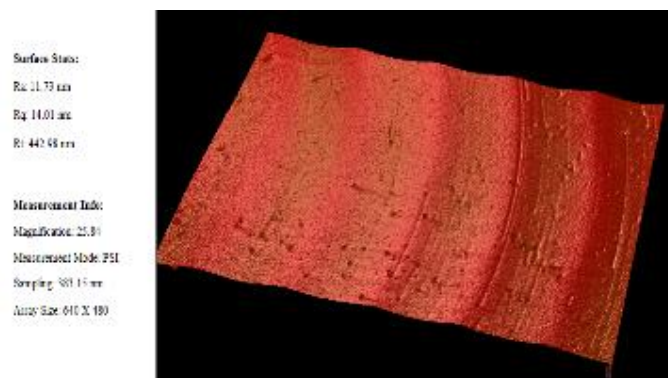


Figure 4.8 Workpiece surface under optimum conditions in second trial (Ra:11.71 nm)

The Spatial Distribution of the surface profile presented in this chapter shows Spatial Amplitude versus Spatial Period, in which Fast Fourier Transforms (FFT) were used to determine spatial amplitudes. The Power Spectral Density (PSD) is used to analyse the surface profile in this chapter. Specific spatial group is used to express the roughness of the surface of the workpiece in the frequency domain. This spatial group is named Equivalent Spatial Surface Roughness (ESSR) in this thesis. ESSR is calculated in a manner to be identical to that of  $R_a$  except that it is specific to a particular spatial group and is only an equivalent term because it cannot fulfill the requirement of any well-received standard measurement of surface roughness. This term DSSR allows for a more intuitive comparison of the surface roughness results detected by the Wyko NT8000 optical profiling system.

As shown in Figure 4.9, the micrograph provides a typical case of non-excessive lapping. The main goal of this low-pressure lapping method is to remove the tool marks from the surface of the workpiece without changing the surface form. In other words, this lapping method requires only lap specific features. In this research, these features are categorized in a preferred spatial group (PSG) while leaving the other spatial groups relatively untouched. For the sample as shown in Figure 4.9, most of the lapping work was done on group IV (23.40%). As long as the lapping time was not excessive, the ESSRs decreased with time for Spatial Groups IV. The SEM monograph also shows that there were no scratches formed when the workpiece was machined

under non-excessive lapping (Figure 4.11).

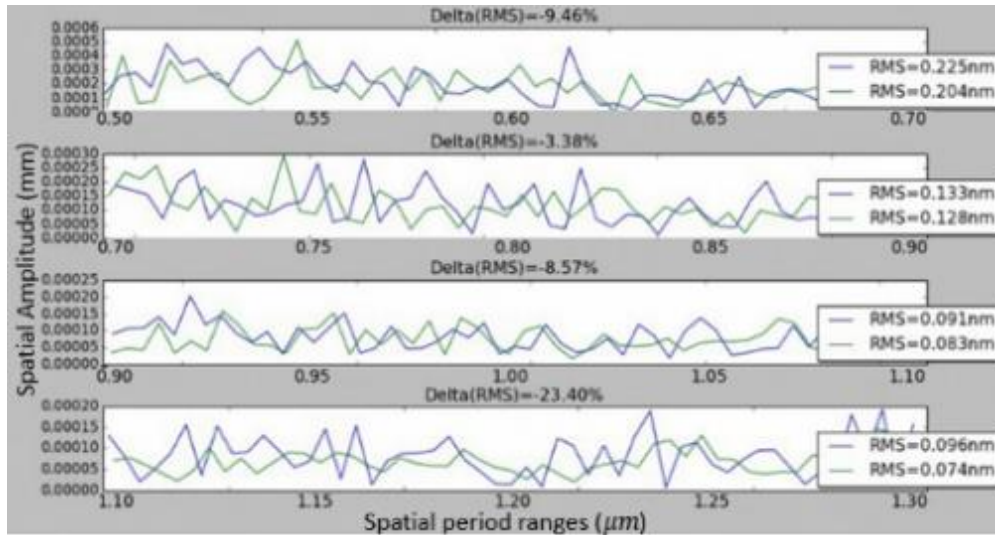


Figure 4.9 Spatial Distribution of surface profile comparison between original surface (Figure 4.6) and lapped surface (Figure 4.7). Most of the lapping work was done on group V(23.40%)

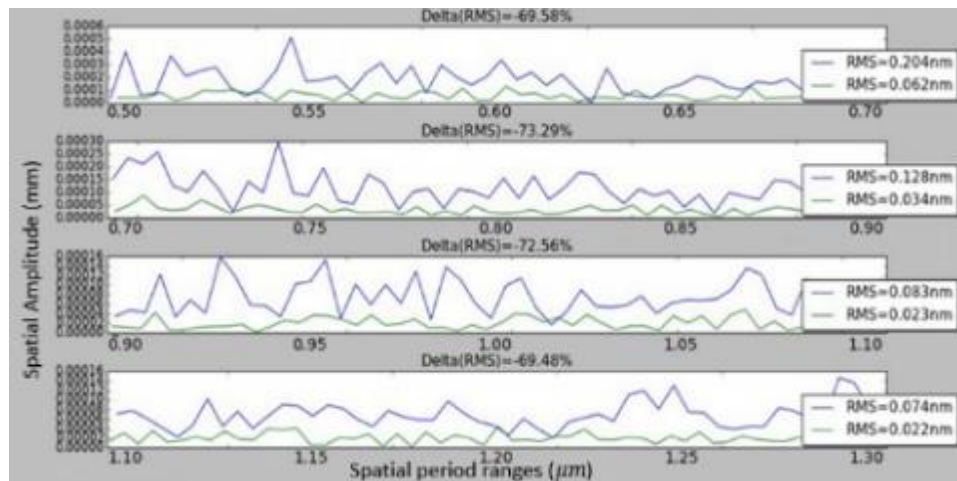


Figure 4.10 Spatial Distribution of surface profile comparison between lapped surface in first trial (Figure 4.7) and lapped surface in second trial (Figure 4.8). Major change in spatial groups shift from long and short period (IV) to middle periods (I II III)



As shown In Figure 4.10, it is found that the PSG was forced to shift from short periods (IV) to long periods (I, II and III) (Table 4.7) as the lapping time increased. The changes of the longer period spatial groups (I, II and III) gave a very good indication of the actual changes that occurred on the form features rather than the surface roughness. As a result, the proposed method can detect the occurrence of excessive lapping.

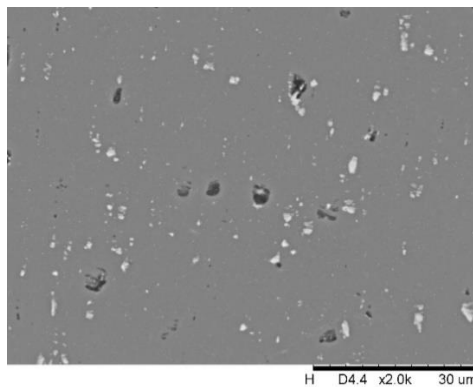


Figure 4.11 SEM: The material surface under 2000X magnification. No scratch occurred on the surface when the workpiece is under non-excessive lapping

Table 4.7 Change rate of Trial 1 is the comparison between the original surface with the lapped surface. Change rate of Trial 2 is the comparison between the lapped surface in trial 1 and the lapped surface in trial 2.

Spatial distribution group	I	II	III	IV
Spatial period ( $\mu m$ )	0.5-0.7	0.7-0.9	0.9-1.1	1.1-1.3
Change rate after Trial 1	9.46%	3.38%	8.57%	23.40%
Change rate after Trial 2	<b>69.58%</b>	<b>73.29%</b>	<b>72.56%</b>	69.48%

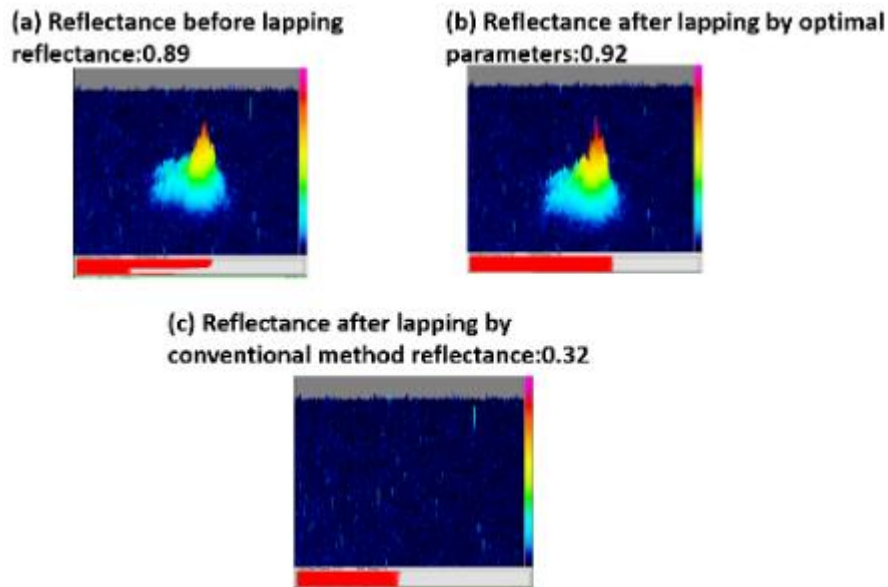


Figure 4.12 Reflectance of Al6061 mirror before lapping (a), after lapping by low-pressure lapping method (b), after lapping by conventional bonnet polishing

#### 4.4. Summary

In this Chapter, a novel lapping method is proposed, in which the Taguchi method was used to investigate the effects of different lapping conditions on aluminium alloy (Al6061). Based on the results, an optimal condition was found that could produce fewer scratch marks, better surface finish and less damages with regard to the form accuracy. The results show that the Taguchi method is an effective method for finding the optimal lapping condition and the predicted values.

Moreover, this approach is more consistent with our prior experimental findings whereby increasing lapping time shifts the PSG to a higher period (lower frequency). The underline reason for this result is possibly due to the fact that the optimal speed (1500 rpm) and time (20 min) are critical in this experiment. As the lapping time

increases, debris may be generated and leads to excessive lapping and damage to the profile of the surface. The Spatial Distribution of the surface profile method proposed in this Chapter provides a new way to evaluate special surface conditions which cannot hardly be assessed by traditional methods. This new assessment method provides a clearer way to control the lapping process and to avoid the occurrence of excessive lapping.

In addition to obtain a better surface finish, the advantage of this new low-pressure lapping method is that it can preserve the reflectance of Al6061 surface as compared to conventional polishing method as shown in Figure 4.12. As a result, the new lapping method is suitable for lapping soft metals and detailed surface generation mechanism is investigated in the next chapter.

# CHAPTER 5 INVESTIGATION ON SURFACE GENERATION MECHANISM OF THE LOW- PRESSURE LAPPING TECHNOLOGY

## 5.1 Introduction

The lapping and polishing process is complicated because it involves many aspects and associated parameters. As mentioned in the literature review, lapping and polishing parameters can be broadly divided into process parameters and material parameters. In the previous chapter, the technical feasibility of the new low-pressure lapping technology has been verified under different process parameters, but it did not discuss the effect of material parameters on the lapping technology. As a result, this chapter is mainly concerned with investigating the influence of material parameters on the lapping results, and the surface generation mechanism in using this method is investigated through a series of lapping experiments.

This chapter is divided into three parts. The first part studies the hydrodynamic effect of this new lapping method by lapping an Al6061 mirror considering different material parameters. In the second part, the influence function of this lapping method is discussed. The last part discusses the surface generation mechanism of the method based on the results of the first two parts which lays the foundation for modeling and simulation work discussed in the next Chapter

## **5.2 Part I: hydrodynamic effect**

In the lapping process, the choice of the lapping pad is important. In this project, since the sample is made of soft metal, in order to avoid scratches on the surfaces, the first consideration is that the fiber of the lapping pad is sufficiently soft. In general, fine polishing, wool felt is used as the polishing pad to avoid scratches, As a result, the wool was chosen as the lapping pad in this research. In addition to the softness of the lapping head, it is also necessary to consider the pressure applied by the lapping head on the workpiece. When the pressure is large, abrasive particles may be pressed into the surface of the workpiece and cause scratches under the driving force of the lapping pad. As a result, a brush was used as the lapping head. In the experiment, the wool fiber contacts the workpiece with almost no pressure and drives the slurry for lapping. The wool brush was compared with the wool polishing head used in bonnet polishing. As it can be seen from the results, although bonnet polishing used small pressure during polishing, which only lasted for one minute, it still left a lot of scratches on the Al6061 mirror surface (see Figure 5.1 (a)). On the contrary, the mirror surface with a brush lapped still remained super mirror surface as shown in Figure 5.1 (b). As a result, it is interesting to note that the lapping/polishing result with the same lapping/polishing fibers but under different pressures is very different in the process of lapping/polishing soft metals such as the Al6061 aluminium alloy.

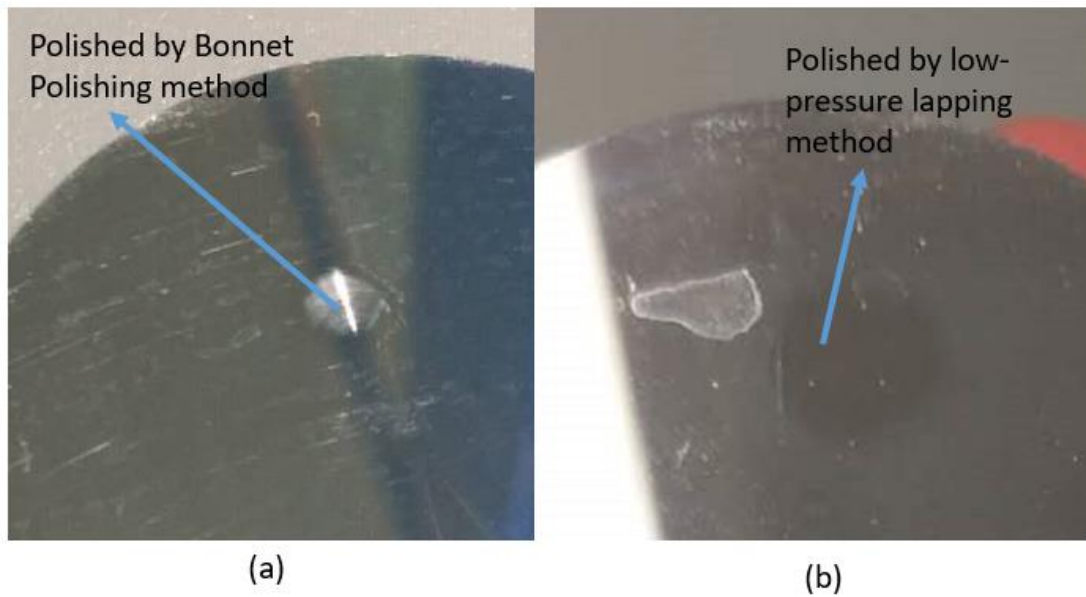


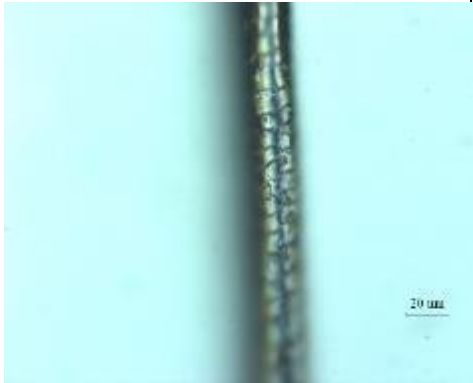





Figure 5.1 Result of Al6061 mirror surface polished by (a) Bonnet polishing method (Inclination angle: 5°, pressure: 0.1 bar, rotational speed: 1000 rpm, time: 1 min) and (b) low-pressure lapping method

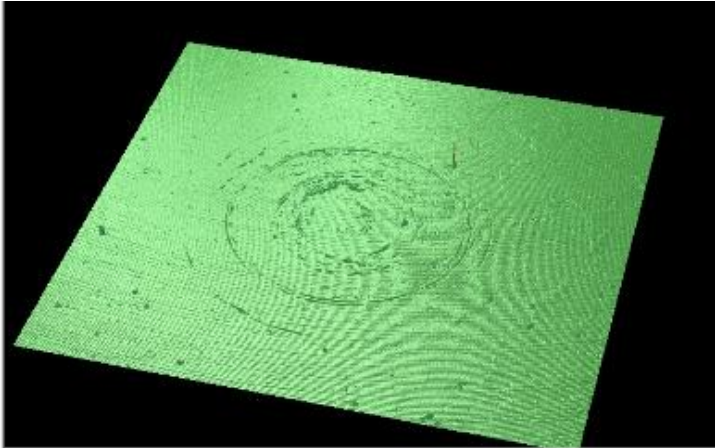
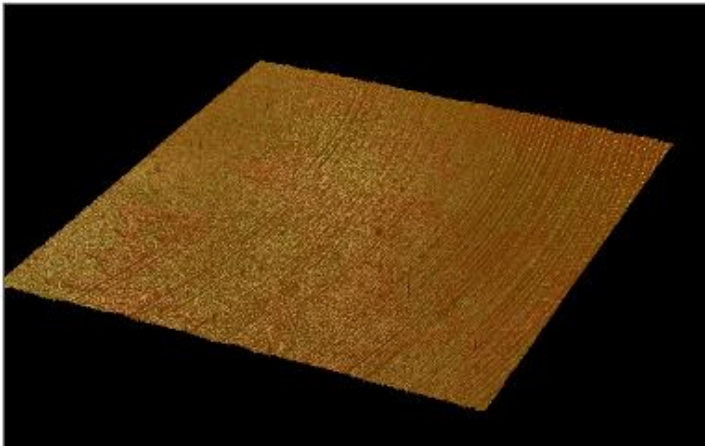
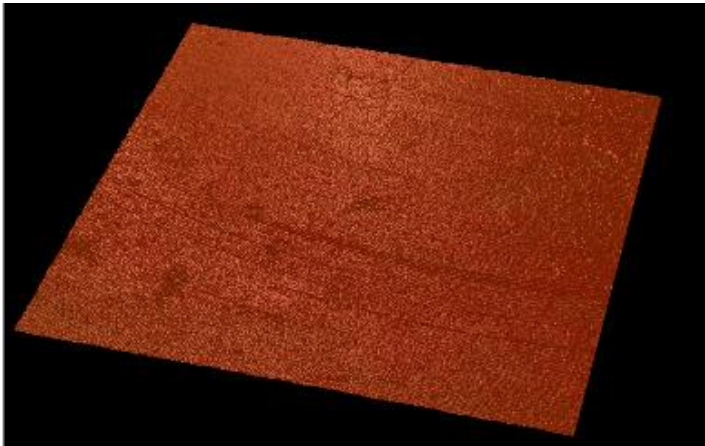
In order to further verify whether wool is suitable as the lapping pad and investigate the hydrodynamic effect of the new lapping process, three different brushes were used in this experiment. These three brushes were made of different animal fibers and had different diameters and hardness (Table 5.1). Each brush lap the Al6061 mirror without media, with water as the medium and with a SiO<sub>2</sub> slurry. The specific lapping parameters and results are shown in the Table 5.2.

Table 5.1 Three different fiber used in the experiment

Fiber type	Bottom of the fiber	Tip of the fiber
Wool		
Rabbit hair		
Weasel hair		

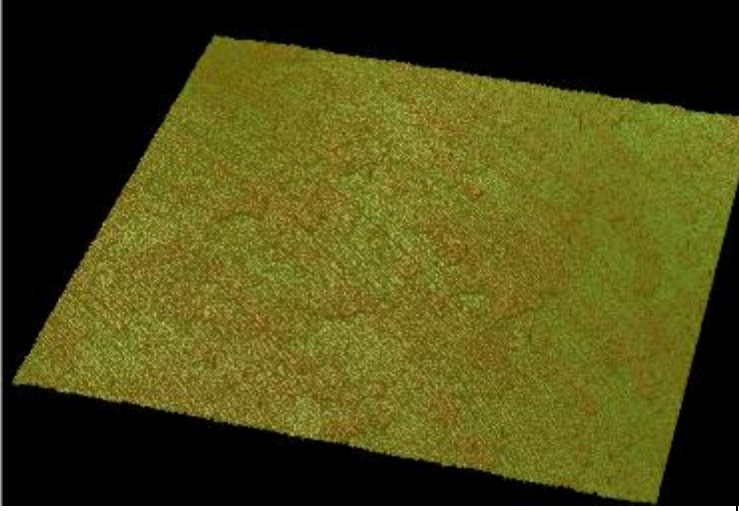
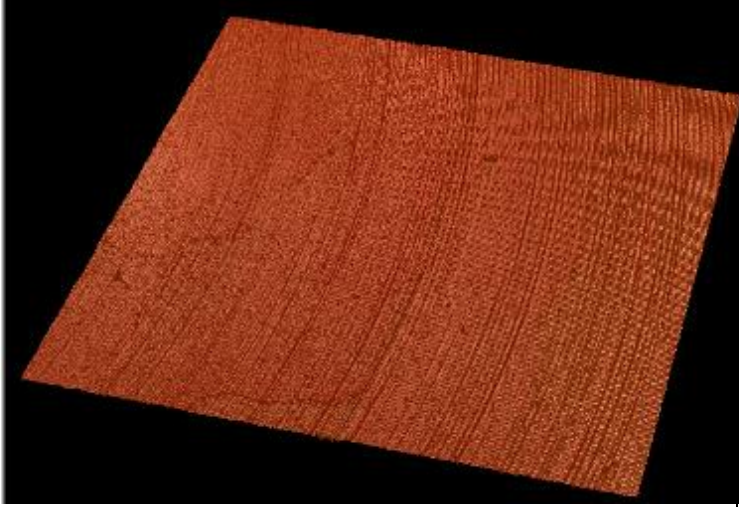
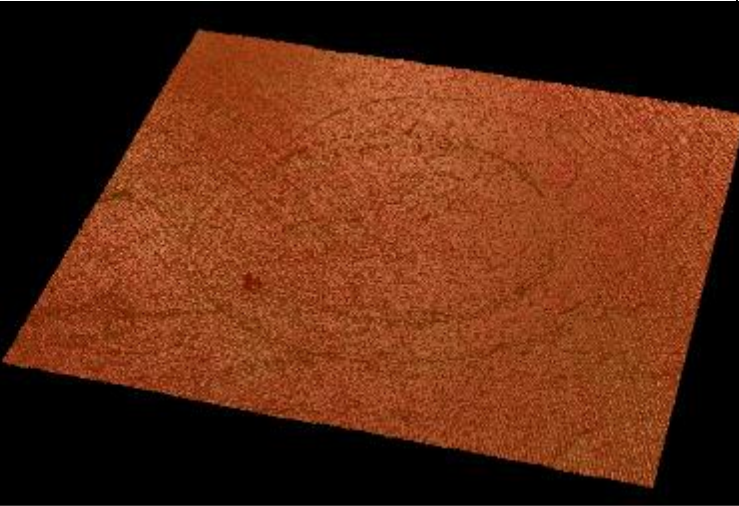
Chapter 5 Investigation on Surface Generation Mechanism of the  
 Low-pressure Lapping technology

Table 5.2 Results of hydrodynamic effect under different lapping fibers

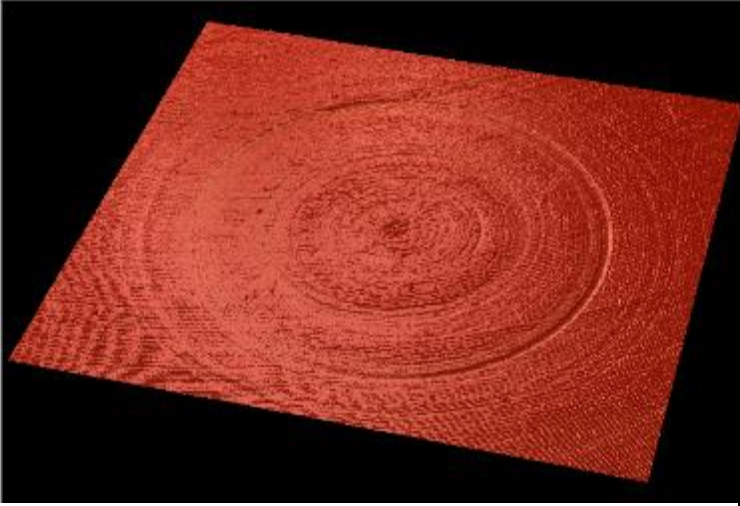
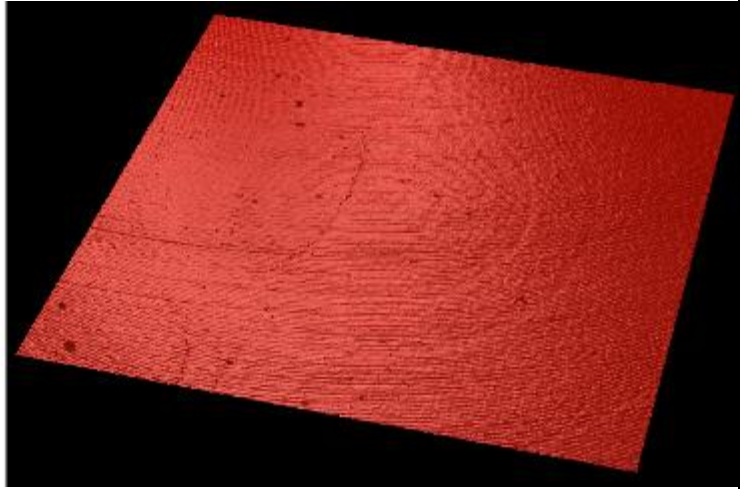
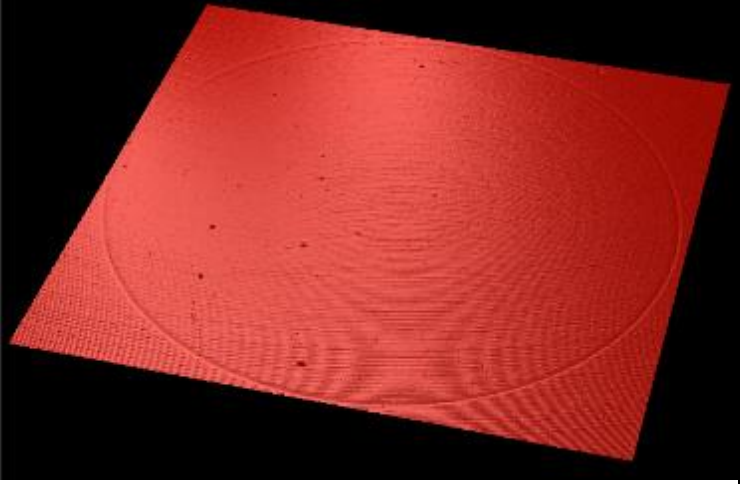
Polishing the Al6061 mirror with no medium (Rotational speed 1000 rpm, time 15 min)	
Wool	<p><b>Surface Stats:</b>                      Ra: 6.29 nm                      Rq: 18.35 nm                      Rt: 2.93 nm</p> <p><b>Measurement Info:</b>                      Magnification: 1.00                      Measurement Mode: PSI                      Sampling: 1.47 um                      Array Size: 1722 X 1638</p> 
Rabbit hair	<p><b>Surface Stats:</b>                      Ra: 4.77 nm                      Rq: 6.50 nm                      Rt: 457.38 nm</p> <p><b>Measurement Info:</b>                      Magnification: 1.00                      Measurement Mode: PSI                      Sampling: 1.47 um                      Array Size: 1480 X 1353</p> 
Weasel hair	<p><b>Surface Stats:</b>                      Ra: 6.36 nm                      Rq: 10.10 nm                      Rt: 762.22 nm</p> <p><b>Measurement Info:</b>                      Magnification: 1.00                      Measurement Mode: PSI                      Sampling: 1.47 um                      Array Size: 1868 X 1838</p> 



Chapter 5 Investigation on Surface Generation Mechanism of the Low-pressure Lapping technology

Polishing the Al6061 mirror in water (Rotational speed 1000 rpm, time 15 min)	
Wool	<p>Surface Stats:            Ra: 4.94 nm            Rq: 6.27 nm            Rt: 353.10 nm</p> <p>Measurement Info:            Magnification: 1.00            Measurement Mode: PSI            Sampling: 1.47 um            Array Size: 1830 X 1770</p> 
Rabbit hair	<p>Surface Stats:            Ra: 5.64 nm            Rq: 8.15 nm            Rt: 646.40 nm</p> <p>Measurement Info:            Magnification: 1.00            Measurement Mode: PSI            Sampling: 1.47 um            Array Size: 1335 X 1417</p> 
Weasel hair	<p>Surface Stats:            Ra: 5.48 nm            Rq: 7.58 nm            Rt: 632.94 nm</p> <p>Measurement Info:            Magnification: 1.00            Measurement Mode: PSI            Sampling: 1.47 um            Array Size: 1971 X 1817</p> 

Chapter 5 Investigation on Surface Generation Mechanism of the Low-pressure Lapping technology

Polishing the Al6061 mirror with SiO <sub>2</sub> slurry (Rotational speed 1000 rpm, time 15 min)	
Wool	<p><b>Surface Stats:</b>            Ra: 8.52 nm            Rq: 11.46 nm            Rt: 1.55 nm</p> <p><b>Measurement Info:</b>            Magnification: 1.00            Measurement Mode: PSI            Sampling: 1.47 nm            Array Size: 1822 X 1741</p> 
Rabbit hair	<p><b>Surface Stats:</b>            Ra: 5.99 nm            Rq: 29.17 nm            Rt: 2.16 nm</p> <p><b>Measurement Info:</b>            Magnification: 1.00            Measurement Mode: PSI            Sampling: 1.47 nm            Array Size: 1405 X 1392</p> 
Weasel hair	<p><b>Surface Stats:</b>            Ra: 5.73 nm            Rq: 28.83 nm            Rt: 6.14 nm</p> <p><b>Measurement Info:</b>            Magnification: 1.00            Measurement Mode: PSI            Sampling: 1.47 nm            Array Size: 1865 X 1833</p> 

It can be seen from the results as shown in Table 5.2 that there was almost no material removal during the lapping process in using the three brushes when there was no medium during the lapping process. Lapping in water also has less effect on the surface of the workpiece. When the medium was changed to a polishing slurry, it was apparent that the material was removed from the Al6061 surface. Among them, wool had the best result, and the worst was weasel hair. Lin et al. (2016) claimed that the friction of the wool, rabbit and weasel hair are about 0.830, 0.692 and 0.303 respectively. As a result, the reason for this result is that the larger friction and coarseness of the fiber can effectively drive the abrasive grains along the workpiece surface. Thereby the abrasive particles can achieve sufficient momentum to remove the surface material.

From the experimental results, it can be concluded that, when the polishing process has no slurry, the surface of the workpiece is substantially unchanged, so it can be said that in this new low-pressure lapping method, the particles in the polishing liquid play the main role not the brush.

### **5.3 Part II: Influence function**

The influence function is an important indicator in the lapping/polishing process. The influence function determines the removal rate of the polishing method and can be used to compensate in the polishing. In this part, according to the conclusion in Chapter 4, wool is used as the lapping pad, and SiO<sub>2</sub> is used as the slurry to investigate

## Chapter 5 Investigation on Surface Generation Mechanism of the Low-pressure Lapping technology

the influence function of the new low-pressure lapping method. The lapping parameters are shown in Table 5.3. Both sets of experiments were lapped on a fixed point on the workpiece surface, the only difference is the lapping time.

Table 5.3 Lapping parameters of the two experiment for investigate the influence  
function

	Rotational speed	Time	Lapping pad	Slurry
Trial 1	1000 rpm	<b>30 min</b>	wool	SiO <sub>2</sub>
Trial 2	1000 rpm	<b>60 min</b>	wool	SiO <sub>2</sub>

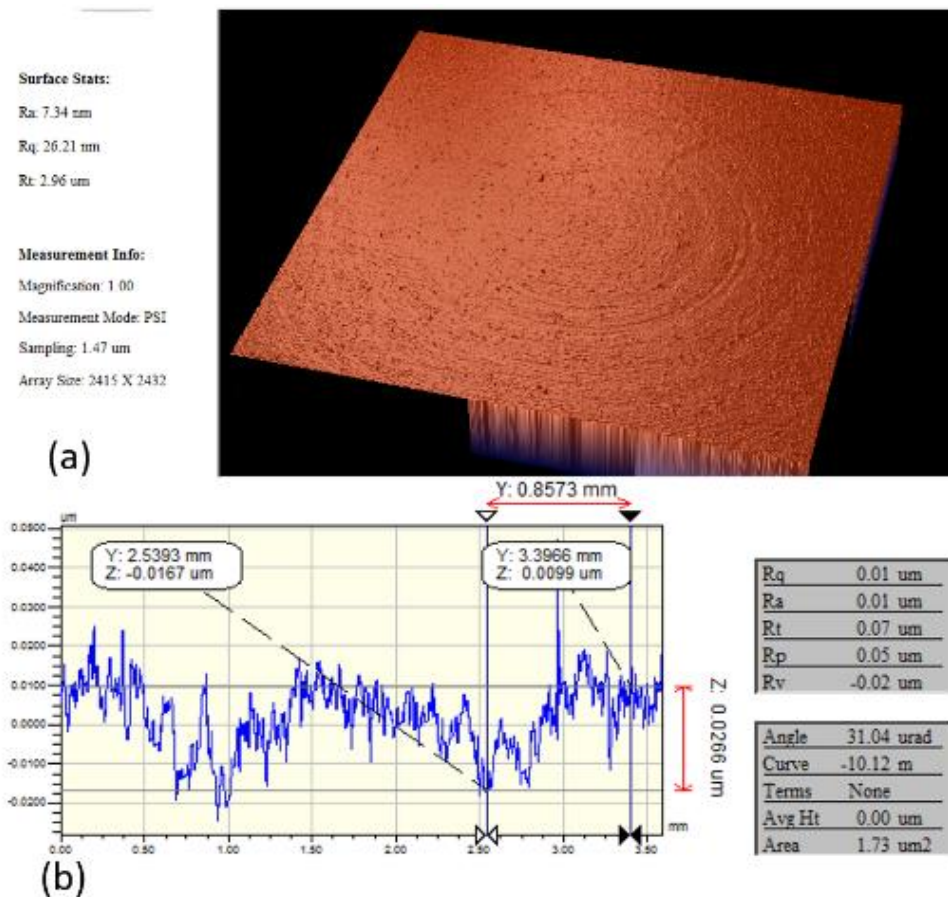


Figure 5.2 Al6061 mirror surface lapped for 30 min (a) and the cross section plot of  
this surface (b)

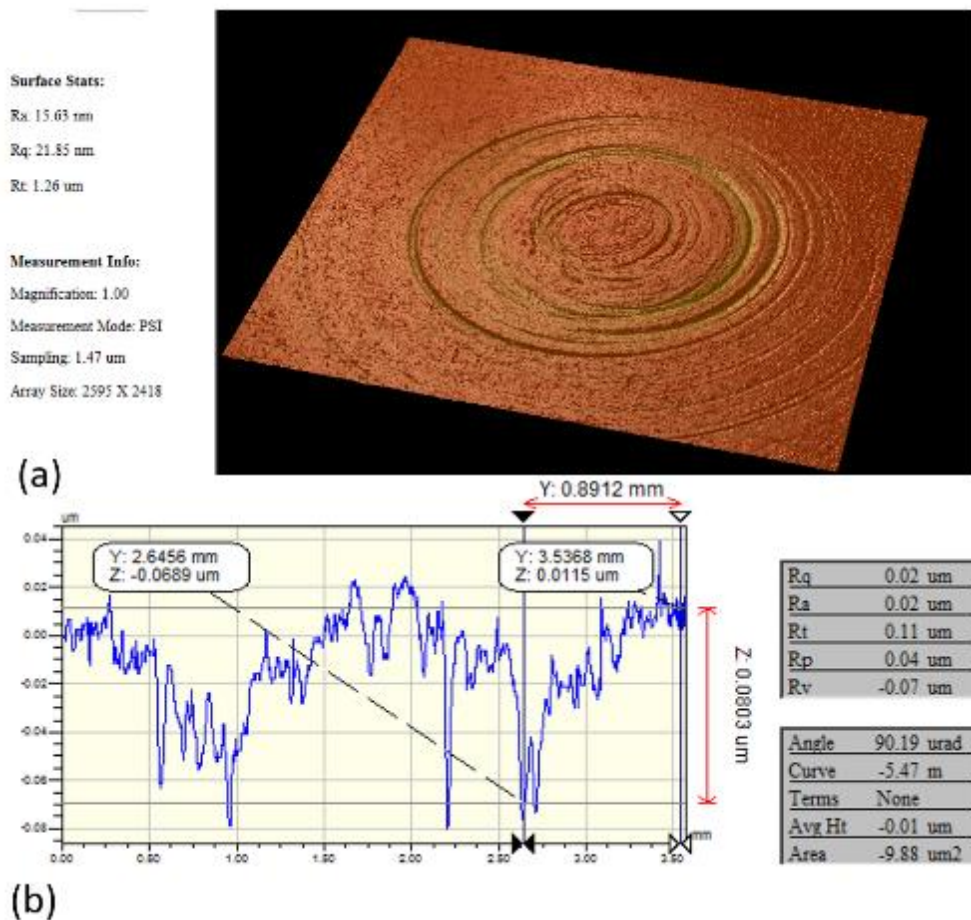


Figure 5.3 Al6061 mirror lapped for 1 hour (a) and the cross section plot of this surface (b)

It can be seen from the experimental results that the removal rate of the new lapping method is very small, and the removal function is not similar to the conventional Gaussian distribution. The reason for this result may be due to the fact that the pressure of the lapping pad is very small, with the abrasive grains always sliding or rolling on the surface of the workpiece during the lapping process, so that there is a small material removal rate.

## Chapter 5 Investigation on Surface Generation Mechanism of the Low-pressure Lapping technology

To further verify this observation that the removal rate is low, another set of samples with large tool marks were also lapped by this low-pressure lapping method for 30 minutes and one hour, respectively. The experimental results are shown in Figure 5.4. The original surface height of the workpiece in this experiment was  $1.3\ \mu\text{m}$ , which was reduced by up to  $0.29\ \mu\text{m}$  after lapping.

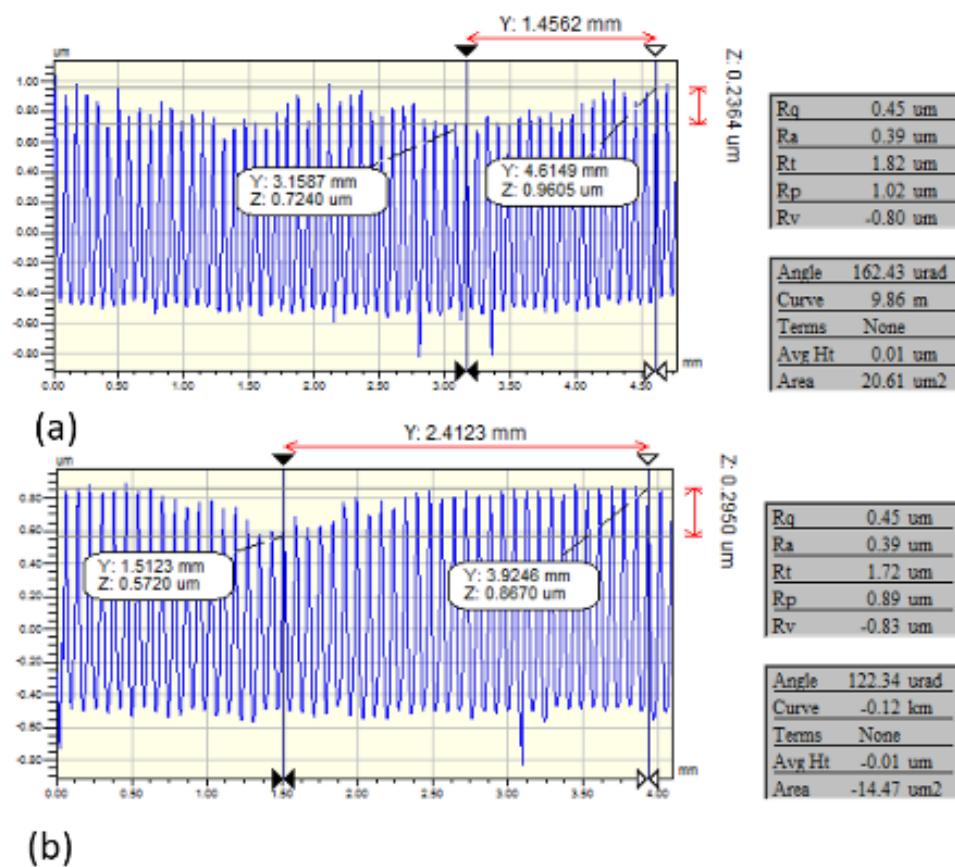


Figure 5.4 Cross section plot of Al6061 surface after lapping for 30 min (a) and 1 hour (b)

It was again verified by the experiment that the material removal rate in this lapping method is very small. It is difficult to describe its influence function with a removal

function. It is found that this lapping method is suitable for lapping soft metal mirrors, which can reduce the surface roughness without affecting the surface form, and the process may also be suitable for lapping soft metal with complex surfaces, such as lenticular lenses or free-form surfaces. However, this method may be difficult to apply on harder materials.

As shown in Figure 2.5 and Figure 2.6, the material removal rate is not a very stable function. The removal function depends on the state of the fiber and where the abrasive particles are during the high-speed rotation process. Referring to the results in Chapter 4, it is known that the lapping time of this method in the fixed point lapping process is better than 20 minutes at the same time,. As a result, the lapping head or the workpiece should not be fixed at a particular point during actual lapping process, so that the fiber can be prevented from forming a stable bond during rotation.

For practical applications, a hexapod can be used to hold the workpiece and move along the lapping path. The path can be set based on the size and shape of the workpiece lapped area. As shown in Figure 5.5, when the workpiece is moving along a path (see Figure 5.5(b)), the cross section plot (Figure 5.5(d)) of the lapped surfaces indicate that this polishing method was a relatively small but stable removal rate.

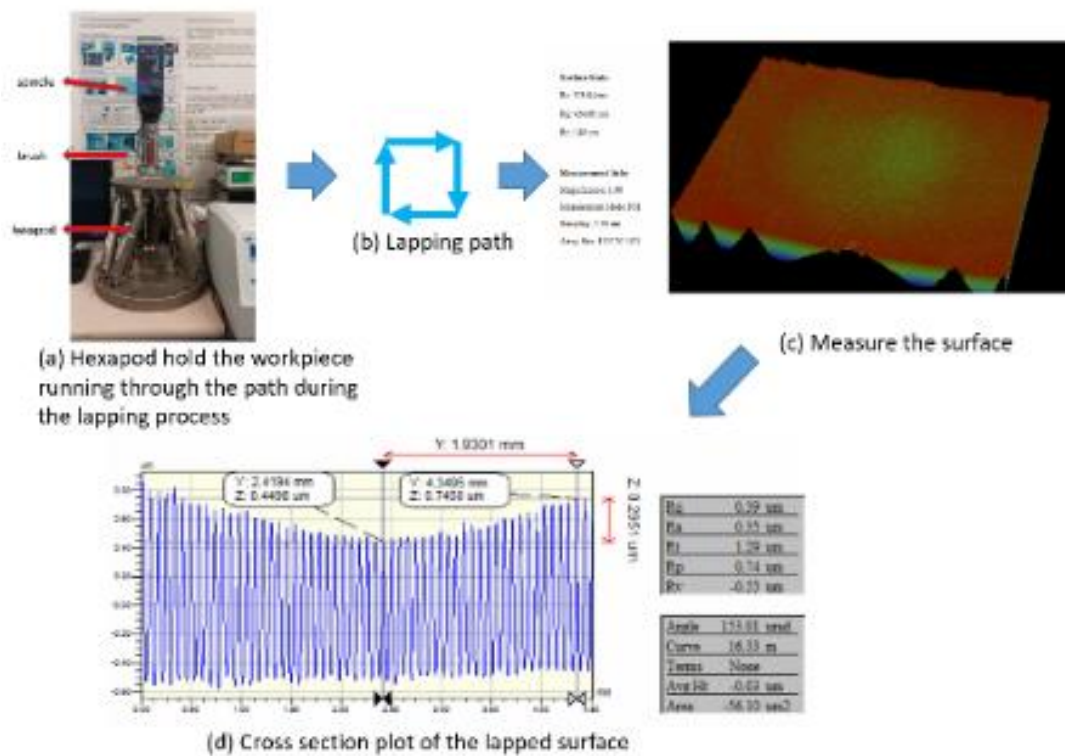


Figure 5.5 AI6061 surface lapped when the workpiece is continue moving through the lapping path

### 5.4 Part III: surface generation mechanism

From the results of Chapter 4, it can be seen that when the rotational speed is low, the change of the polished surface is small. In section 5.1, it was shown that the abrasive particles play a major role in the lapping process which indicates that the surface generation mechanism is mainly due to the interaction between the abrasive particles and the workpiece. Figure 5.6 shows a measurement image of the original workpiece surface and the lapped surface by the low-pressure lapping method under the optimized parameters.



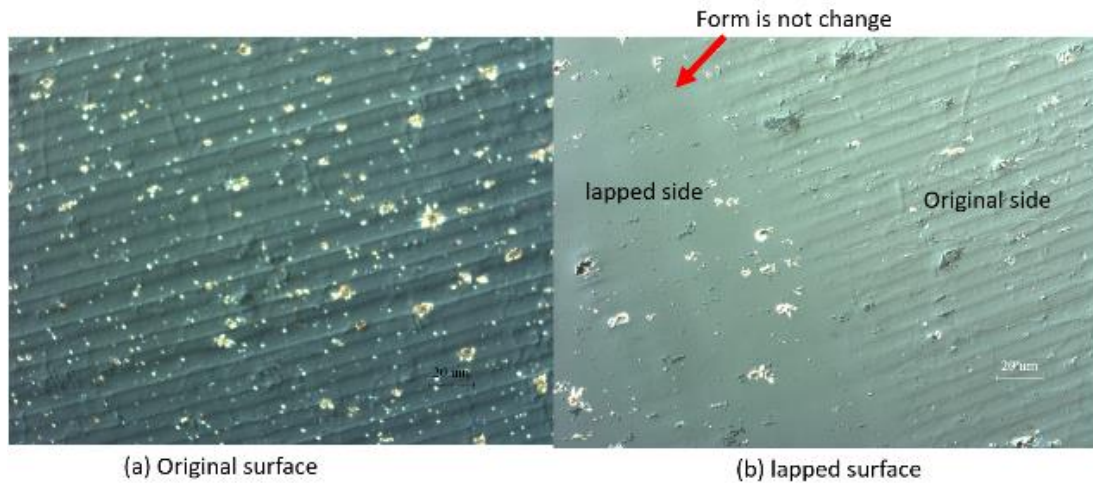


Figure 5.6 Measurement image of the original Al6061 surface (a) and lapped surface  
(b) by Olympus BX60 microscope

As shown in Figure 5.6, the left side is the unlapped surface and the right side is the lapped surface. It can be seen from Figure 5.6(b) that the form of the workpiece surface has not been changed after lapping and the tool mark is removed from the surface. In this lapped surface, it is hard to see pits and scratches. By comparing Figure 5.6(a) and 5.6(b), it can be seen that there is no trace of the Chemical Mechanical Polishing (CMP) process on the workpiece surface, such as the etching layer, before and after lapping. As a result, this low-pressure lapping process is mechanical polishing rather than CMP. Research studies have also indicated that lapping Al6061 alloys with colloidal silica slurry ( $\text{SiO}_2$  particle dispersed in the slurry) as the lapping/polishing liquid is a mechanical lapping/polishing process (Toozandehjani et al. 2016, Sabirov et al. 2010).

In the mechanical lapping process, the contact process between the particles and the

workpiece determines the surface generation mechanism. In this research, the diameter of the wool fiber was around 100 nm, and the diameter of the abrasive particle was 15 nm. Studies have shown that SiO<sub>2</sub> particles are generally circular in the slurry (Turley 1981). As a result, the possible modes of interaction between a particle and the workpiece surface can be generalised into three categories:

**Mode 1:** The abrasive particles roll freely on the surface of the workpiece. The efficiency of material removal would be small, close to zero.

**Mode 2:** The abrasive particles plow a groove on the surface of the workpiece, and the material in the groove is extruded to the front and sides of the groove. In this case, the material removal rate is also close to zero, but the material stacked on the edge of the groove may be taken away by the subsequent abrasive particles.

**Mode 3:** The abrasive particle cuts a groove while a long strip of chip is removed from the groove. Ideally, the material is completely removed from the groove, and the material removal rate is close to 100%.

Mode 1 is usually called three body abrasion, and the other two are generally known as two-body abrasion. Since the metal surface is soft, the abrasive particles move at a high speed under the action of the fiber, and may be embedded in the workpiece surface, thereby changing from mode 1 to mode 2 or mode 3. However, since the material removal rate of this lapping method is very low, the mode 1 should play the main role.

It can be seen from the SEM image that some mottled surfaces are formed on the

## Chapter 5 Investigation on Surface Generation Mechanism of the Low-pressure Lapping technology

lapped surface (Figure 5.7), and some platelet-like materials are taken away during the lapping process (Figure 5.8). Some researchers believe that when the abrasive particles are small, to a certain extent, such as less than 0.5 micrometer, the main mechanism in the lapping process is platelet delamination. However, it is still hard to explain why there is a wide range of scratch-free areas on the lapped surface.

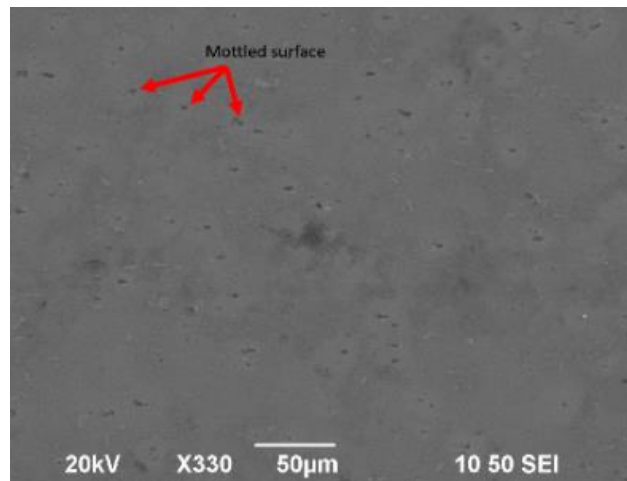


Figure 5.7 Mottled surface after lapping process (Rotational speed 1000 rpm, Time 15 min, Slurry: SiO<sub>2</sub>)

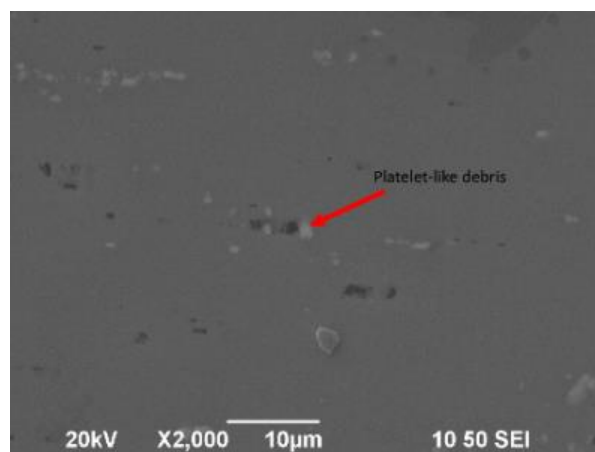


Figure 5.8 Platelet-like debris on the surface after lapping process (Rotational speed 1000 rpm, Time 15 min, Slurry: SiO<sub>2</sub>)

For a single abrasive particle, it can microcut or plow the workpiece surface during the lapping process. However, it can be seen from the SEM image in Figure 5.9, the groove is rarely produced on the surface during the lapping process. In addition, the abrasive particles themselves are relatively round. As a result, the single particle erosion mechanism only occupies a small proportion of material remove in the low-pressure lapping process.

For the mechanism in which the abrasive particles are embedded on the fiber to form a cantilever system to produce a removal rate, the surface of the workpiece should have many shallow, long scratches. Although this method makes it is easier to lap a mirror surface, it can be seen from Figure 5.9 that only one shallow and long scratch exists. As a result, this mechanism is not suitable for this lapping method.

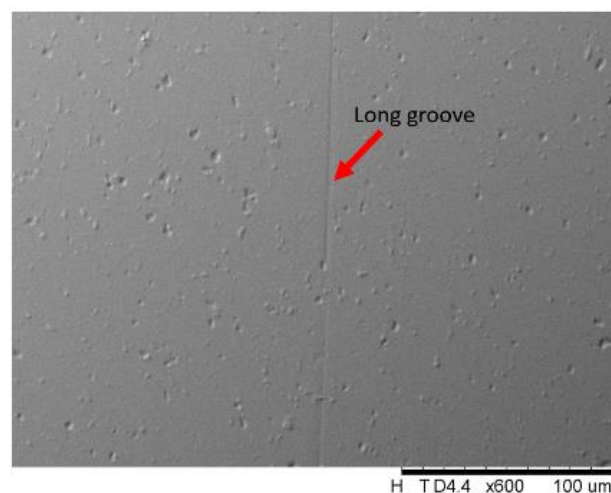


Figure 5.9 Long scratch on the lapped surface (Rotational speed 1000 rpm, Time 15 min, Slurry particle:  $\text{Al}_2\text{O}_3$ )

Micromachining by abrasives contained in a carrier paste is a mechanism which has no microcutting behavior. This mechanism requires the lapping pad to be softer than the workpiece and the abrasive particles to be sufficiently small. At the same time, the abrasive particles should be easily embedded on the fiber. In this low-pressure lapping process, the fiber of the brush is far softer than the surface of the workpiece, the abrasive grain is much smaller than the fiber and because the fiber has a good friction, the abrasive grain should be easily embedded on the fiber or driven by the fiber for high-speed motion. As a result, this mechanism is more suitable for the low-pressure lapping process. The high-speed movement of the abrasive particles means that there is sufficient momentum to laterally impact the surface. When the momentum is accumulated to a certain level, the asperities on the surface of the workpiece are worn away, thereby reducing the surface roughness.

Through the above discussion, the possible mechanism for the low-pressure lapping method is that the fiber containing the carrier paste is worn away by the tiny asperities (tool mark in this case) from the workpiece. This mechanism is difficult to observe experimentally, so the next chapter describe the use of finite element method to simulate the surface condition of the abrasive particles sliding from the workpiece surface at high speed so as to verify the surface generation mechanism of the low-pressure lapping method.

## 5.5 Summary

In this chapter, the hydrodynamic effect, influence function and possible surface formation mechanisms of the new lapping method were investigated. The results show that, wool is the ideal lapping pad for lapping soft metal mirrors for material parameters. This lapping method does not have a distinct influence function, but is well suited for lapping soft metal mirrors (referred to as Al6061 in this study). The surface generation mechanism of this method is closer to wearing than microcutting or erosion. When the abrasive grains are rolled or slid with high speed driven by the fiber, the particles have sufficient momentum to wear away the asperities from the rough surface, and scratches were rarely generated in this process. As a result, this new low-pressure lapping method can remove tool marks while maintaining the reflectance of the workpiece surface at the same time.

# CHAPTER 6 MODELLING AND SIMULATION OF THE SURFACE GENERATION MECHANISM OF THE LOW-PRESSURE LAPPING TECHNOLOGY

## 6.1. Introduction

The low-pressure lapping technology used in this study has a very a small material removal rate as compared with other conventional lapping/polishing methods. The traditional lapping model based on the Preston formula is not suitable for this method. In the general lapping/polishing process, the common mechanisms are microcutting, delamination, slurry erosion, chemical mechanical polishing, etc. (Samuels et al. 2003). In this study, the brush touches the lapped surface very gently during the lapping process and drives the abrasive particles to move on the surface. The possible mechanism as discussed in Chapter 5 is that the abrasive particles receive large momentum during the lapping process. As a result, the abrasive particles impinge the asperities of the workpiece surface during the sliding and rolling process, causing the plastic deformation of the asperities which are worn away and thereby reducing the surface roughness.

Since the asperities of the surface are removed by the impingement of the abrasive particles, the finite element method (FEM) can be used to model and simulate the surface generation in this low-pressure lapping. The simulation results provide a better

understanding of the surface generation mechanism and can be used to design the polishing parameters of the actual experiment.

The finite element method (FEM) is an important analytical method for analyzing the deformation process of materials. Komvopoulos et al. (1993) used the finite element software named Abaqus to simulate an area changing from elastic to plastic deformation under load. This research shows that the material change process depends on strain hardening characteristics and accumulated plastic deformation at a specific load, but has little to do with the elastic modulus. Kogut and Etsion studied the deformation process of the contact between a sphere and a rigid plane by the finite element simulation software named ANSYS in 2002. The Von Mises yield criterion was introduced to analyze the deformation process of the material, from elastic to plastic. The results show that the elastic model cannot fully explain the elastic to plastic deformation process.

For the micro-contact model, the basic contact model proposed by Greenwood and Williamson in 1966 is the basis of many subsequent micro-contact models. In this study, it is assumed that the contact surface is rough, the asperities heights on the surface follow a Gaussian distribution with the same curvature, and the asperities do not affect each other when they are under pressure. Contact in this model makes use of the Hertzian approach to calculate the pressure distribution during the contact process. The significance of this model was that it provides a preliminary contact model, and makes use of a plasticity index that determines when the material transforms from



elastic deformation to plastic deformation under a specific load.

Another classic model was established by Chang et al. (1987) based on the Chang, Etsion and Bogy (CEB) elastic-plastic model by Tabor in 1951. This model was the first attempt to determine the boundary state of a material from elastic to plastic. This model and the Greenwood and Williamson model (1966) provide good simulation for the contact process in a real contact area at very high or very low plasticity index.

Based on the Greenwood and Williamson model, Jackson and Green (2005) calculated the yield point of the material based on the asperity contact and the von Mises criterion. Kadin et al. (2006) found that the yield point of the material was greatly affected by Poisson's ratio and strain hardening. Peng et al. (2013) simulated the elastic-plastic contact process of rough surfaces by the finite element method. The simulation model involves asperity contact with a rigid body. In 2017, Almuramady and Borodich conducted a theoretical and experimental comparison of the plastic behavior of an actual rough surface. Although researchers have been continually studying the elastic-plastic contact of rough surfaces by finite element methods, they are rarely used to simulate the actual lapping process.

Since the core of the low-pressure lapping method is the abrasive particles continuously impinge on the tool marks, which are deformed and worn away gradually. In this chapter, the surface generation mechanism is simulated based on the current elastic-plastic contact models.

## 6.2 Modeling processes

### 6.2.1 Parameter setting

The simulation software Abaqus is used in this chapter. In the simulation, two different heights of tool marks on the Al6061 surfaces were designed to be 1  $\mu\text{m}$  and 20 nm. In order to reduce the calculation time, only the tip of the tool mark was used, which means that the intercepted tool mark height are 1 nm and 0.02 nm, respectively in this simulation. Due to the surface with a tool mark height of 20 nm is almost close to the plane. As a result, in this simulation, it can be assumed that each tool mark is independent, and the movement of the abrasive particles on the surface is not affected by the adjacent tool mark. In this simulation, the tool mark is a long ridged shape form, so when the abrasive grains collide from the side, it can be simplified into a 2D tool mark model. According to the experiment, the diameter of the abrasive particles in this simulation is 15 nm. In order to make the operation converge, a plane surface is added at the beginning side as shown in Figure 6.1.

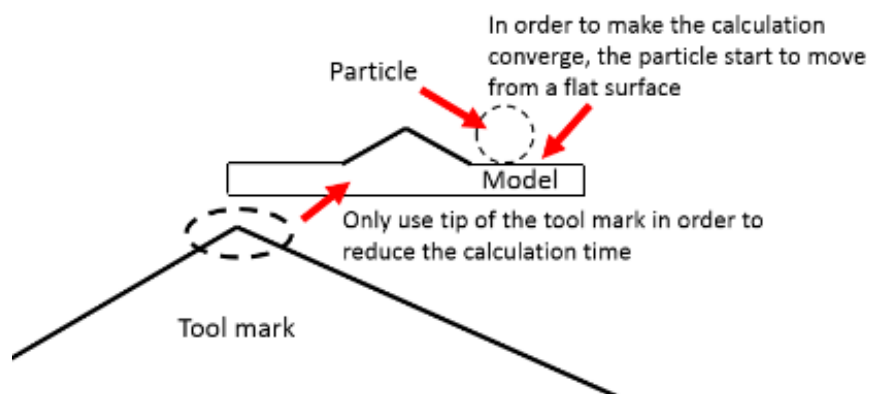


Figure 6.1. Schematic of the finite element model

## Chapter 6 Modelling and Simulation of the Surface Generation Mechanism of the Low-pressure Lapping technology

---

Since this simulation only has a mechanical relationship and no variables like temperature and magnetism are involved, the material parameters only need to be set with mass density, elastic behavior and plastic behavior. In the Abaqus software, there is no unit system, and it is necessary to set the unit according to the content of the simulation. In order to ensure the correct operation result, the unit setting need to ensure the consistency, otherwise the results have no actual physical meaning. In Abaqus, units can be divided into two types: fundamental units, and derived units. A derived unit is a combination of fundamental units. Since this simulation is in the micrometer range, the common meter-scale units are converted into micrometer units (Table 6.1) and is used in the simulation. The workpiece material in this simulation is aluminium allow (Al6061) with the density of  $2.7 \times 10^{-15} \text{ kg}/\mu\text{m}^3$ , Young's modulus is  $6.89 \times 10^4 \text{ MPa}$ , yield stress is  $276 \text{ MPa}$ . In the assembly process, the initial position of the abrasive particle is on the right side of the tool mark and the moving direction is from right to the left.

Table 6.1 Units used in the simulation

Fundamental units	
Length	Mm
Force	$\mu\text{N}$
Time	S
Mass	Kg
Derived units	
Pressure	MPa
Velocity	$\mu\text{m}/\text{s}$
Density	$\text{Kg}/\mu\text{m}^3$
Young's Modulus	MPa
Yield stress	276MPa

In the simulation, Al6061 alloy was designed as an elastic-plastic material based on the Johnson Cook plasticity model (Fish et al. 2005). The model can be expressed as:

$$\bar{\sigma} = \left[ S + V(\bar{\epsilon}^{pl})^n \right] \left[ 1 + Z \ln \left( \frac{\dot{\epsilon}^{pl}}{\dot{\epsilon}_0} \right) \right] \left( 1 - \frac{\theta}{\theta_{melt}} \right)^m \quad (6.1)$$

where  $\bar{\sigma}$  is the yield,  $\bar{\epsilon}^{pl}$  and  $\dot{\epsilon}^{pl}$  are the equivalent plastic strain and plastic strain rate, S, V, Z, n, m and  $\dot{\epsilon}_0$  are material parameters. when the material temperature is lower than transition temperature and detail coefficients are as shown in Table 6.2

Table 6.2: Johnson Cook Coefficients

S	V	Z	n	M	$\dot{\epsilon}_0$	$\theta_{melt}$	$\theta_{transition}$
289.6MPa	203.4MPa	0.011	0.35	1.34	1.0s <sup>-1</sup>	925.37K	294.26K

When the abrasive particles slide and roll on the surface of the workpiece. The polishing time is  $T$ , the rotational speed is  $S$ , the wool is bent after contact with the workpiece, and the angle of bending is  $\theta$ . Since the diameter  $d$  of the thickest part of the wool is about 100  $\mu\text{m}$ , one fiber sweeps  $N$  times on point  $P$ , and can be expressed, as shown in Figure 6.2:

$$N = \mu \frac{2\pi (R - \tan\theta \cdot D) T}{d} \quad (6.2)$$

The speed at which the abrasive particle pass through the P point is:

$$v = 2\pi\kappa \cdot S \cdot R \quad (6.3)$$

where  $\kappa$  is a constant that represents how much of the fiber speed is transmitted to the abrasive particles.

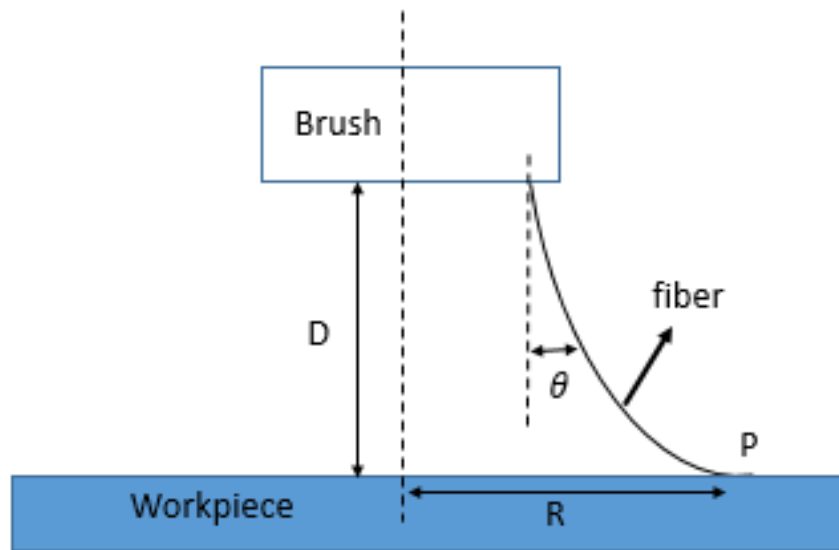


Figure 6.2. Schematic of the lapping process. One fiber on the brush is swept from the workpiece surface

The wear model for the nodes in this simulation is built based on the Archard model.

$$q = \frac{k P A \eta}{H} \quad (6.4)$$

where  $q$  is wear rate,  $k$  a dimensionless constant,  $P$  is the normal pressure,  $\eta$  interface slip rate.  $H$  is the material hardness. In this simulation, the surface is expressed by the change of nodes on the surface. Each node transmits the force to the next node according to the software settings. The wear rate can be expressed as:

$$q(t) = \frac{k}{H} \int P(x, t) \eta(x, t) dx \quad (6.5)$$

where  $x$  is the node position, and  $t$  is the time. Then based on the Eulerian steady-state transport procedure (Qi et al., 2007), the model can change to a time-independent expression:

$$q = \frac{k}{H} \int P(\eta) u(T) u(d) \quad (6.6)$$

where  $u$  is the position along the edge of the grid,  $T(u)$  is the width of the adjacent grid at position  $u$ . The wear rate can be expressed as a function of local material change:

$$q(t) = \int w(u) T(u) du \quad (6.7)$$

Since the software needs a discrete form expression, Eq. (6.7) and Eq. (6.8) are combined and discrete as:

$$\sum_{i=1}^N w_i A_i = \frac{k}{H} \sum_{i=1}^N P_i \eta_i A_i \quad (6.8)$$

where  $w$  is the node wear velocity and  $A_i$  is the node contact area. The expression for  $w$ :

$$w = \frac{k \sum_{i=1}^N P_i \eta_i A_i}{H \sum_{i=1}^N A_i} \quad (6.9)$$

In this simulation, the momentum of the abrasive particles depends on the weight and speed of the abrasive particles. Since the individual abrasive particles are very small, the weight of the individual abrasive particles is about  $5 \times 10^{-18}$  Kg based on the density of the abrasive material ( $2.65 \text{ g/cm}^3$ ) and the size. From Eq. (6.3), it can determine that different speeds of the abrasive particles when  $R$  is 5 mm as in Table 6.3.

Table 6.3 Speed of the particle in the simulation

1	Rotational speed: 200 rpm	$6.28 \times 10^6 \mu\text{m/s}$
2	Rotational speed: 400 rpm	$1.26 \times 10^7 \mu\text{m/s}$
3	Rotational speed: 600 rpm	$1.88 \times 10^7 \mu\text{m/s}$
4	Rotational speed: 800 rpm	$2.51 \times 10^7 \mu\text{m/s}$
5	Rotational speed: 1000 rpm	$3.14 \times 10^7 \mu\text{m/s}$

### 6.2.2 Software setting

In the pre-processing stage, a two-dimensional model is first established in Abaqus and the model is meshed. The boundary conditions and contact conditions of the contact model are then defined, and the abrasive particles are given an initial velocity. In the process of simulating the elastic-plastic contact between the abrasive particles and the surface of the workpiece, the contact process of the finite element simulation is a discontinuous constraint behavior, allowing the forces of the various nodes to be transmitted to other nodes. The premise of this constraint is that the two surfaces are to make contact. As a result, when analyzing the contact process, it is necessary to confirm that the two surfaces have been in contact and produced constraints.

Since the simulation is an impact process, the simulation makes use of the Dynamic Explicit module from Abaqus. The software stores the simulation results as a binary file for the post-processing stage. In the post-processing stage, the simulation process can be visually displayed by Abaqus software. At the same time, the basic variables can also be calibrated using the simulation results, such as displacement, stresses, forces, etc.

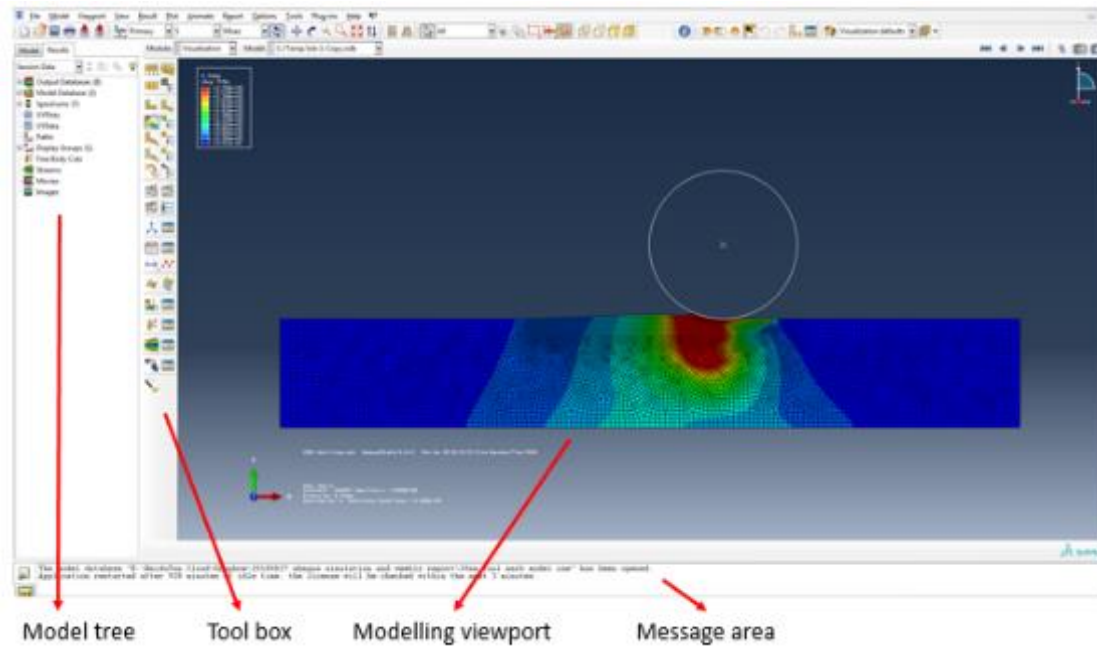


Figure 6.3 Abaqus interface

In the simulation, fatigue failure generally begins with micro-cracks in the material. When the stress was accumulated sufficiently in the structures, such as impurities, dislocations, etc., the material begins to yield (Oila and Bull 2005). Generally, the fatigue crack is divided into three stages: initiation, propagation and final fracture. (Verdu et al. 2008). The early fatigue models were generally based on Hertzian contact to determine the maximum point of force to determine crack initiation. The recent rolling contact fatigue studies consider rough surface as an important parameter (Terrin et al. 2017; Paulson et al. 2017).

Fatigue life is usually defined as: a series of cycles or times that cause fatigue damage and cause a final failure. (Suresh, 1998). In this simulation, the fatigue life is the stage at which the tool mark begins to plastically deform after the abrasive grain repeatedly



impacts the tool mark.

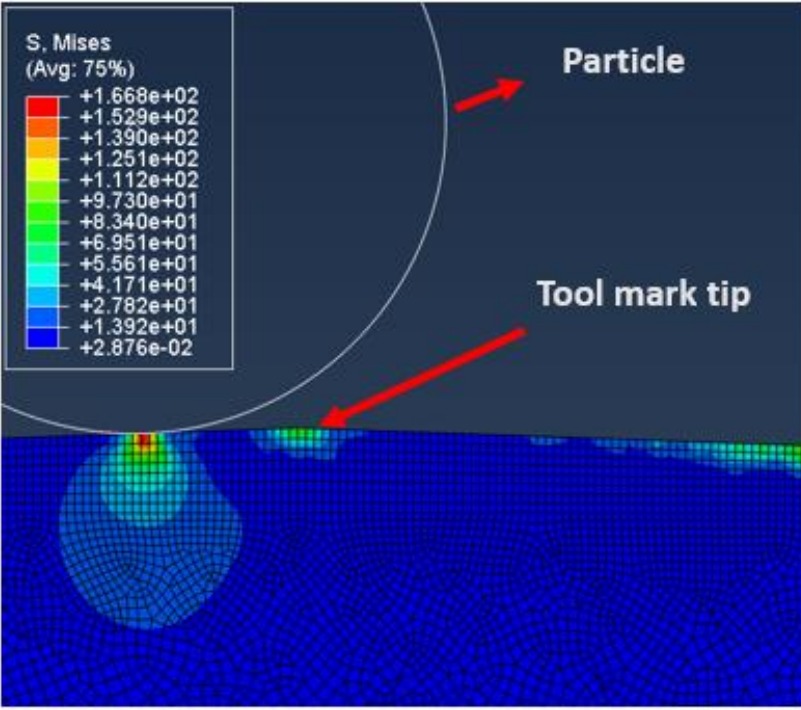
### 6.3 Results and discussion

Table 6.4 and Table 6.5 show the stress map of the two different tool marks height models impacted by particles at different speeds. It can be seen from the two sets of simulation results that when the abrasive grains rolling and sliding at high speed on the surface of the workpiece. The greater the speed, the greater the impact force on the surface. When the abrasive grain hits the tool mark fast enough, it bounces after the impact, and then be pressed back by the fiber and repeated follow the hit-bounce process. It can be seen from (d) and (e) in Table 6.4 and (d) and (e) in Table 6.5 that as the momentum of the abrasive particles increases, the stress on the contact surface becomes larger, and the distance between the two high stress area becomes wide. This result indicates that high rotational speed of the lapping pad does not mean a good lapping result for the actual lapping experiment. When the speed of the particle is high enough, the surface would start to show pits and scratches because the particle impact on the surface is not even.

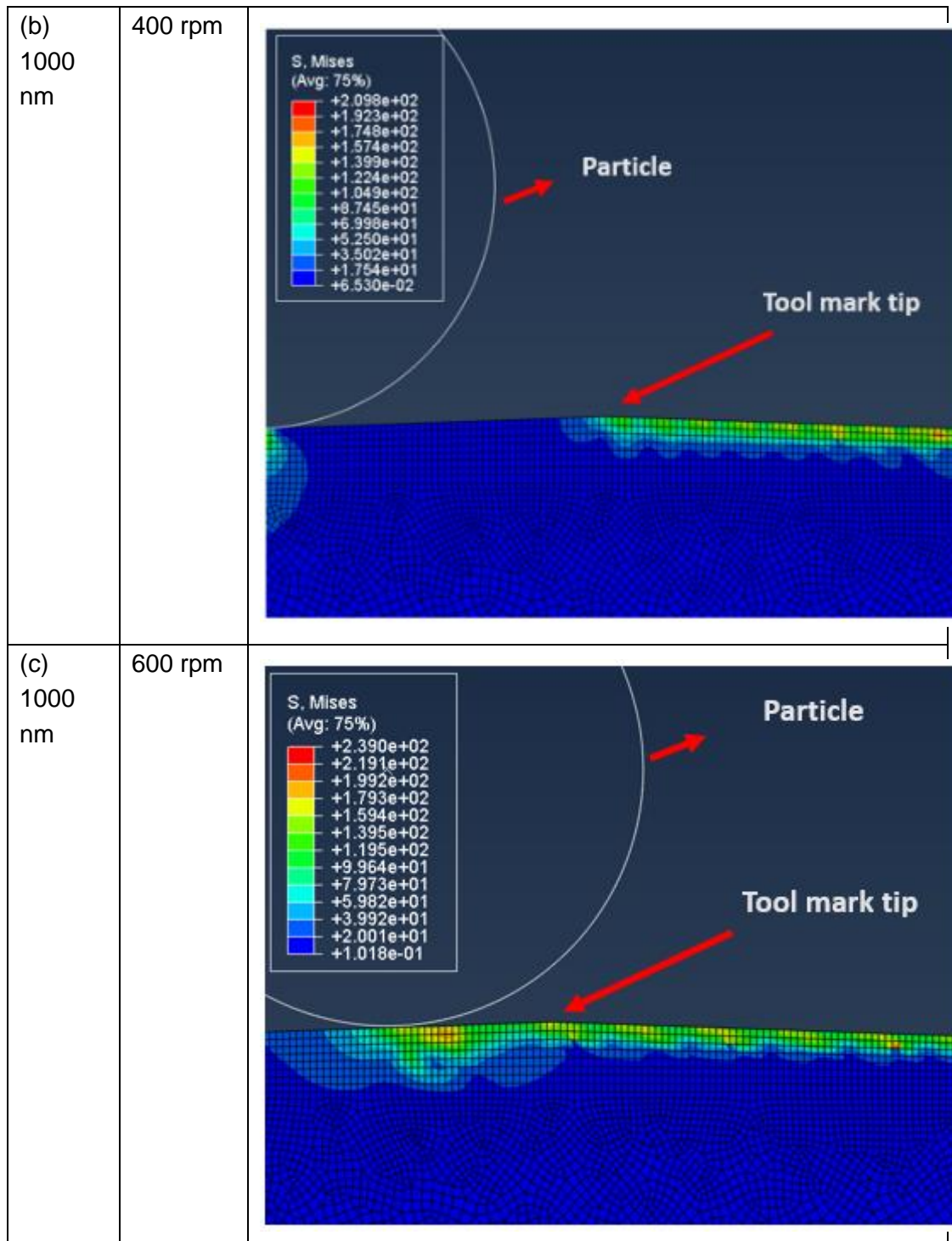
Figure 6.4 and Figure 6.5 show the stress map of the tool marks under different impacts speeds of the particles. Since the yield strength of the workpiece in this simulation is 276 MPa, it can be seen from Figure 6.4 and Figure 6.5 that when the rotational speed is above 800 rpm, the stress of the abrasive grains in the simulation reaches the material yield limit, and the contact area begins to change from elastic deformation to

plastic deformation. It can find from Figure 6.6 and Figure 6.7 that when the rotational speed reaches 1000 rpm, the plastic strain begins to occur on the surface of the workpiece.

Table 6.4 1000nm high tool mark workpiece surface under particle impact at different speeds

Tool mark height	Rotational speed	Results
(a) 1000 nm	200 rpm	 <p>The simulation image shows a particle (indicated by a red arrow) impacting the tip of a tool mark (also indicated by a red arrow) on a workpiece surface. A color scale legend for 'S. Mises (Avg: 75%)' is shown, with values ranging from +2.876e-02 (dark blue) to +1.668e+02 (dark red). The workpiece surface is represented by a grid of elements, with the highest stress concentrations (red and orange) occurring at the point of impact.</p>

Chapter 6 Modelling and Simulation of the Surface Generation Mechanism of the Low-pressure Lapping technology



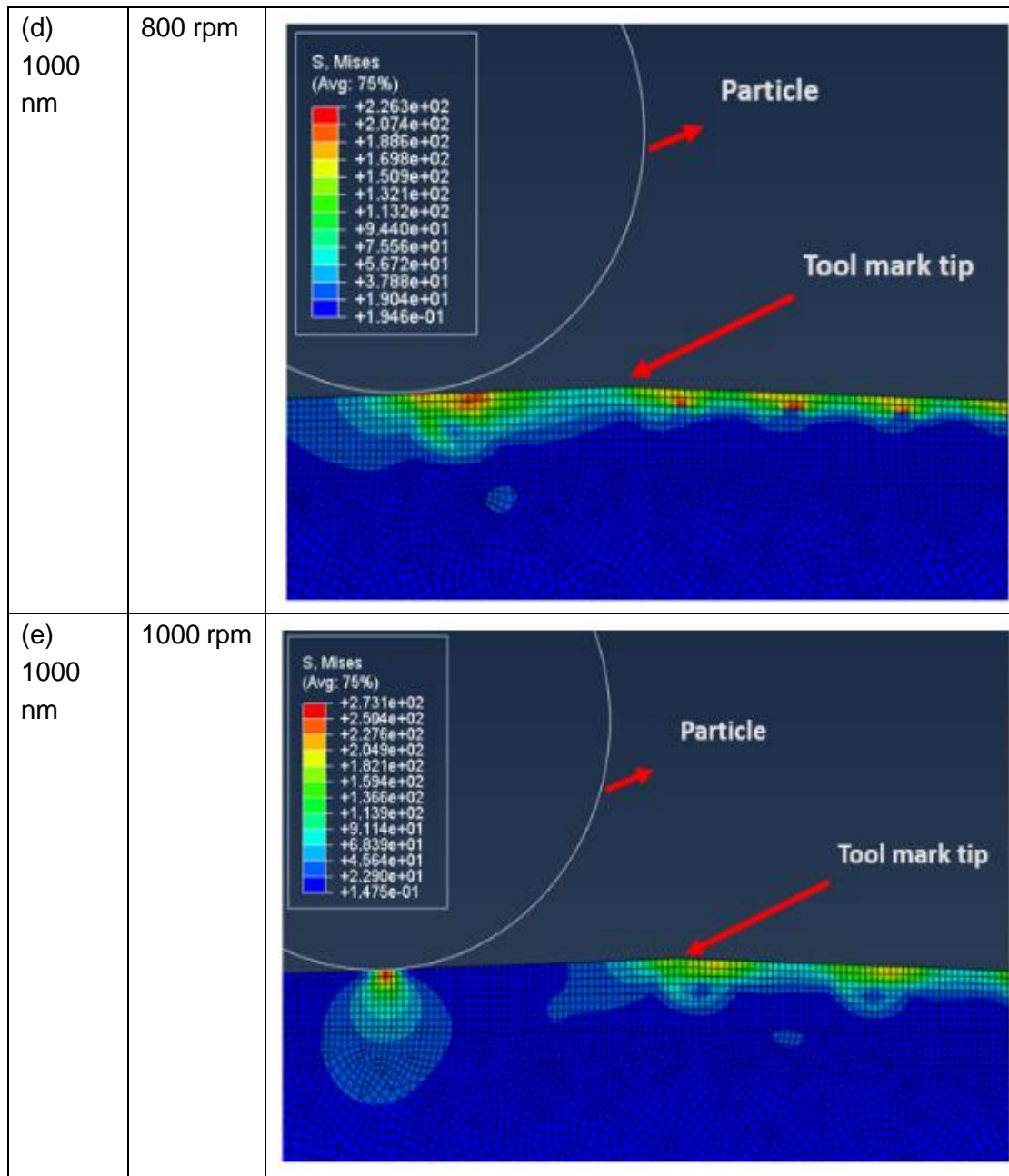
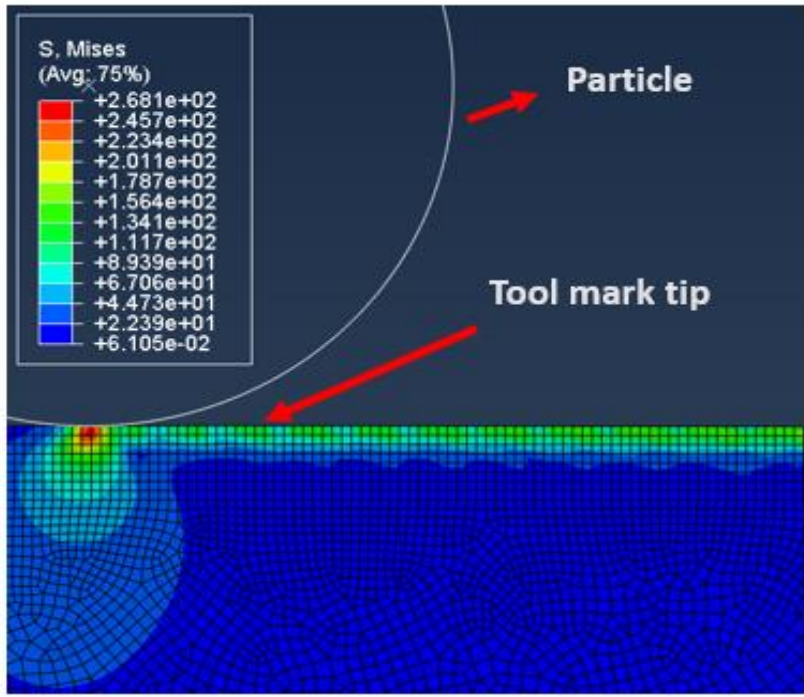
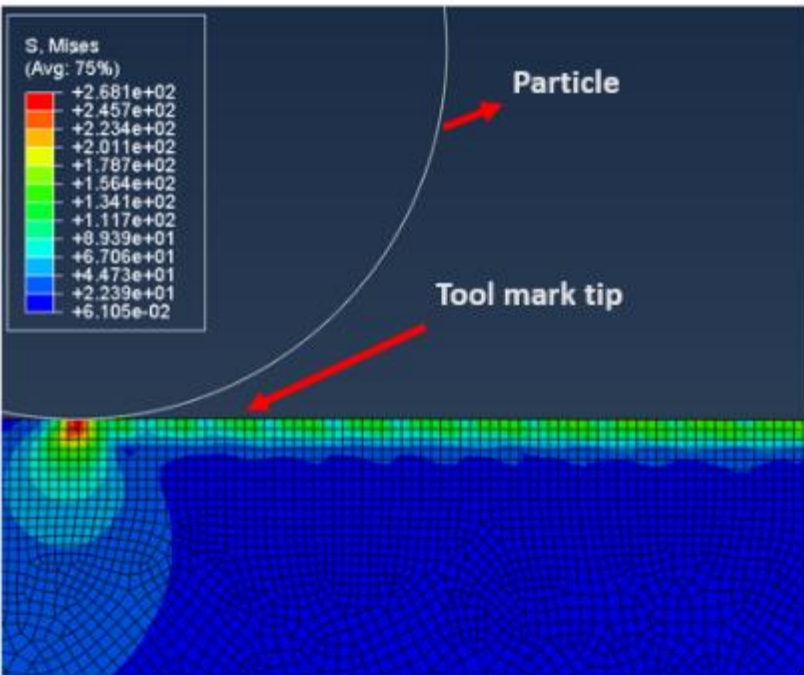
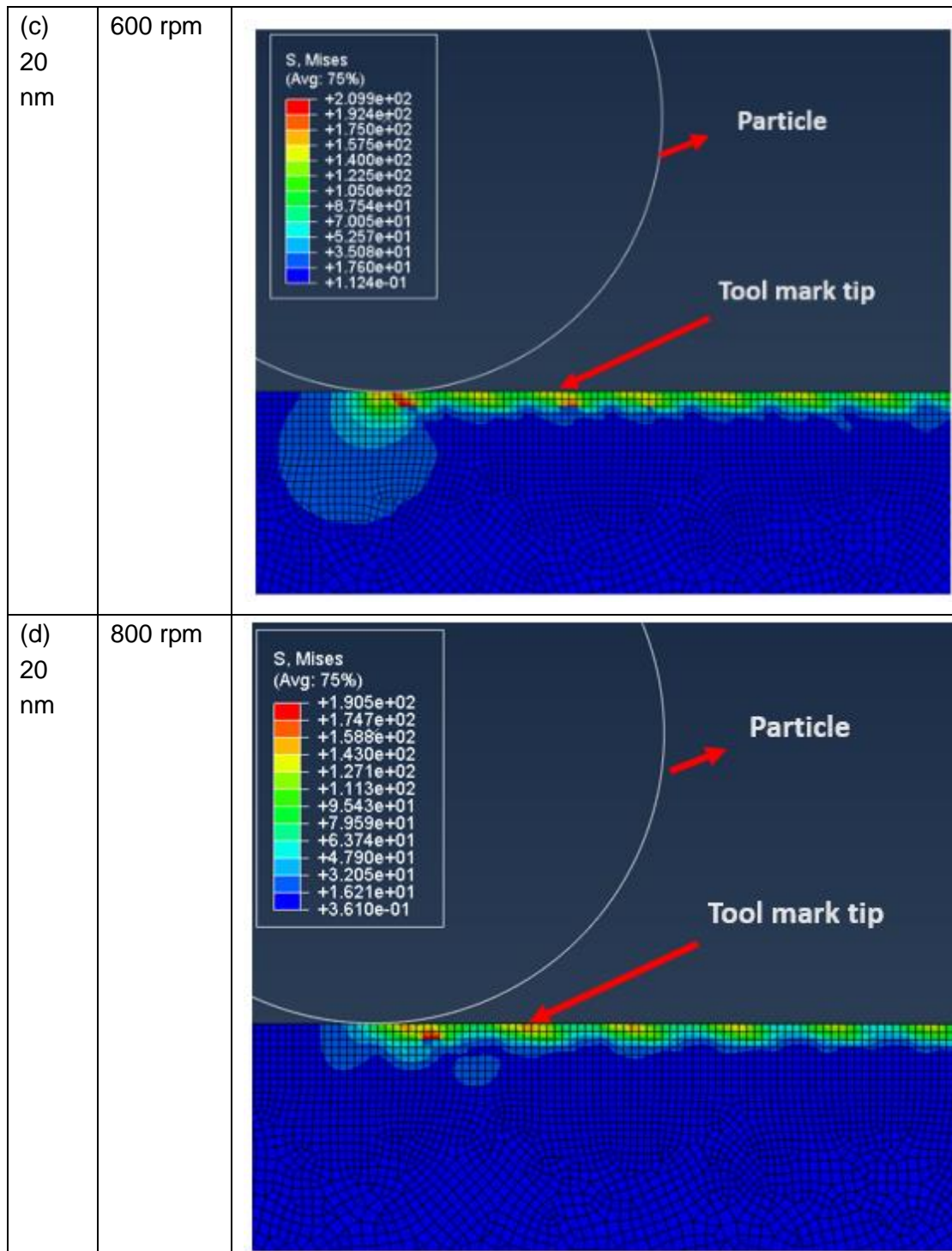


Table 6.5 20nm high tool mark workpiece surface under particle impact at different speeds

Tool mark height	Rotational speed	Results
(a) 20 nm	200 rpm	 <p>The simulation shows a particle impacting the workpiece surface at 200 rpm. The stress distribution is visualized using a color scale from blue (low stress) to red (high stress). The highest stress is concentrated at the point of impact, with a peak value of <math>+2.681 \times 10^2</math>. The tool mark tip is clearly visible, and the stress field extends into the subsurface. Labels 'Particle' and 'Tool mark tip' are present with red arrows pointing to their respective locations.</p>
(b) 20 nm	400 rpm	 <p>The simulation shows a particle impacting the workpiece surface at 400 rpm. The stress distribution is visualized using the same color scale as in (a). The stress field is more localized and intense at the impact point compared to 200 rpm, with a peak value of <math>+2.681 \times 10^2</math>. The tool mark tip is visible, and the stress field extends into the subsurface. Labels 'Particle' and 'Tool mark tip' are present with red arrows pointing to their respective locations.</p>

Chapter 6 Modelling and Simulation of the Surface Generation Mechanism of the Low-pressure Lapping technology



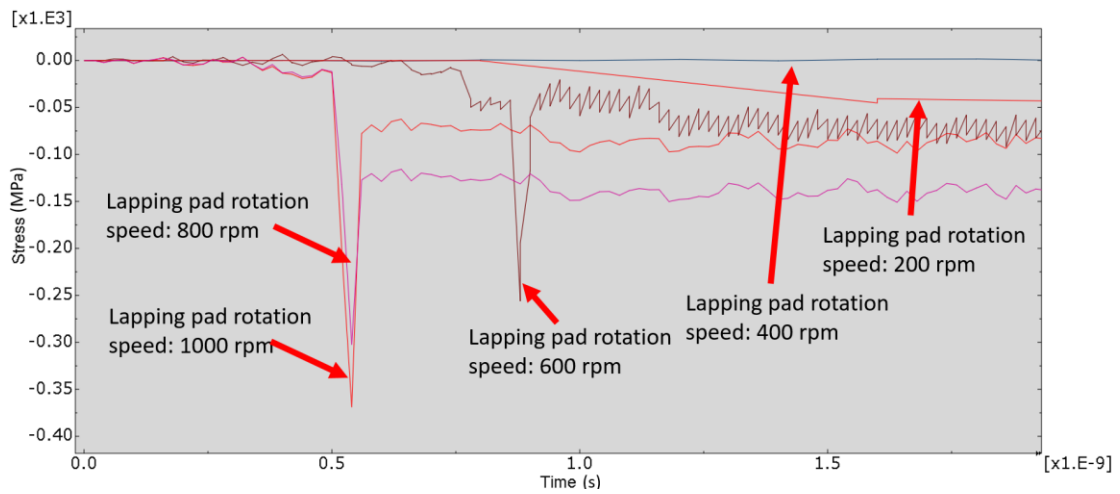
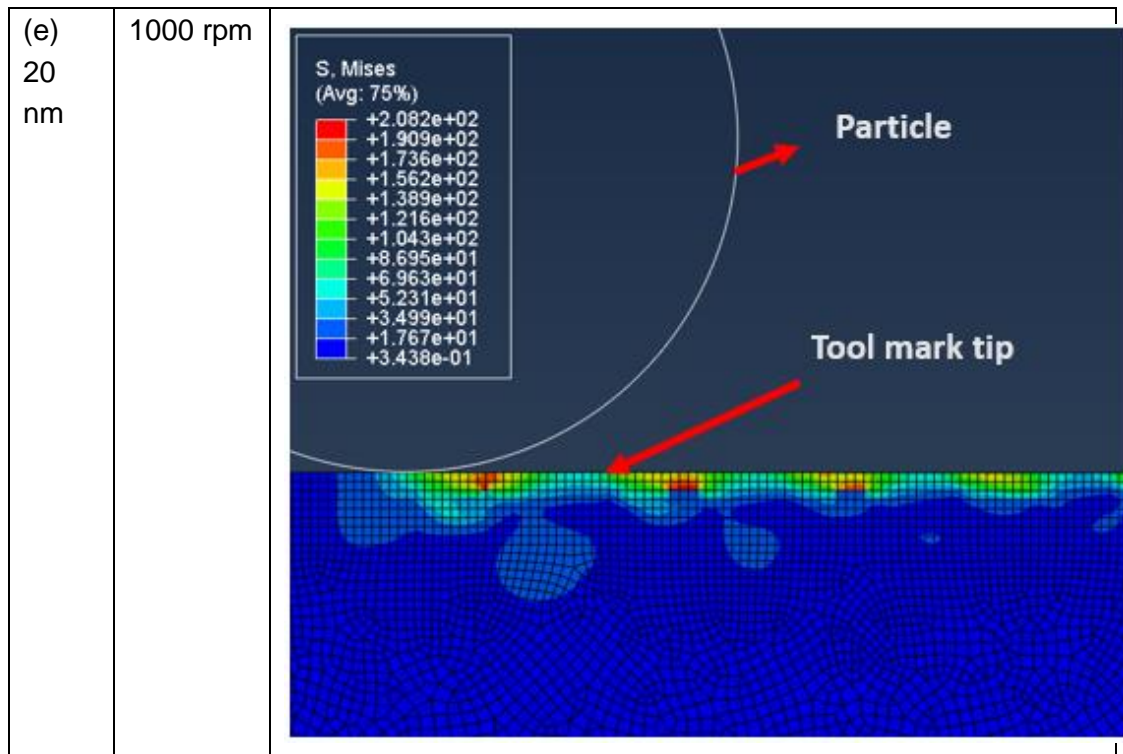


Figure 6.4 Stress-time curve of 1000nm tool mark surface under different speed

## Chapter 6 Modelling and Simulation of the Surface Generation Mechanism of the Low-pressure Lapping technology

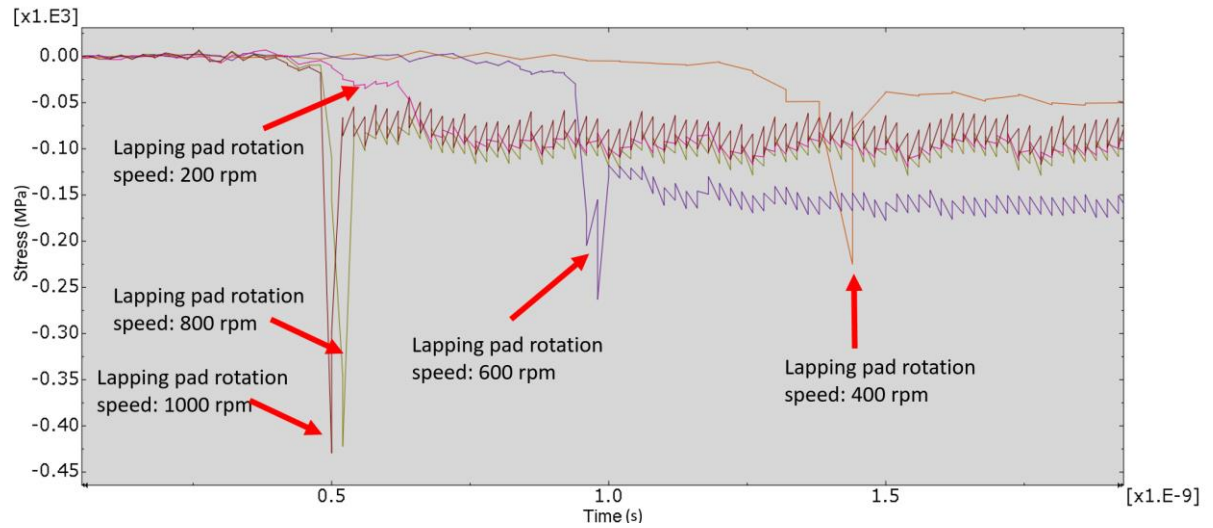


Figure 6.5 Stress-time curve of 20nm tool mark under different speed

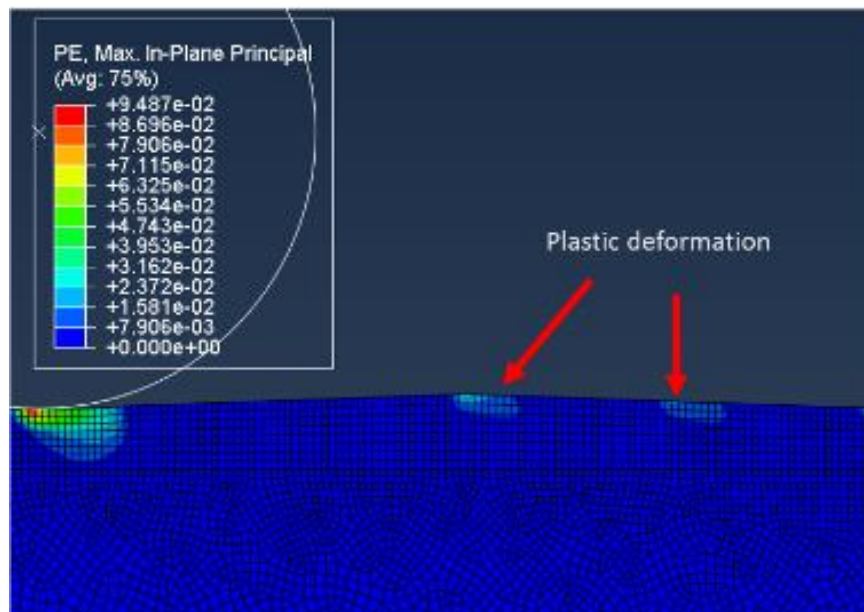


Figure 6.6 Plastic strain map of the 1000 nm high tool mark surface



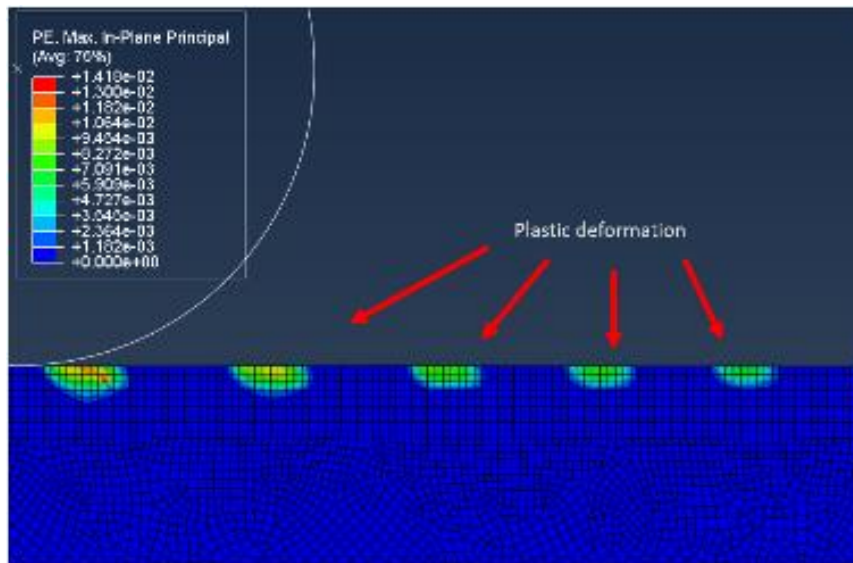


Figure 6.7 Plastic strain map of the 20 nm high tool mark surface

Although the simulation assumes that the speed of the abrasive particles is equal to the speed of the fiber on the lapping pad, the surface formation mechanism of the polishing method can be well verified from the simulation results. That is, the tool marks or asperities on the surface of the workpiece is deformed by the continuous impact of the abrasive grains and finally removed. The number of impacts is calculated according to Eq. (6.3). When it is lapped for 10 minutes, the surface has been impacted  $3 \times 10^6$  times. It is far more than the  $10^5$  times of impact required for high cycle fatigue of typical materials. This cyclic stress is large enough to cause fatigue. As a result, it can be regarded as micro-scale high-cycle fatigue, and can also be seen as impact fatigue for tool marks or asperities. These asperities and tool marks are worn away after fatigue, and the worn surface continues to be impacted by the abrasive particles, which leads to the small scale material removal rate.

It can be seen from the experiment in Chapter 4 that there is almost no change in the lapped surface when the rotational speed is 500 rpm. By finite element simulation, it state that, the rotational speed is the most important lapping parameter in this polishing method. When the rotational speed is lower than a certain level, it will be difficult to produce material removal. This also explains why the asperities on the tool mark surface are removed first, followed by the tool mark itself (Figure 6.8).

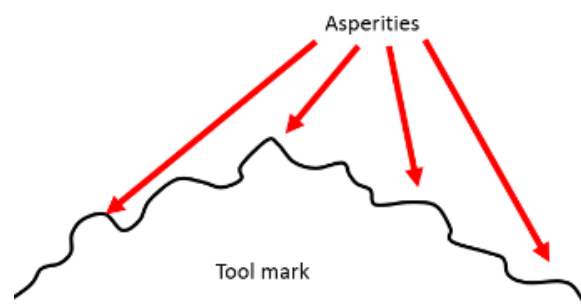


Figure 6.8 The asperities on the tool mark surface are removed first, then the tool mark itself are worn away

## 6.4 Summary

This chapter describes the modelling and simulation of the surface generation mechanism of the novel low-pressure lapping method by the finite element method. The results indicate that the rotational speed plays a major role in the low-pressure lapping process. When the rotational speed is higher than a certain level, i.e. 1000 rpm in the experiment, the abrasive particles driven by the fiber obtain sufficient momentum to impinge on the surface of the workpiece. This causes fatigue on the surface of the workpiece and finally wears asperities and tool marks away. This model not only

## Chapter 6 Modelling and Simulation of the Surface Generation Mechanism of the Low-pressure Lapping technology

---

describes the surface generation mechanism of the low-pressure lapping method, but also can be used to predict the possible lapping parameters when different material and forms of the workpiece are used.

# CHAPTER 7 OVERALL CONCLUSION AND SUGGESTIONS FOR FURTHER WORK

## 7.1 Overall conclusion

Ultra-precision polishing technology has been developed as a post machining process for more than 50 years (Komanduri et al. 1997). Technologies such as Bonnet polishing or Fluid Jet Polishing (FJP) have been developed for polishing materials such as cobalt chrome alloys (Zeng and Blunt 2014), NiCu alloys (Cheung et al. 2010) and SKD61 mould steel (Tsai et al. 2008), but these techniques cannot be applied to polished Al6061 alloy because it is a relatively soft metal in which it is very easy to generate scratches when the vertical force between polishing pad and material is large. Up to present, only Chemical Mechanical Polishing (CMP) has been reported for successfully polishing plano mirrors made from an Al6061 alloy (Horst et al. 2008, Moeggenborg 2008). However, little attention has been focused on the reflectance when the surface roughness is in the nanometer scale.

Sharma et al. (2014) used Al6061 alloy as the specimen material to compare the reflectivity spectrum from a deterministic surface machined by SPDT, and random finished surfaces machined by Chemo Mechanical Magneto Rheological Finishing (CMMRF). They claimed that CMMRF has a higher reflectivity because there are less irregularities and defects on the surface. This indicated that Al6061 alloy can achieve a high reflectance by ultra-precision lapping/polishing methods. As a result, an

experimental and theoretical investigation has been conducted to gain a better understanding of the reflectance characteristics, and to remove the tool marks on the Al6061 mirror surface.

The results of the reflectance experiments show that there is a complex relationship between optical reflectance and surface roughness. The reflectance might not always decrease monotonically with the decreasing surface roughness. The reason for the changes of the reflectance in this study may be due to the changes in the amount of  $Mg_2Si$  particles on the machined surface. When the aluminium alloy (Al6061) is being cut under low feed rate (1 mm/min), it lead to a burnishing effect (Rahman et al 2017): the  $Mg_2Si$  particles were firmly pressed to the surface rather than being removed or knocked-out and these remaining  $Mg_2Si$  particles caused the reduction of the reflectance of the Al6061 alloy.

As a result, a novel low-pressure lapping method for the lapping of Al6061 alloy was investigated to lap the surface machined by higher feed rate (larger than 3 mm/min in this study), and a theoretical model of analyzing the surface generation mechanism of the low-pressure lapping process has been developed. The effects of processing parameters on the surface quality of the workpiece were explored through a series of experiments. Results indicate that parameters such as rotational speed and lapping time play a more important role compares to the grit size and pressure.

The spatial distribution of the surface profile method proposed in this research provides a new way to evaluate surface conditions and to control the lapping process to avoid the occurrence of excessive lapping.

By comparison between the surface lapped by the new method and traditional bonnet polishing method in Chapter 4, it can be clearly see that the novel low-pressure lapping method not only can obtain a better surface finish, but also can preserve the reflectance of aluminium alloy (Al6061) surface.

The finite element method was used to simulate the lapping process of the novel low-pressure lapping method. The simulation combined with the experiment results provide a deep understanding of the surface generation mechanism of the lapping process.

The investigation reported in this thesis contributes significantly to the improvement of understanding of the surface reflectance characteristics on Al6061 alloys machined by SPDT at low feed rates. The developed low-pressure lapping process provides a new post-processing method that can remove the tool marks and preserve the reflectance of Al6061 alloy mirrors at the same time. The development of the finite element model for the new lapping method provides an important means for understanding the surface generation mechanism and making the new lapping process more predictable and efficient.

### **7.2 Suggestions for further work**

The new lapping method studied in this research can be applied to the lapping of soft metal. However, this method is still far from perfect. As a result, some suggestions for further work are provided as follows:

(i)The combination of different parameters during the lapping process can result in very different results. At present, the methods still at the laboratory stage, and is a long way

from actual application. The Taguchi method used in this study reduced the time and trials for finding the optimal lapping parameters, but more combinations of different parameters, such as slurry concentration, need to be evaluated in detail. The results of lapping different soft metals and workpiece with different surface forms need to be further explored. The effect of the lapping path is also an important research direction in order to transform this novel technology from the laboratory level to industry application.

(ii) Lapping process is a complex process that any small changes of the parameters may lead to a different lapping results, which means more parameters involve in the simulation process may lead to a more precisely simulation result. However, finite element method do not have sufficient module to simulate this complex process. As a results, a secondary development is needed in order to simulate the lapping process more precisely. Subsequent simulation should be combined with more experimental results to simulate the particle impinge process on the workpiece, as well as define a more precision adaptive mesh by using subroutine UMESHMOTION tool in Abaqus, in order to simulate the surface generation mechanism of this lapping method in more accurate manner.

(iii) In discussing the relationship between the reflectance and roughness of Al6061 alloy machined by SPDT, it was found that in addition to the surface roughness and surface form of the workpiece influencing the surface reflectance, the amounts of

Mg<sub>2</sub>Si particles contained in the workpiece material may also have a correlation with the surface reflectance. In this study, when the workpiece was machined with different feed rates, the reflectance of the workpiece surface with roughness (Ra) at 7 nm was better than the surface with a smaller roughness (Ra: 4 nm). After using EDX and XRD to inspect the surface of the two workpieces, it was found that the low reflectance surface had more Mg<sub>2</sub>Si particles. This may be due to the small feed rate leading to a burnishing effect, causing the particles being firmly pressed to the surface rather than being removed. These particles lead to the decrease in the reflectance. However, there is no further study on the relationship between the amounts of Mg<sub>2</sub>Si particles and the surface reflectance. Subsequent research should further explore and quantify the relationship between the amounts of Mg<sub>2</sub>Si particles and the surface reflectance through image analysis methods. Further investigation on whether other processing factors in SPDT will also affect the reflectance of this material should be undertaken. In addition, more common materials for ultra-precision machining should be explored to observe whether this phenomenon is universal.



## REFERENCES

Abdullah, A.B., Chia, L.Y. and Samad, Z. The effect of feed rate and cutting speed to surface roughness. *Asian Journal of Scientific Research*, 3(4), pp.278-287. 2010.

Ahmed, S.A., Ko, J.H. and Yeo, S.H. Fabrication of 3D submicron to micro textured surfaces using backside patterned texturing (BPT). *Precision Engineering*, 47, pp.397-405. 2017

Ahmedi, G., and Xia, X., 2001, A Model for Mechanical Wear and Abrasive Particle Adhesion during the Chemical Mechanical Polishing Process, *J. Electrochem. SOC.* 148: G99-GI 09, 2001

anapathy Srinivasan, R., Shanmugan, S. and Palani, S., Application of Magnetorheological Fluid in Machining Process, 2016

Arnold, T. and Böhm, G. Application of atmospheric plasma jet machining (PJM) for effective surface figuring of SiC. *Precision Engineering*, 36(4), pp.546-553. 2012

Arnold, T., Böhm, G., Fechner, R., Meister, J., Nickel, A., Frost, F., Hänsel, T. and

Schindler, A. Ultra-precision surface finishing by ion beam and plasma jet techniques—status and outlook. *Nuclear Instruments and Methods in Physics Research Section A: Accelerators, Spectrometers, Detectors and Associated Equipment*, 616(2), pp.147-156. 2010.

ASM International Handbook Committee. *Metals Handbook: Vol. 2, Properties and selection—nonferrous alloys and pure metals*. 1990

Baker, P.C., Sonderman, J.B. and Saitot, T.T. Finishing of precision generated metal optical components. In *Design, Manufacture and Application of Metal Optics, International Society for Optics and Photonics*. (Vol. 65, pp. 42-48). 1976

Barrick, D.E. Rough surface scattering based on the specular point theory. *Antennas and Propagation, IEEE Transactions on*, 16(4), pp.449-454. 1968.

Bass, M., Van Stryland, E.W., Williams, D.R. and Wolfe, W.L. eds. *Handbook of optics* (Vol. 2). New York: McGraw-Hill. 2001.

Beheshti, A. and Khonsari, M.M. Asperity micro-contact models as applied to the deformation of rough line contact. *Tribology International*, 52, pp.61-74. 2012

Beilby, S.G.T., 1921. *Aggregation & Flow of Solids*. Macmillan. 1921

Bennett, H.E.J. and Porteus, J.O. Relation between surface roughness and specular reflectance at normal incidence. *JOSA*, 51(2), pp.123-129. 1961.

Bingham, R.G., Walker, D.D., Kim, D.H., Brooks, D., Freeman, R. and Riley, D. October. Novel automated process for aspheric surfaces. In *International Symposium on Optical Science and Technology*. pp. 445-450. 2000.

Blateyron, F. The areal field parameters. In *Characterisation of Areal Surface Texture* (pp. 15-43). Springer Berlin Heidelberg. 2013.

Bowden F.P. and Hughes T.P., Proc. R.Soc. (London) A, Vol 160, p575. 1921

Bowden F.P. and Tabor D. The friction and lubrication of solids, Clarendon Press, 1950

Brinksmeier, E., W. Preuß, and J. Schmütz. Manufacture of microstructures by ultrasonic lapping. *Proceedings of the 13th Annual Meeting of the ASPE*. 1998.

Brown, N. J., Baker, P. C., & Maney, R. T. Optical polishing of metals. In *25th Annual Technical Symposium*. pp. 42-57. 1982.

Cao, Z.C., and Cheung C. F. Theoretical modelling and analysis of the material

removal characteristics in fluid jet polishing. *International Journal of Mechanical Sciences* 89. pp. 158-166. 2014.

Cha, J.W., Hwang, S.C. and Lee, E.S. Evaluation of Y<sub>2</sub>O<sub>3</sub> surface machinability using ultra-precision lapping process with IED. *Journal of mechanical science and technology*, 23(4), pp.1194-1201. 2009.

Chang , W. R. , Etsion , I. and Bogy , D. B. An Elastic-plastic Model for the Contact of Rough Surfaces , *ASME Jour. of Trib. ,* 109 , pp 257 – 263 1987

Chen, S., Lv, B., Yuan, J., Zhao, P., Shao, Q. and He, Q. Parameter Optimization by Taguchi Methods for Polishing LiTaO<sub>3</sub> Substrate Using Force-induced Rheological Polishing Method. 2018

Chen, S.S., Li S.Y., Hu H., Tie G.P., Guan C.L., and Li Qi. Analysis of surface quality and processing optimization of magnetorheological polishing of KDP crystal. *Journal of Optics* 44, no. 4. pp.384-390. 2015.

CHENG H.B., FENG Y.P., WANG Y.T. Research on free-form optics [J]. *Laser & Optoelectronics Progress*, (12): 17-22. 2009

Cheung, C.F. and Lee, W.B. A multi-spectrum analysis of surface roughness formation

in ultra-precision machining. *Precision Engineering*, 24(1), pp.77-87. 2000.

Cheung, C.F. and Lee, W.B. Characterisation of nanosurface generation in single-point diamond turning. *International Journal of Machine Tools and Manufacture*, 41(6), pp.851-875. 2001.

Cheung, C.F., Ho, L.T., Charlton, P., Kong, L.B., To, S. and Lee, W.B. Analysis of surface generation in the ultraprecision polishing of freeform surfaces. *Proceedings of the Institution of Mechanical Engineers, Part B: Journal of Engineering Manufacture*, 224(1), pp.59-73. 2010.

Cheung, C.F., Kong, L.B., Lee, W.B. and To, S. Modelling and simulation of freeform surface generation in ultra-precision raster milling. *Proceedings of the Institution of Mechanical Engineers, Part B: Journal of Engineering Manufacture*, 220(11), pp.1787-1801. 2006.

Childs, T.H.C., Evans, C.J., Browy, E.C., Troutman, J.R. and Paul, E. Tool Temperatures and Wear in Micro-machining Cu-Ni Alloys with Diamond Tools: Models, Simulations and Experiments. *Procedia CIRP*, 31, pp.270-275. 2015.

Choi, Seung-Geon, Seong-Hyun Kim, Woong-Kirl Choi, and Eun-Sang Lee. The optimum condition selection of electrochemical polishing and surface analysis of the

stainless steel 316L by the Taguchi method. *The International Journal of Advanced Manufacturing Technology*. 1-7. 2015.

Chuang, Ho-Chiao, and Pei-Lum Tso. An investigation of lapping characteristics for improving the form error of an aspheric lens. *Journal of materials processing technology* 176.1. 183-190. 2006.

Cogburn, G., Mertus, L. and Symmons, A. April. Mounding aspheric lenses for low-cost production versus diamond turned lenses. In SPIE Defense, Security, and Sensing (pp. 766020-766020). *International Society for Optics and Photonics*. 2010.

DAI Y.F. , ZHOU L., XIE X.H. Deterministic figuring in optical machining by ion beam[J]. *Acta Optica Sinica*, 28(6): 1131-1135. 2008

DIN 8589-15. Manufacturing process chip removal. Part 15. Lapping; classification, subdivisions, terms and definitions. *German National Standard*. 1985.

Doyle, E.D. and Turley, D.M. *Wear*, Vol 51, 1978, p269

EITobgy, M., Ng, E. G., & Elbestawi, M. A. Modelling of abrasive waterjet machining: a new approach. *CIRP Annals-Manufacturing Technology*, 54(1), 285-288. 2005.

Enomoto, T., Satake, U., Miyake, T., & Tabata, N. A newly developed polishing pad for achieving high surface flatness without edge roll off. *CIRP Annals-Manufacturing Technology*, 60(1), 371-374. 2011.

Evans, C.J., Paul, E., Dornfeld, D., Lucca, D.A., Byrne, G., Tricard, M., Klocke, F., Dambon, O. and Mullany, B.A. Material removal mechanisms in lapping and polishing. *CIRP Annals-Manufacturing Technology*, 52(2), pp.611-633.2003.

Fähnle, O.W., Van Brug, H. and Frankena, H.J. Fluid jet polishing of optical surfaces. *Applied optics*, 37(28), pp.6771-6773. 1998.

Fish, J., Oskay, C., Fan, R. and Barsoum, R. Al 6061-T6-elastomer impact simulations. *Electronic document*. 2005

Gennaro, A., Sánchez-Sánchez, C.M., Isse, A.A. and Montiel, V. Electrocatalytic synthesis of 6-aminonicotinic acid at silver cathodes under mild conditions. *Electrochemistry communications*, 6(7), pp.627-631. 2004.

Germer, T.A., Zwinkels, J.C. and Tsai, B.K. *Spectrophotometry: Accurate measurement of optical properties of materials* (Vol. 46). Elsevier. 2014.

Gindele, K., Köhl, M. and Mast, M. Spectral reflectance measurements using an integrating sphere in the infrared. *Applied optics*, 1985; 24(12), pp.1757-1760.

Greenwood, J.A. and Williamson, J.B.P., December. Contact of nominally flat surfaces. In Proceedings of the Royal Society of London A: *Mathematical, Physical and Engineering Sciences* Vol. 295, No. 1442, pp. 300-319. 1966,

Guo, Jiang. Corrective finishing of a micro-aspheric mould made of tungsten carbide to 50 nm accuracy. *Applied optics* 54.18. pp. 5764-5770. 2015.

Han, X., Hu, Y., & Yu, S. Investigation of material removal mechanism of silicon wafer in the chemical mechanical polishing process using molecular dynamics simulation method. *Applied Physics A*, 95(3), 899-905. 2009.

Hanrahan, P. and Krueger, W. September. Reflection from layered surfaces due to subsurface scattering. In *Proceedings of the 20th annual conference on Computer graphics and interactive techniques* pp. 165-174. ACM. 1993.

Harvey, J.E., Vernold, C.L., Krywonos, A. and Thompson, P.L. Diffracted radiance: a fundamental quantity in nonparaxial scalar diffraction theory. *Applied optics*, 38(31), pp.6469-6481. 1999.



Hashmi, S. Comprehensive materials processing. Newnes; 2014.

Huang, B., Lai, L., Xia, M., Cheng, W. and Lin, F, October. Research on calibration of lux meter based on integrating sphere source. In International Symposium on Optoelectronic Technology and Application 2016 (pp. 101552F-101552F). International Society for Optics and Photonics; 2016.

Imanaka, O. and Okutomi, M. New concepts on surface finishing and its application to ceramics recent progress in ultra-fine finishing in Japan. *NBS Publication, 562*, pp.157-169. 1979

*Jackson, R.L. and Green, I. A finite element study of elasto-plastic hemispherical contact against a rigid flat. Transactions of the ASME-F-Journal of Tribology, 127(2), pp.343-354. 2005*

Jacobs, S.D., Golini, D., Hsu, Y., Puchebner, B.E., Strafford, D., Prokhorov, I.V., Fess, E.M., Pietrowski, D. and Kordonski, W.I. August. Magnetorheological finishing: a deterministic process for optics manufacturing. In *International Conferences on Optical Fabrication and Testing and Applications of Optical Holography*. pp. 372-382. 1995.

Jain, V.K. Magnetic field assisted abrasive based micro-/nano-finishing. *Journal of Materials Processing Technology*, 209(20), pp.6022-6038. 2009

Jeon, M.W., Hyun, S.W., Bae, J.Y., Jeong, B.J., Oh, E.S., Kang, et al. Development of an off-axis TMA telescope for coastal water remote sensing. *International Journal of Precision Engineering and Manufacturing*, 17(5), pp.685-689. 2016

Ji, S., Yu, H., Zhao, J., Liu, X. and Zhao, M. Ultra-Precision Machining of a Large Amplitude Sinusoidal Ring Surface Based on a Slow Tool Servo. *Strojniški vestnik- Journal of Mechanical Engineering*, 62(4), pp.213-219. 2016

Jiang, X., Scott, P.J., Whitehouse, D.J. and Blunt, L. September. Paradigm shifts in surface metrology. Part I. Historical philosophy. In *Proceedings of the Royal Society of London A: Mathematical, Physical and Engineering Sciences* (Vol. 463, No. 2085, pp. 2049-2070). The Royal Society. 2007.

Kadin, Y., Kligerman, Y. and Etsion, I. Multiple loading–unloading of an elastic–plastic spherical contact. *International journal of solids and structures*, 43(22), pp.7119-7127. 2006

Kaplan, B.A., Goldstein, G.R., Vijayaraghavan, T.V. and Nelson, I.K. The effect of three polishing systems on the surface roughness of four hybrid composites: a profilometric and scanning electron microscopy study. *Journal of prosthetic dentistry*, 76(1), pp.34-38. 1996

Kinast, J., Schlegel, R., Kleinbauer, K., Steinkopf, R., Follert, R., Dorn, R.J., Lizon, J.L., Hatzes, A. and Tünnermann, A. Manufacturing of aluminum mirrors for cryogenic applications. In *Advances in Optical and Mechanical Technologies for Telescopes and Instrumentation. International Society for Optics and Photonics.III* (Vol. 10706, p. 107063G). 2018

Klocke, E.F. and Kuchie, A. Lapping and Polishing. In *Manufacturing Processes 2* (pp. 1-32). Springer Berlin Heidelberg. 2009

Klocke, F., Dambon, O., & Zunke, R. Modeling of contact behavior between polishing pad and workpiece surface. *Production Engineering*, 2(1), 9-14. 2008.

Kogut, L. and Etsion, I. Elastic-plastic contact analysis of a sphere and a rigid flat. *Journal of applied Mechanics*, 69(5), pp.657-662. 2002

Komanduri, R., Lucca, D.A. and Tani, Y. Technological advances in fine abrasive processes. *CIRP Annals-Manufacturing Technology*, 46(2), pp.545-596. 1997.

Kong, L.B. and Cheung, C.F. Modeling and characterization of surface generation in fast tool servo machining of microlens arrays. *Computers & Industrial Engineering*, 63(4), pp.957-970. 2012.

Kordonski, W., & Golini, D. Progress update in magnetorheological finishing. *International Journal of Modern Physics B*, 13(14n16), 2205-2212. 1999.

Kral, E.R., Komvopoulos, K. and Bogy, D.B. Elastic-plastic finite element analysis of repeated indentation of a half-space by a rigid sphere. *Journal of applied mechanics*, 60(4), pp.829-841. 1993

Kuriyagawa, T. Development of electrorheological fluid assisted machining for 3-dimensional small parts. *Journal of the Japan Society of Precision Engineering*, 65(1), p.145. 1999

Kuriyagawa, T., Saeki, M. and Syoji, K. Electrorheological fluid-assisted ultra-precision polishing for small three-dimensional parts. *Precision engineering*, 26(4), pp.370-380. 2002.

Lambropoulos, John C., Su Xu, and Tong Fang. Loose abrasive lapping hardness of

optical glasses and its interpretation. *Applied optics* 36.7: 1501-1516.1997.

Lauro, C.H., Brandão, L.C., Baldo, D., Reis, R.A. and Davim, J.P. Monitoring and processing signal applied in machining processes—A review. *Measurement*, 58, pp.73-86. 2014.

Leach, R.K. *Characterisation of areal surface texture* (pp. 36-37). Berlin: Springer. 2013.

Lee, E.H. Elastic-plastic deformation at finite strains. *Journal of Applied Mechanics*, 36(1), pp.1-6. 1969

Lee, H.S. and Jeong, H.D. Chemical and mechanical balance in polishing of electronic materials for defect-free surfaces. *CIRP Annals-Manufacturing Technology*, 58(1), pp.485-490. 2009.

Lee, W.B. and Cheung, B.C. *Surface generation in ultra-precision diamond turning: Modelling and Practices* (Vol. 12). John Wiley & Sons. 2003.

Lewandowski, Henry S., and Richard R., An automated method for the preparation of orthogonal arrays for use in Taguchi designed experiments. *Computers & industrial*

*engineering* 17.1. 502-507. 1989.

Li, L., Collins, S.A. and Allen, Y.Y. Optical effects of surface finish by ultraprecision single point diamond machining. *Journal of Manufacturing Science and Engineering*, 132(2), p.021002. 2010.

Li, W., Wang, G., Wu, S. and Liaw, P.K. Creep, fatigue, and fracture behavior of high-entropy alloys. *Journal of Materials Research*, 33(19), pp.3011-3034. 2018

Li, Y., Wu, Y., Zhou, L., & Fujimoto, M. Vibration-assisted dry polishing of fused silica using a fixed-abrasive polisher. *International Journal of Machine Tools and Manufacture*, 77, 93-102. 2014.

Liao, W., Dai, Y. and Xie, X. Influence of material removal programming on ion beam figuring of high-precision optical surfaces. *Optical Engineering*, 53(9), p.095101. 2014

Lin H J, Hong X Y, Xu Z X, The dynamic analysis of writing brush furcation phenomenon based on experiments, online, 2016.

Liu, X., Liu, Y., Liang, Y., Liu, H., Zhao, Z., and Gao, B. Effect of slurry components on chemical mechanical polishing of copper at low down pressure and a chemical kinetics

model. *Thin Solid Films*, 520(1), 400-403. 2011.

Mandal, S., Mishra, V., Tiwari, U., Hanumaiah, N. and Sarepaka, R.G. Fiber Bragg grating sensor for temperature measurement in micro turning of optical surfaces with high surface integrity. *International journal of optomechatronics*, 7(4), pp.244-252. 2013.

Marinescu I., Uhlmann E., Toshiro D., *Handbook of lapping and polishing* (1st ed.) CRC Press ISBN 11 57444 670 3. 2006.

Miao, C., Shafrir, S. N., Lambropoulos, J. C., Mici, J., and Jacobs, S. D. Shear stress in magnetorheological finishing for glasses. *Applied Optics*, 48(13), 2585-2594. 2009.

Moeggenborg, K.J., Barros, C., Lesiak, S., Naguib, N. and Reggie, S. Low-scatter bare aluminum optics via chemical mechanical polishing. In *Optical Engineering+ Applications* pp. 706002-706002. 2008.

Moeggenborg, Kevin., Vincer, T., Lesiak, S. and Salij, R. August. Super-polished aluminum mirrors through the application of chemical mechanical polishing techniques. In *SPIE Optics+ Photonics*. pp. 62880L-62880L. 2006.

Moeggenborg, Kevin.J., Barros, C., Lesiak, S., Naguib, N. and Reggie, S. August. Low-

scatter bare aluminum optics via chemical mechanical polishing. In *Optical Engineering+ Applications* pp. 706002-706002. 2008.

Mori, Y., Yamauchi, K., Yamamura, K. and Sano, Y. Development of plasma chemical vaporization machining. *Review of scientific instruments*, 71(12), pp.4627-4632. 2000

Namba, Y., Abe, M. and Kobayashi, A. Ultraprecision grinding of optical glasses to produce super-smooth surfaces. *CIRP Annals-Manufacturing Technology*, 42(1), pp.417-420. 1993.

Ogilvy, J.A. *Theory of wave scatter. from random rough surf.* Adam Hilger, Bristol, 1991.

Olver, A.V. The mechanism of rolling contact fatigue: an update. Proceedings of the Institution of Mechanical Engineers, Part J: Journal of Engineering Tribology, 219(5), pp.313-330. 2005

Oren, M. and Nayar, S.K. Generalization of the Lambertian model and implications for machine vision. *International Journal of Computer Vision*, 14(3):227–251. 1995.

Paulson, N.R., Sadeghi, F. and Habchi, W. A coupled finite element EHL and continuum damage mechanics model for rolling contact fatigue. *Tribology International*, 107, pp.173-183. 2017



Peiponen, K.E. and Tsuboi, T. Metal surface roughness and optical reflectance. *Optics & Laser Technology*, 22(2), pp.127-130. 1990

Peng, H., Liu, Z., Huang, F. and Ma, R. A study of elastic–plastic contact of statistical rough surfaces. Proceedings of the Institution of Mechanical Engineers, Part J: *Journal of Engineering Tribology*, 227(10), pp.1076-1089. 2013

Pitschke, E., Schinhaerl, M., Rascher, R., Sperber, P., Smith, L., Stamp, R., & Smith, M. Simulation of a complex optical polishing process using a neural network. *Robotics and Computer-Integrated Manufacturing*, 24(1), 32-37. 2008.

Preston, F. W. The theory and design of plate glass polishing machines. *J. Soc. Glass Tech.* 11: 214.1927.

Pugh E.N. and Samuels L.E. *J. Electrochem. Soci.* , Vol 111, p1429. 1964

Qi, J. Herron J.R., Sansalone K.H., Mars W.V., Du Z.Z., Snyman M. and Surendranath H. (2007) Validation of a Steady-State Transport Analysis for Rolling Treaded Tires. *Tire Science and Technology*: September, Vol. 35, No. 3, pp. 183-208. 2007

Ragheb, H. and Hancock, E.R. Testing new variants of the Beckmann–Kirchhoff model against radiance data. *Computer Vision and Image Understanding*, 102(2), pp.145-168. 2006.

Rahman, M.A., Rahman, M. and Kumar, A.S. Chip perforation and ‘burnishing–like’finishing of Al alloy in precision machining. *Precision Engineering*, 50, pp.393-409. 2017

Raja, J., Muralikrishnan, B. and Fu, S. Recent advances in separation of roughness, waviness and form. *Precision Engineering*, 26(2), pp.222-235. 2002.

Ren, L., Zhang, G., Zhang, L., Zhang, Z. and Huang, Y. Modelling and investigation of material removal profile for computer controlled ultra-precision polishing. *Precision Engineering*. 2018

Richardson, J. H., W. De La Torre, and H. E. Mendoza: "An SEM Study of Polishing Cloths," *Microstructural Science*, vol. 3B, Elsevier Publishing Company, New York, pp551-566. 1975

Sabirov, I., Perez-Prado, M.T., Murashkin, M., Molina-Aldareguia, J.M., Bobruk, E.V.,

Yunusova, N.F. and Valiev, R.Z. Application of equal channel angular pressing with parallel channels for grain refinement in aluminium alloys and its effect on deformation behavior. *International Journal of Material Forming*, 3(1), pp.411-414. 2010

Saito, T.T. and Simmons, L.B. Performance characteristics of single point diamond machined metal mirrors for infrared laser applications. *Applied optics*, 13(11), pp.2647-2650. 1974.

Samuels L.E. Polishing Wear, Friction, Lubrication, and Wear Technology, Vol18, ASM Handbook, ASM international, p191. 1992

Samuels, L.E., Coade, R.W. and Mann, S.D. Precracking structures in a creep-ruptured low-carbon Cr Mo steel: Their nature and detection by light microscopy and scanning electron microscopy. *Materials characterization*, 29(3), pp.343-363. 1992

Samuels, L.E. Metallographic polishing by mechanical methods. Asm International. 2003

Sanchez L. E. A., Jun N. Z. X., and Fiocchi A. A. Surface finishing of flat pieces when submitted to lapping kinematics on abrasive disc dressed under several overlap factors. *Precision Engineering* 35.2. 355-363. 2011.

Sata, T., Li, M., Takata, S., Hiraoka, H., Li, C.Q., Xing, X.Z. and Xiao, X.G. Analysis of surface roughness generation in turning operation and its applications. *CIRP Annals-Manufacturing Technology*, 34(1), pp.473-476. 1985.

Shankar, S. and Mayuram, M.M. Effect of strain hardening in elastic–plastic transition behavior in a hemisphere in contact with a rigid flat. *International Journal of Solids and Structures*, 45(10), pp.3009-3020. 2008

Shiou, Fang-Jung, and Quoc-Nguyen Banh. Development of an innovative small ball-burnishing tool embedded with a load cell. *The International Journal of Advanced Manufacturing Technology*. 1-11. 2016.

Shorey, A. B. *Mechanisms of material removal in magnetorheological finishing (MRF) of glass*. 2000.

Si, L., Guo, D., Luo, J., & Lu, X. Monoatomic layer removal mechanism in chemical mechanical polishing process: A molecular dynamics study. *Journal of Applied Physics*, 107(6), 064310. 2010.

Spizzichino, A. and Beckmann, P. *The Scattering of Electromagnetic Waves from Rough Surfaces*. New York, Paris. 1963.

Srinivasa-Murthy, C., Wang, D., Beaudoin, S. P., Bibby, T., Holland, K., and Cale, T. S. Stress distribution in chemical mechanical polishing. *Thin Solid Films*, 308, 533-537. 1997.

St'aihli, A.W. *The technique of lapping*. 1998.

Strong, J. *Procedures in experimental physics*. 1938.

Su, J.X., Guo, D.M., Kang, R.K., Jin, Z.J., Li, X.J. and Tian, Y.B. Modeling and analyzing on nonuniformity of material removal in chemical mechanical polishing of silicon wafer. In *Materials Science Forum* (Vol. 471, pp. 26-31). Trans Tech Publications. 2004

Suh, N.P. et al., The delamination Theory of wear, *Wear*, Vol 44, p1, 1977

Suresh, S. *Fatigue of materials*. Cambridge university press. 1998

Tabor D. *The Hardness of Metals* , *Clarendon Press* , Oxford. 1951

Tam, H.Y. and Cheng, H. An investigation of the effects of the tool path on the removal of material in polishing. *Journal of Materials Processing Technology*, 210(5),

pp.807-818. 2010

Tam, H.Y., Cheng, H. and Dong, Z. Peano-like paths for subaperture polishing of optical aspherical surfaces. *Applied optics*, 52(15), pp.3624-3636. 2013

Tam, H.Y., Cheng, H. and Dong, Z. Peano-like paths for subaperture polishing of optical aspherical surfaces. *Applied optics*, 52(15), pp.3624-3636. 2013

ter Horst, R., Tromp, N., de Haan, M., Navarro, R., Venema, L. and Pragt, J. Directly polished lightweight aluminum mirror. In SPIE Astronomical Telescopes+ Instrumentation pp. 701808-701808. 2008.

Terrin, A., Dengo, C. and Meneghetti, G. Experimental analysis of contact fatigue damage in case hardened gears for off-highway axles. *Engineering Failure Analysis*, 76, pp.10-26. 2017

Toozandehjani, M., Mustapha, F., Ariffin, M.K.A., Zahari, N.I., Matori, K.A., Ostovan, F. and Fadaeifard, F. Effect of Artificial Aging on the Microstructure and Mechanical Properties of Aluminum Alloy AA6061-T6. *Metal Science and Heat Treatment*, 58(5-6), pp.283-286. 2016

Torrance, K.E., Sparrow, E.M. and Birkebak, R.C. Polarization, directional distribution,

and off-specular peak phenomena in light reflected from roughened surfaces. *JOSA*, 56(7), pp.916-924. 1966.

Trent, E. M. and Wright, P. K. *Metal Cutting, fourth edition*, pp. 98-102. 2000.

TRICARD M, KORDONSKI W I, SHOREY A B. Magnetorheological jet finishing of conformal, freeform and steep concave optics[J]. *Annals of the CIRP*, 55: 309-312. 2006

Tsai, F.C., Yan, B.H., Kuan, C.Y. and Huang, F.Y. A Taguchi and experimental investigation into the optimal processing conditions for the abrasive jet polishing of SKD61 mould steel. *International Journal of Machine Tools and Manufacture*, 48(7), pp.932-945. 2008.

Turley D.M. and Samuels L.E. *Metallography*, Vol 14, 1981, p275

van Ginneken, B., Stavridi, M. and Koenderink, J.J. Diffuse and specular reflectance from rough surfaces. *Applied optics*, 37(1), pp.130-139. 1998.

Verdu, C., Adrien, J. and Buffière, J.Y. Three-dimensional shape of the early stages of fatigue cracks nucleated in nodular cast iron. *Materials Science and Engineering: A*, 483, pp.402-405. 2008

Whitehouse, D.J. *Handbook of surface and nanometrology*. CRC press. 2010.

Whitehouse, D.J. *Handbook of surface metrology*. CRC Press. 1994.

Whitehouse, D.J. *Surfaces and their Measurement*. Elsevier. 2004.

Whitley, J.Q., Kusy, R.P., Mayhew, M.J. and Buckthal, J.E. Surface roughness of stainless steel and electroformed nickel standards using a HeNe laser. *Optics & Laser Technology*, 19(4), pp.189-196. 1987

Wolff, L.B., Nayar, S.K. and Oren, M. Improved diffuse reflection models for computer vision. *International Journal of Computer Vision*, 30(1), pp.55-71. 1998.

Xie, D. G., Gao, B., Yao, Y. X., and Yuan, Z. J. Study of Local Material Removal Model of Bonnet Tool Polishing. *Key Engineering Materials*, 304, 335-339. 2006.

Yen, Y.C. Modeling of metal cutting and ball burnishing-Prediction of tool wear and surface properties Doctoral dissertation, The Ohio State University. 2004.

Yi, J. On the wafer/pad friction of chemical-mechanical planarization (CMP) processes-



part I: modeling and analysis. *IEEE transactions on semiconductor manufacturing*, 18(3), pp.359-370. 2005

Yin, Z. and Yi, Z. Direct polishing of aluminum mirrors with higher quality and accuracy. *Applied optics*, 54(26), pp.7835-7841. 2015.

Yonehara, M., Matsui, T., Kihara, K., Isono, H., Kijima, A. and Sugibayashi, T. Experimental relationships between surface roughness, glossiness and color of chromatic colored metals. *Materials Transactions*, 45(4), pp.1027-1032. 2004.

Yu T.K., Yu C.C. and M. Orłowski , in Proceeding of the *International Electro Devices Meeting*, page 35.4.1. 1993

Yuan, J long, and WU. Review on Ultra-precision Polishing Technology of Aspheric Surface. *Journal of Mechanical Engineering* 48.23(2012):167. 2012

Zeng, S. and Blunt, L. Experimental investigation and analytical modelling of the effects of process parameters on material removal rate for bonnet polishing of cobalt chrome alloy. *Precision Engineering*, 38(2), pp.348-355. 2014.

Zeng, S. *Bonnet Polishing of Cobalt Chrome Alloys for Artificial Implants* (Doctoral dissertation, University of Huddersfield). 2014.

ZHANG Lei, HE Xinsheng, ZHANG Ying, et al. Development of new type ER fluid-assisted polishing tool and its polishing experiment[J]. *Journal of Jilin University*, 40(4): 1009-1014. 2010

Zhang, J., Zhang, X., Tan, S. and Xie, X. Design and Manufacture of an Off-axis Aluminum Mirror for Visible-light Imaging. *Current Optics and Photonics*, 1(4), pp.364-371. 2017

Zhang, J. H. Theory and technique of precision cutting, *Pergamon Press*, pp.92-94. 1991.

Zhao, P., Tao, L., & Wang, Z. W. Review on trace of plane lapping/polishing. *Aviation Precision Manufacturing Technology*, 45(2), 1-6. 2009